# Neuronal Nitric Oxide Synthase – A biomarker for Alzheimers disease:

## Interaction of neuronal Nitric oxide synthase with beta – amyloid peptides in the brain

---

A thesis submitted in fulfillment of the requirements for the degree of

**Master of Science**
**(Biochemistry)**

at

Rhodes University

by

**Eden Padayachee**

March 2010

# Abstract

High levels of the amino acid arginine and low levels of the product citrulline in the cerebrospinal fluid of Alzheimer's patients could mean that there is a decrease in the enzymes that metabolize this amino acid. One such enzyme is neuronal nitric oxide synthase (nNOS). In this study, neuronal nitric oxide synthase (nNOS), sourced from bovine brain was extracted and concentrated using two methods of precipitation: poly (ethylene glycol) 20 000 (PEG) and ammonium sulphate [$(NH_4)_2SO_4$]. These two techniques gave no increase in yield nor fold purification and hence were abandoned in favour of ion exchange chromatography by DEAE-Sepharose. The enzyme was then successfully purified by anion-exchange and after dialysis produced a 38 % yield and three fold purification and yielded the highest specific activity of 2.27 U/mg. Neuronal nitric oxide synthase (nNOS) was a heterodimeric protein with a total molecular mass of ± 225 kDa (95 and 130 kDa monomers). The temperature and pH optima of the enzyme were 40 °C and 6.5, respectively. The kinetic parameters ($K_M$ and $V_{max}$) of nNOS were 70 μM and 0.332 μmol.min$^{-1}$, respectively. Moreover neuronal nitric oxide synthase (nNOS) was relatively stable at 40 °C ($t_{½}$ = 3 h). It was also confirmed that ß-amyloid peptides inhibited nNOS when bound to the enzyme and that nNOS behaved as a catalyst in fibril formation through association-dissociation between enzyme and ß-amyloid peptide. It was further shown that $Aß_{17-28}$ inhibited nNOS the most with a $K_i$ of 1.92 μM and also had the highest Stern-Volmer value ($K_{SV}$) of 0.11 μM$^{-1}$ indicating tight binding affinity to nNOS and easier accessibility to fluor molecules during binding. Congo red, turbidity, thioflavin-T assays and transmission electron microscopy were successfully used to detect and visualize the presence of fibrils by studying the process of fibrillogenesis. Computerized molecular modeling successfully studied protein dynamics and conformational changes of nNOS. These results correlated with resonance energy transfer (FRET) results which revealed the distance of tryptophan residues from the arginine bound at enzyme active site. Both the aforementioned techniques revealed that in the natural state of the enzyme with arginine bound at the active site, the tryptophan residues ($TRP_{625}$ and $TRP_{721}$) were positioned at the surface of the enzyme 28 Å away from the

active site. When the amyloid peptide ($A\beta_{17-28}$) was bound to the active site, these same two amino acids moved 14 Å closer to the active site. A five residue hydrophobic fragment $A\beta_{17-21}$ [$Leu_{17}$ – $Val_{18}$ – $Phe_{19}$ – $Phe_{20}$ – $Ala_{21}$] within $A\beta_{17-28}$ was shown by computer modeling to be critical to the binding of the peptide to the active site of nNOS.

# Table of Contents

# List of Figures

# List of Tables

# List of Schemes

# List of Equations

$$\text{Enzyme activity} = \frac{\Delta A.V_T.D_f}{e.t.l.V_e} = \mu\text{mol/min}$$

Eq (1).....32

$$\frac{[S]}{V} = \frac{[S]}{V_{max}} + \frac{K_M}{V_{max}}$$

Eq (2).....35

$$k_{cat} = \frac{V_{max}}{[E_t]}$$

Eq (3).....44

$$\text{Catalytic efficiency} = \frac{k_{cat}}{K_M}$$

Eq (4).....44

$$K_i = \frac{A\beta.\ V_{max}^{app}}{V_{max} - V_{max}^{app}}$$

Eq (5)..... 51

$$[A\beta_{FIB}] = \left(\frac{A_{540}}{25\,295} - \frac{A_{480}}{46\,306}\right)$$

Eq (6).....67

$$\frac{F_0}{F} = 1 + Tkq$$

Eq (7).....91

$$\frac{F_0}{\Delta F} = \frac{1}{\Theta K_{SV}[q]} + \frac{1}{\Theta}$$

Eq (8).....92

$$\text{Efficiency of Transfer} = 1 - \frac{F^{D,A}}{F^{D}} = \frac{1}{1+(R/R_0)^6}$$

Eq (9).....94

$$R_0 = 8.79 \times 10^{-5} (Q_D k^2 n^{-4} J)$$

Eq (10).....94

# List of Abbreviations

| | |
|---|---|
| γ-secretase | gamma-secretase |
| ß-secretase | beta-secretase |
| < | less than |
| λ | wavelength |
| % | percent |
| $\Delta F_{max}$ | maximum change in fluorescence |
| 3-D | three-dimensional |
| µL | microlitre |
| µM | micromolar |
| $A_{max}$ | absorption maximum |
| Aß | amyloid beta peptide |
| A | amperes |
| AD | Alzheimer's disease |
| ADMA | asymmetric $N^G$, $N^G$ –dimethyl-L-arginine |
| AFM | atomic force microscopy |
| Al | aluminium |
| ApoE | apoliprotein E |
| APP | amyloid precursor protein |
| AU | arbitrary units |
| BACE | beta-secretase or beta-site APP cleaving enzyme |

| | |
|---|---|
| BAEE | benzoyl-L-arginine ethyl ester hydrochloride |
| $BH_4$ | tetrahydro-L-biopterin dichloride |
| BSA | bovine serum albumin |
| C | concentration of amyloid peptide |
| CaM | calmodulin |
| CNS | central nervous system |
| c* | critical micelle concentration |
| $CaCl_2$ | calcium chloride |
| CSF | cerebrospinal fluid |
| Cu | copper |
| D | donor |
| Da | dalton |
| DAF-2 | 4,5-diaminofluorescein |
| DAF-2 DA | 4,5-diaminofluorescein diacetate |
| DAF-2T | triazolofluorescein |
| DEAE | diethyl-amino ethylene |
| DTT | dithiothreitol |
| DMSO | dimethyl sulfoxide |
| [E] | FRET efficiency/ efficiency of energy transfer |
| EDTA | ethylenediaminetetraacetic acid |
| ESI | enzyme-substrate – inhibitor |
| eNOS | endothelial nitric oxide synthase |
| F | fluorescence intensity |
| FAD | flavin adenine dinucleotide |

| | |
|---|---|
| Fe | iron/heme |
| $FeCl_3$ | ferric chloride hexahydrate |
| FMN | flavin mononucleotide |
| $F^{D,A}$ | fluorescence between donor and acceptor |
| FRET | fluorescence resonance energy transfer |
| HEPES | 4-(2-hydroxyethyl) piperazine-N'-(2-ethane-sulphonic acid monosodium salt |
| h | hour |
| HCL | hydrochloric acid |
| 80 HG | 8- hydroxyguanosine |
| CoA HMG-CoA-reductase | 3-hydroxy-3-methyl-glutaryl-CoA reductase |
| iNOS | inducible nitric oxide synthase |
| j | overlap integral between acceptor emission and donor excitation |
| $k^2$ | orientation factor of donor and acceptor |
| $k_{cat}$ | enzyme turn-over number |
| $k_{cat}$ /$K_M$ | catalytic efficiency |
| kDa | kilodalton |
| $K_a$ | association constant |
| $K_d$ | dissociation constant |
| $K_i$ | inhibitor constant |
| $K_M$ | Michaelis-Menten constant |
| $K_{sv}$ | Stern -Volmer constant |
| kV | kilovolts |
| L | ligand |

| | |
|---|---|
| L-NHA | $N^G$-hydroxy –L-arginine |
| M | molar |
| mins | minutes |
| ml | milliliter |
| mM | millimolar |
| mtNOS | mitochondrial nitric oxide synthase |
| MCI | mild cognitive impairment |
| MRI | magnetic resonance imaging |
| $M_r$ | molecular weight |
| methHb | methemoglobin |
| nM | nanomolar |
| nm | nanometer |
| NaOH | sodium hydroxide |
| NAMD | nanoscale molecular dynamics |
| NADPH | nicotinamide adenine dinucleotide phosphate reduced tetrasodium salt |
| NMDA | *N*-methyl-D-aspartate |
| NOS | nitric oxide synthase |
| nNOS | neuronal nitric oxide synthase |
| $NADP^+$ | nicotinamide adenine dinucleotide phosphate |
| NO | nitric oxide |
| $NH_4Cl$ | ammonium chloride |
| $(NH_4)_2\ SO_4$ | ammonium sulphate |
| NFT | neurofibrillary tangle |

| | |
|---|---|
| NMMA | $N^G$-monomethyl-L-arginine |
| NPA | *N*-propyl-L-arginine |
| $O_2$ | oxygen |
| oxyHb | oxyhemoglobin |
| $ONOO^-$ | peroxynitrate |
| PAGE | poly-acrylamide gel electrophoresis |
| PDB | protein data bank |
| PEG | poly (ethylene glycol) |
| PET | positron emission tomography |
| Phe | phenylalanine |
| PS 1 | presenilin 1 |
| PS 2 | presenilin 2 |
| pM | picomolar |
| PMSF | phenylmethylsulphonylfluoride |
| QCMD | quartz crystal microbalance with dissipation monitoring |
| Q | quantum yield |
| R | distance between donor and acceptor molecules |
| $R_0$ | Förster distance |
| ROS | reactive oxygen species |
| RFU | relative fluorescence units |
| RT | room temperature |
| S.E.M | standard error of mean |
| SDS | sodium dodecyl sulphate |
| SDS-PAGE | Sodium dodecyl sulphate-polyacrylamide gel electrophoresis |

| | |
|---|---|
| s | second |
| TEMED | *N,N,N'*, *N*-tetramethyl-ethylenediamine |
| ThT | thioflavin -T |
| TRP | tryptophan |
| V | volt |
| vs. | versus |
| v/v | volume per volume |
| w | tryptophan |
| w/v | weight per volume |
| Zn | zinc |

# Acknowledgements

I would like to express my sincere gratitude and appreciation to the following people:

- To Jehovah God, my Best friend, Helper, Protector and Provider, in you I have trusted and through your holy spirit you have guided me to the ultimate success and completion of this thesis. Despite the odds and perils I encountered, I have come off victorious. All the praise and honour must go to YOU for you have endowed me with intellectual ability and reason.
- To my supervisor and mentor, Professor Chris Whiteley, thank you for constantly reminding me about the importance of focus and hard work in research. Your constructive criticism, guidance and motivation have been invaluable in the completion of this thesis. You have inspired me to question all possibilities to a research problem before arriving at a solution and I am now passionate to pursue my PhD in Medicinal Biochemistry.
- To my team mates of Lab 309 (2008/2009), thank you for sharing your ideas and suggestions with me. It has been a pleasure and an honour working with you all in the name of scientific research.
- To my dearest gran, Manormanie Naidoo (02/07/1930-10/10/09), your legacy of hard work, endurance and perseverance through tough times will continue to live on in me. I am a stronger woman today because of you.
- To my beloved sister and brother, Sandra and Lionel Padayachee. There is no better friend than a brother or sister and there is no better friend than you both. You cried with me in my hardships, you rejoiced with me my triumphs-I couldn't have done it without you both by my side.
- To my friends who stood by me during the last two years, in particular Pearl Mzobe who was always by my side and supported me down to the last-I couldn't have done it without you.
- The financial assistance from the National Research Foundation (NRF) and Medical Research Council (MRC) toward this research is hereby acknowledged. Opinions expressed and conclusions arrived at, are those of the author and are not necessarily attributed to the NRF or MRC.

"After much thought, my research has lead me to the conclusion that the human brain is the most complicated object in the universe, the more we learn about the brain and the mind, the more magnificent and unknowable it becomes"

# Case Study

***"Often, Mary was afraid, a nameless, shapeless fear. Her impaired mind could not put a name or an explanation to her fear. People came, memories came, and then they slipped away. She could not tell what was reality and what was memory of people past. The bathroom was not where it was yesterday. Dressing became an insurmountable ordeal....Mary gradually lost the ability to make sense out of what her eyes and ears told her....She worried about her things: a chair, and the china that had belonged to her mother. They said they had told her over and over, but she could not remember where her things had gone. Perhaps someone had stolen them. She had lost so much....***

***Mary was glad when her family came to visit. Sometimes she remembered their names; more often she did not. She never remembered that they had come last week, so she regularly scolded them for abandoning her....She was glad when they didn't try to remind her of what she had just said or tell her they had come last week, or ask her if she remembered this person or that one. She liked it best when they just held her and loved her"***

*Adapted from (Rodgers, 2003)*

# I

# Literature Review

## 1.1 Introduction

Alzheimer's disease (AD) is defined as a progressive and fatal neurodegenerative disorder manifested by cognitive and memory deterioration, progressive impairment of activities of daily living, and a variety of neuropsychiatric symptoms and behavioral disturbances (De Meyer *et al.*, 2006). Dr Alois Alzheimer first described the disease in 1906 (Parihar and Hemnani, 2004). One of the most important facts about AD is that even though its victims, often exhibit strange, irrational and emotionally upsetting behavior, the disease in itself is not a psychological or mental illness but rather it is a medically related disease involving neurodegenerative mechanisms in the brain. Moreover it is the symptoms of the disease which are psychologically and psychiatrically based. In view of this, it is necessary to elucidate these AD-related degenerative pathways within the brain in order to provide a medical and scientific based understanding of the disease. This is critical in order to develop an early diagnostic marker for the disease. In addition, AD belongs to a group of diseases called dementias- a term that literally means 'deprived of mind' and is the most common type of dementia which accounts for 60 %-80 % of all dementia cases (Sigel *et al.*, 2006).

## 1.2 Impact of Alzheimer's disease (AD)

Future growth in the public-health impact of AD depends strongly on age distribution, specifically on the growth of the oldest age groups of the population (Cummings, 2003). In view of this fact, AD is set to grow at an alarming rate because the projected growth of citizens over the age of 65 is unprecedented on a global scale (Cummings, 2003). Moreover, the greatest risk factor for AD is advancing age. As individuals age the risk of dementia increases, which increases the probability of AD (Mebane-Sims, 2009). Dementia doubles in frequency every five years after the age of 60. Figure 1.1 graphically indicates the increasing percentage of the population with dementia from the ages 60-85+, doubling every 5 years (Cummings, 2003). The results (Fig. 1.1), however, do not include that smaller percentage of the population of the ages 40-50 who are also affected by AD.

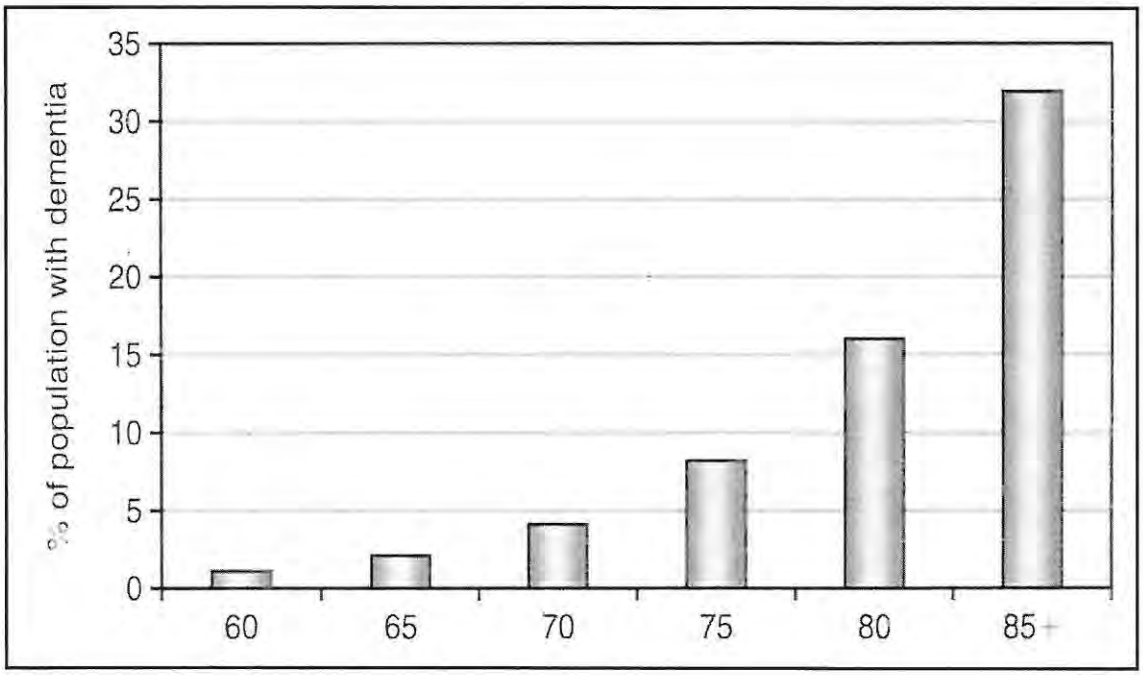


**Figure 1.1 Increasing percent of the population with dementia from age 60-85+ (Cummings, 2003).**

In addition, in the U.S.A alone, AD accounts for over 65 000 deaths per year in individuals over the age of 65 and it is estimated that the number of people older than 65 years will approach 370 million by the year 2050 (Cummings ,2003). In Africa, between

1997 and 2025, the number of individuals over the age of 65 will increase from 17.7 million to 37.9 million. Presently in South Africa, more than 140 000 aged suffer from dementia (Cummings, 2003). It is clear from these statistics that AD has both a national and international impact on society and this adds a heavy social and economic burden on family members and society in general (De Felice *et al.*, 2002). For example, in the U.S.A. alone, the annual direct and indirect economic costs associated with AD are estimated at $80-100 billion (National Institute of Aging, 1998). The socio-economic impact is, however, more drastic for developing countries like South Africa because developing countries have developing economies with limited healthcare budgets and limited health care facilities. Thus, it is essential to question the possible causes of AD.

## 1.3 Genetic causes of AD

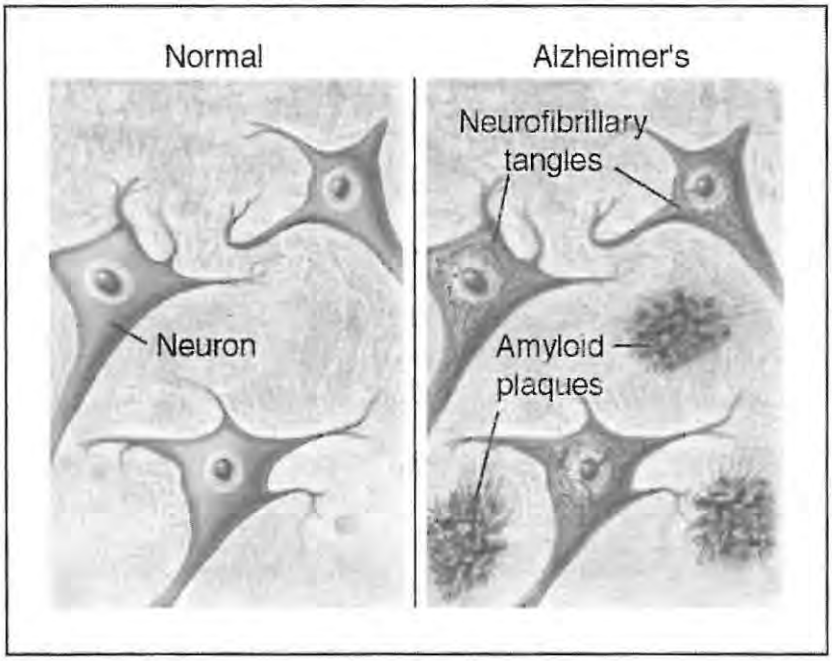


**Figure 1.2 The presence of plaques and tangles in Alzheimers (http://www.ahaf.org).**

Recent advances in molecular genetics of AD indicate that the disease is a complex disorder with mutations in many genes. At most, 5 % of all cases of AD are associated with gene mutations and are classified as familial AD, whereas the majority of AD cases are sporadic; , resulting from a single genetic mutation (Perry *et al.*, 2005). These genetic causes include protein abnormalities in one specific type of protein amongst others;

namely the amyloid precursor protein (APP). Mutations in this protein type create the hallmarks of AD pathogenesis; namely, the formation of amyloid plaques and subsequent formation of neurofibrillary tangles (NFTs) (De Meyer *et al.*, 2006). Differentiation between the brain of a normal patient compared to the brain of an Alzheimer's patient is noted (Fig.1.2).

# 1.4 Mechanisms of amyloid precursor protein (APP) mutation

## 1.4.1 Mutation in amyloid precursor protein (APP)

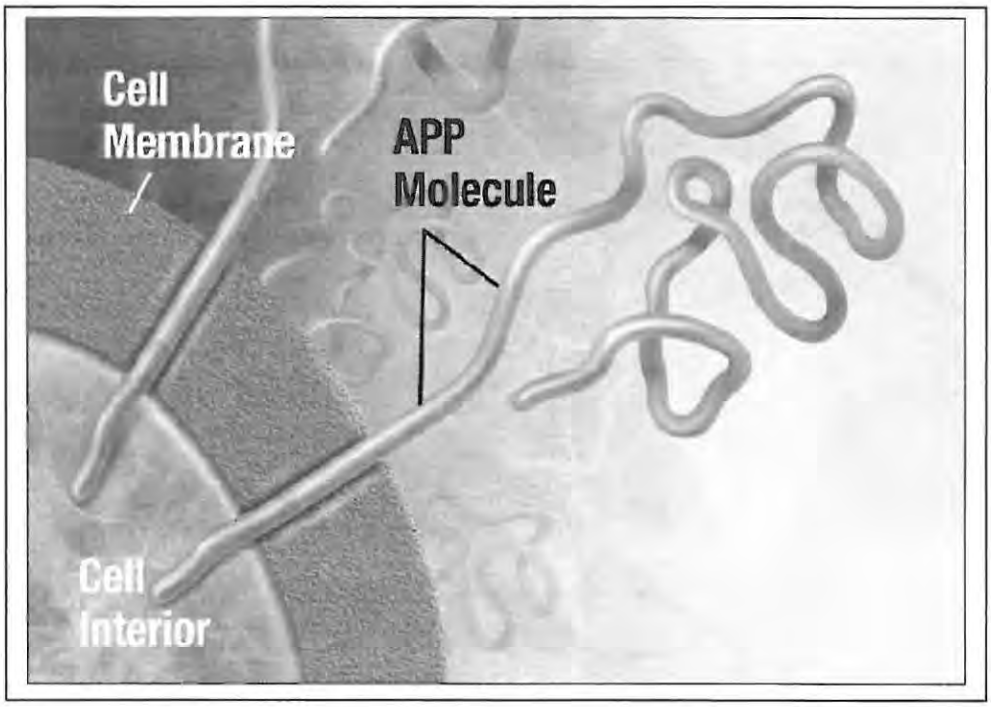


**Figure 1.3 Diagram illustrating the location of APP embedded in the cell membrane (Sigel *et al.*, 2006).**

Since amyloid peptides are generated from APP, it is important to understand the underlying mechanisms involved in both protein mutations. APP is a transmembrane cell surface glycoprotein, encoded by a gene located on chromosome 21. The protein matures in the endoplasmic reticulum and golgi apparatus and exhibit post-translational modifications including phosphorylation, glycosylation and sulphation within these organelles (Parihar and Hemnani, 2004). In addition, the protein has a large hydrophilic

amino terminal extracellular domain, a single hydrophobic putative transmembrane domain and a small carboxy-terminal cytoplasmic domain (Parihar and Hemnani, 2004). Thus, the protein is intracellulary inserted into the cell membrane with part of the protein 'sticking' out from the cell membrane (Fig. 1.3). It is this extracellular part of the protein which is known to be cleaved by secretase enzymes.

Moreover, APP is involved in viability, growth, morphological and functional plasticity of nerve cells and also plays a role in learning or memory processes. Thus a mutation in the protein blocks these processes and leads to eventual neuron death (Parihar and Hemnani, 2004). More significantly, the abnormal processing of the APP triggers the aggregation, deposition and toxicity of beta-amyloid peptides (Aß) via secretase cleavage in a process called amyloidogenesis (Parihar and Hemnani, 2004).

Two secretase enzymes; namely, ß-secretase and γ-secretase are involved in amyloidogenesis. The third secretase namely a-secretase plays a partial role in the process. The precise molecular identity of γ-secretase remains elusive. However, recent evidence suggests that membrane-associated presenilin proteins 1 and 2 (PS 1 and PS 2), which act in association with another protein called nicastrin, may constitute the γ-secretase complex (De Felice *et al.*, 2002). Moreover, ß-secretase (also known as BACE or memapsin) has recently been identified as an aspartic protease (De Felice *et al.*, 2002). The process of Aß production starts when a- and ß-secretase cleave the APP molecule at different positions leading to the release of large soluble N-terminal fragments; namely, a-APPs and ß-APPs, respectively (Fig. 1.4). APP is cleaved by a-secretase at residue 687 to produce a-APPs and the C-terminal fragment C 83. However, cleavage by a-secretase does not contribute to Aß formation. In contrast, ß-secretase cleavage generates the free N-terminus of Aß and is, therefore, considered the first critical step in amyloid formation. The aspartyl protease cleaves at residue 671 to produce ß-APPs and the C-terminal fragment C 99. C 99 is further cleaved by γ –secretase within the APP transmembrane domain to release Aß, which is critical in the pathogenesis and etiology of AD (Fig. 1.4) (Parihar and Hemnani, 2004).

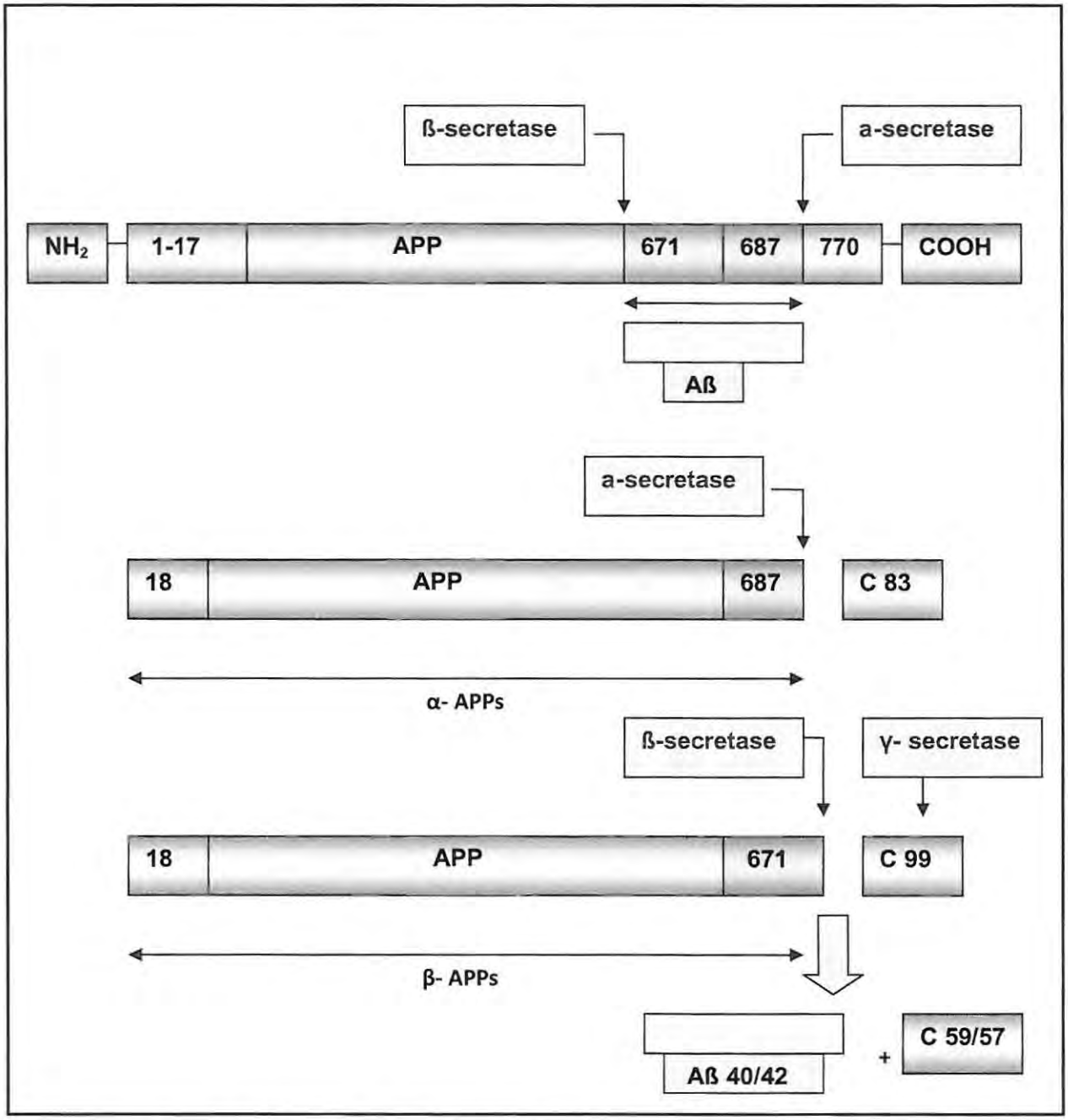


**Figure 1.4 Schematic diagram of processing of amyloid precursor protein (APP) and production of amyloid ß-peptide (Aß) (Parihar and Hemnani, 2004).**

Cleavage of APP may also be regulated by a protein ligand called F-spondin which binds to the central APP domain and inhibits the initial a- and ß-secretase cleavage of APP, thereby regulating cleavage. This may indicate a potential pharmaceutical target to inhibit APP cleavage by synthesizing new molecules which bind to the central APP domain (Sigel *et al.*, 2006). Moreover, the trafficking and processing of APP can also be

regulated by adaptor proteins e.g. members of the Fe65 families which can bind to the cytosolic tail. Fe65 is involved in gene transcription regulation and appears to promote Aß secretion (Sigel *et al.*, 2006). It is clear that the presence of amyloid peptides is crucial in the underlying mechanism of AD. Hence, it is necessary to understand their origin, nature and function within the brain.

## 1.5 Amyloid peptides–their origin, nature and function in the brain

The term 'amyloid' was coined by Virchow on the basis of its histological staining by iodine (Virchow, 1854). The term is derived from amylose or amylon and means 'starchlike'. The general nature of the carbohydrate present in the amyloid was known to be glycosaminoglycans. However it was quickly recognized that the amyloid deposits were constructed largely of protein (Fraser *et al.*, 1993). More recently, the term 'amyloid' generally refers to many types of ß- pleated sheet proteins found in the central nervous system (Mathis *et al.*, 2007). To be more specific, in AD, the term 'amyloid' is equated to beta-amyloid protein (Aß) (Mathis *et al.*, 2007).

Aß protein contains 42 amino acids in its peptide sequence and is associated with lipoprotein particles which make Aß highly hydrophobic such that it is partially inserted into lipids by its hydrophobic C-terminal tail (Kontush, 2001). Under all cell conditions, Aß is produced by neurons and many other cells such as astrocytes, neuroblastoma, hepatoma cells, fibroblasts and platelets. However, neuronal cells are more active than other cells in producing Aß and seem to be the major source of Aß in the brain (Kontush, 2001). It is interesting to note that Aß can exist in three biochemical fractions in the brain namely; membrane-associated, aggregated and soluble.

The fact that Aß is normally present in human cerebrospinal fluid (CSF) and plasma of both healthy subjects and Alzheimer patients suggests that it can behave as a pro-oxidant or an anti-oxidant in the brain, i.e., contribute to toxicity or help lower toxicity. Various mechanisms have being proposed to explain Aß toxicity which induces neuronal cell death. These mechanisms include reactive oxygen species, nitric oxide productions, decreased membrane fluidity and inflammatory processes that contribute to the pro-

oxidant nature of Aß (Parihar and Hemnani, 2004). All of these processes result in oxidative stress which is classically defined as the occurrence of an imbalance between the generation of reactive oxygen species (ROS) and nitrogen species and anti-oxidant defenses and Aß plays a role in triggering such responses (Perry *et al.*, 2005). Moreover, the presence of transition metals such as Cu, Fe, Zn and Al interaction with Aß is also known to generate ROS and mediates toxicity of Aß (Perry *et al.*, 2005).

On the other hand, it is surprising that an unexpected increase in Aß deposition is associated with decreased oxidative damage. This fact is in agreement with two recent findings on the distribution of oxidative damage to diseased neurons. A major product of nucleic acid oxidation called 8-hydroxyguanosine (8 HG) markedly accumulates in the cytoplasm of cerebral neurons in AD. Unexpectedly, an increase in Aß deposition in the AD cortex was associated with a decrease in neuronal level of 8 HG; namely, decreased oxidative damage (Nunomura *et al.*, 1999). A similar negative correlation between Aß deposition and oxidative damage was found in patients with Down syndrome (Nunomura *et al.*, 2000). It was also suggested that an increased synthesis of APP and Aß is an attempt by brain cells to detoxify elevated levels of redox active metals such as Cu and Fe (Fraser *et al.*, 1993).

Thus, the protective role afforded by Aß in the initial stages of AD should not be underestimated (Perry *et al.*, 2005). This is interesting since the complete removal of this form of peptide from the nervous system may upset homeostatic balance within the nervous system. Thus, it may be necessary to find ways to regulate Aß production rather than totally eliminating the peptide from the nervous system. It is thus clear that the mechanistic basis of AD is associated with APP and amyloid peptides. Such mechanistic understanding of the nature of AD is vital so as to find a way of detecting the disease in its early stages. This is significant as the only form of diagnosis is postmortem. Nevertheless, considerable research has recently been undertaken into drug design and development in the hope of managing the symptomatic nature of AD.

# 1.6 Drug development

No treatment has up till now (2010) been clinically proven to modify the disease process in a way that significantly slows or prevents the progression of AD (De Meyer *et al.*, 2006). However, there are several different pharmacological agents that may temporarily suppress certain debilitating symptoms as well as possible agents that may target the underlying cause of AD. There exist typical treatment modes, among others, that may be applied to the treatment of AD and the prevention of excessive amyloid production in the brain. Such treatment strategies are summarized below (Figure 1.5).

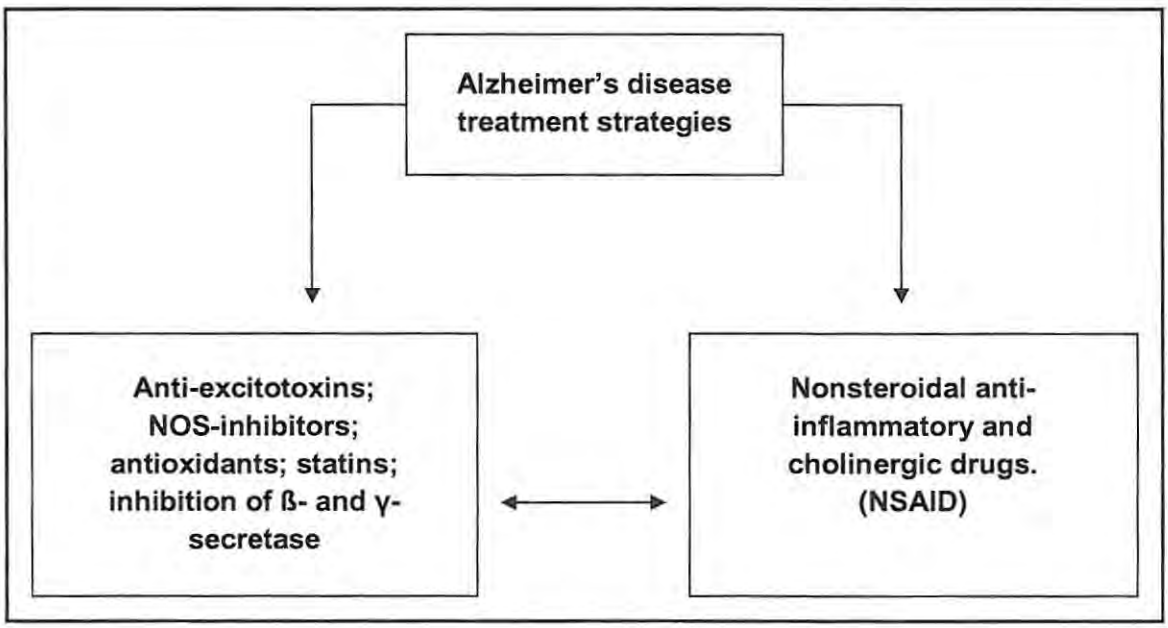


**Figure 1.5 A few Alzheimer drug treatment strategies (Citron, 2002).**

## 1.6.1 Cholinergic drugs and non-steroidal anti-inflammatory drugs (NSAIDs)

Cholinergic drugs include cholinesterase inhibitors (ChE-Is) and acetylcholinesterase inhibitors such as donepezil, galantamine and rivastigmine (De Meyer *et al.*, 2006). ChE-Is improve cholinergic function in AD by inhibiting the destruction of intrasynaptic acetylcholine by acetylcholinesterase. This increases the synaptic residence time of acetylcholine and increases the likelihood of a signal in the postsynaptic cholinergic

neuron (Cummings, 2003). In addition, NSAIDs down regulate pro-inflammatory signals as well as the autoimmune response from microglia cells which produces free radicals within amyloid plaques (Parihar and Hemnani, 2004). Excessive free radical generation poses the risk of oxidative stress. Hence, epidemiological studies suggest that NSAIDs, e.g., aspirin, may provide some degree of protection from oxidative stress. However, the results from the drug remain inconsistent and NSAIDs carry the risk of cardiovascular disease (Citron, 2002).

### 1.6.2 Antioxidants

Owing to the beneficial effects of the a-tocopherol and ascorbic acid in reducing free radical load in the hippocampus and cortex, a considerable interest in the use of these vitamins for the treatment of AD has been made. Both a-tocopherol and ascorbic acid have been shown to slow the progression of the disease and reduce the risk of AD (Cummings, 2003).

### 1.6.3 Anti-excitotoxins

Glutamate is the principle excitatory neurotransmitter in cortical and hippocampal neurons. Glutamate is oxidized in the brains of AD patients, leading to excess glutamate. Excessive activation of NMDA (*N*-methyl-D-aspartate) receptors by glutamate increases the vulnerability of CNS neurons leading to neuronal degeneration. An anti-excitotoxin called memantine blocks glutamate gated NMDA channels, thereby slowing down neuronal death (Castellani *et al.*, 2008).

### 1.6.4 Statins

Finally, there is renewed hope that statin treatment might prevent AD, or at least slow its development before more direct amyloid therapy becomes available. An example of a statin called simvastatin is known to have a protective effect against dementia (Castellani *et al.*, 2008). Statins are inhibitors of the cholesterol-synthesizing enzyme HMG-CoA-reductase which has a proposed effect on Aß production (Citron, 2002). Three case control studies found that in elderly patients with hypercholesterolemia the risk of developing dementia was reduced 60-70 % when they were treated with a statin (De

Meyer *et al.*, 2006). However, although statins may slow the progression of the neurodegenerative process, they not be able to reverse neuronal degeneration once it has occurred (Castellani *et al.*, 2008).

Another relatively new strategy in preventing Alzheimer's is the potential of nitric oxide synthase (NOS) enzyme inhibitors and the blocking of a- and ß secretase pathways (Fig.1.5). Thus, it is essential to study the nature of the synthase enzyme and its relation to AD and the potential inhibitors of the enzyme in the field of AD.

# 1.7 Nitric oxide synthases (NOSs)

Nitric oxide synthases (NOSs) are a class of enzymes found in mammals and other species that utilize L-arginine to generate nitric oxide (NO), an important signaling molecule in the brain (Poulos *et al.*, 2002). Like many enzymes, the nitric oxide synthases (NOSs) have being designed to function as active dimers comprised of identical subunits. There are three isoforms of NOS; namely, neuronal NOS (nNOS); endothelial NOS (eNOS) and inducible NOS (iNOS) (Zhang and Snyder., 1995).

## 1.7.1 Neuronal NOS (nNOS)

nNOS was the first nitric oxide synthase to be identified and was found in neuronal tissue in both the central and peripheral nervous system and is also known as NOS1. Neuronal NOS also performs a role in cell communication and is associated with plasma membranes. The enzyme is a 150 kDa protein (Zhang and Snyder, 1995) and its quaternary structure is indicated (Fig.1.6).

## 1.7.2 Inducible NOS (iNOS)

iNOS can be found in the immune system but is also found in the cardiovascular system. Originally isolated from murine macrophages, iNOS is expressed in cells upon immunologic or inflammatory stimulus. The enzyme is a 130 kDa protein and is cytosolic (Zhang and Snyder, 1995).

### 1.7.3 Endothelial NOS (eNOS)

Endothelial NOS was the third isoform to be identified. Endothelial NOS generates NO in blood vessels and is involved with regulating vascular functions. The enzyme is has a size of 135 kDa and it is the only isoform that is membrane bound (Zhang and Snyder, 1995).


**Figure 1.6 Ribbon structure of homodimeric nNOS illustrating active site (A). Image was generated using Rasmol (Raswin molecular graphics [V 2.7.2.1](Sayle and Bernstein,1998-2001) (PDB: 1zvi).**

## 1.8 Properties of nNOS

### 1.8.1 Structure of neuronal NOS (nNOS)

nNOS consists of two parts-an oxygenase domain and a reductase domain aligned in a head to head manner (Fig. 1.7) with a short calmodulin (CaM) linker. The N-terminal oxygenase domain contains binding sites for L-arginine (ARG); tetrahydro-L-biopterin

dichloride ($H_4B$) and heme (Fe). The C-terminal domain of the enzyme represents the reductase domain which binds the flavin co-factors, FMN and FAD and NADPH; a calmodulin–binding sequence (CaM) is present between FMN and FAD (Fig. 1.7). Active NOS may assemble in two sequential post-translational steps that each involves a separate domain of the enzyme. The protein first acquires a functional reductase domain by binding FAD or FMN and CaM (Stuehr, 1997). This generates a folded NOS monomer that is capable of catalyzing electron transfer from NADPH but is inactive regarding NO synthesis. The monomers then assemble into a dimer in a reaction that requires sufficient heme to be present and may be promoted by the presence of L-arginine and tetrahydro-L-biopterin dichloride to activate NO synthesis (Stuehr, 1997).

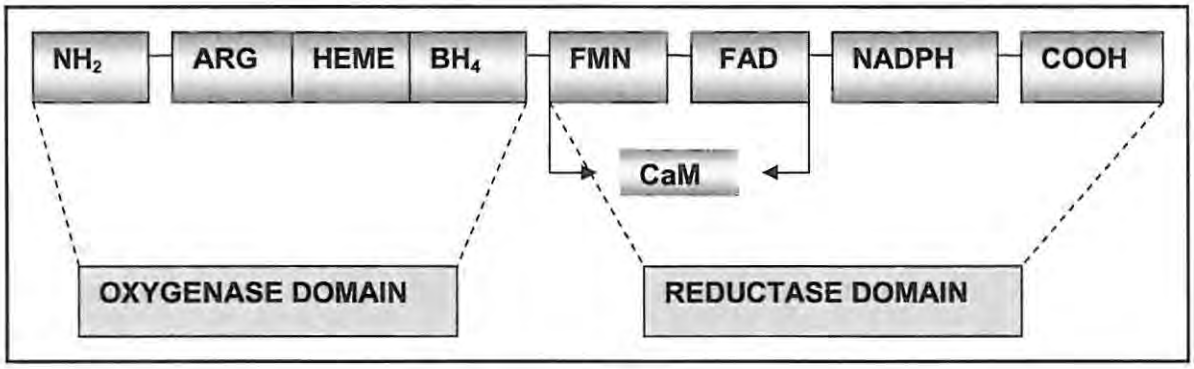


**Figure 1.7 Domain structure of human nNOS, depicting two parts: oxygenase and reductase domain (Stuehr, 1997).**

# 1.9 Catalysis of nNOS

Although there will be some isoform-specific differences, the major aspects of catalysis are likely to be quite similar of all isoforms of NOS. This is because all isoforms have the same cofactors and the same co-substrate requirements (Marletta *et al.*, 1998). Hence, the neuronal nitric oxide synthase-catalyzed conversion of L-arginine to L-citrulline and nitric oxide is known to be the sum of two partial reactions namely; oxygenation of arginine to *N*-hydroxyarginine, followed by oxygenation of *N*-hydroxyarginine to citrulline and nitric oxide (Campos *et al.*, 1995).

The first step in the reaction is the *N*-hydroxylation of L-arginine, yielding $N^G$-hydroxy – L-arginine (L-NHA) as an intermediate. L-NHA is further oxidized to L-citrulline and

NO in an NADPH–and $O_2$-dependent step (Fig. 1.8) (Marletta *et al.*, 1998). It is L-NHA which functions effectively as a substrate for nNOS and requires not only a guanidinium moiety but also an amino acid head group for catalysis to occur (Fig. 1.8) (Poulos *et al.*, 2002). Moreover, NO synthesis requires a sequential transfer of three electrons between the reductase and oxygenase domains to convert L-arginine to citrulline and NO. The nitrogen of NO is derived from the guanidino nitrogen atoms of L-arginine while the oxygen is derived from molecular oxygen ($O_2$) (Bruckdorfer, 2005). A schematic diagram (Fig. 1.9) describes the electron shuttling between the reductase and oxygenase domain of nNOS.

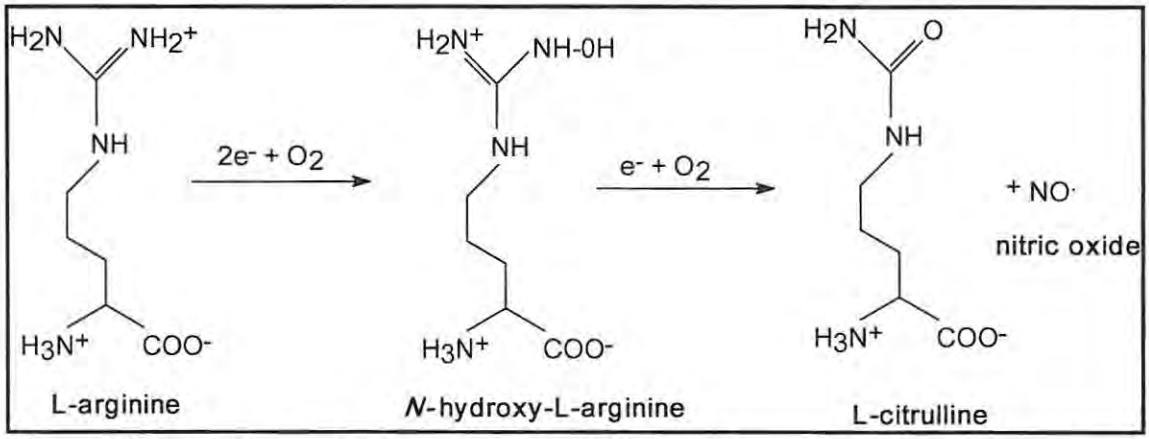


**Figure 1.8 Catalytic mechanism of neuronal nitric oxide synthase.**

The reductase domain converts NADPH into $NADP^+$ and feeds electrons via FAD or FMN (either one of the flavin cofactors are necessary for catalysis) to an iron protoporphyrin IX (Fe site) in the oxygenase domain (Fig. 1.9). The heme (Fe) center and $BH_4$ in the oxygenase domain converts arginine and oxygen into citrulline and NO. It must be noted that electron flow through the reductase domain requires the presence of bound calcium ion or calmodulin ($Ca^{2+}$/CaM) (Knowles *et al.*, 2001).

Moreover, the nNOS isoform contains a 250-amino acid N-terminal leader sequence not present in the other two NOS isoforms. The leader sequence is not required for dimerization, prosthetic group binding, or catalysis of NO synthesis, but it is involved in binding proteins that target nNOS to discrete regions in the cell. In addition, the presence of a PDZ domain also sets nNOS apart form other isoforms (Marletta *et al.*, 1998). The

PDZ domain (named for domains within 3 proteins: PSD95, Dh/G and ZO-1/ ZO-2) targets the enzyme to sites in the nerve synapses (Bruckdorfer, 2005).

Since nNOS catalyzes the substrate arginine (an amino acid associated with AD) it can serve to regulate levels of arginine and subsequently citrulline levels in the brain. This indicates the potential of the enzyme to behave as a biomarker for AD relative to substrate concentration levels in the brain of an AD patient.

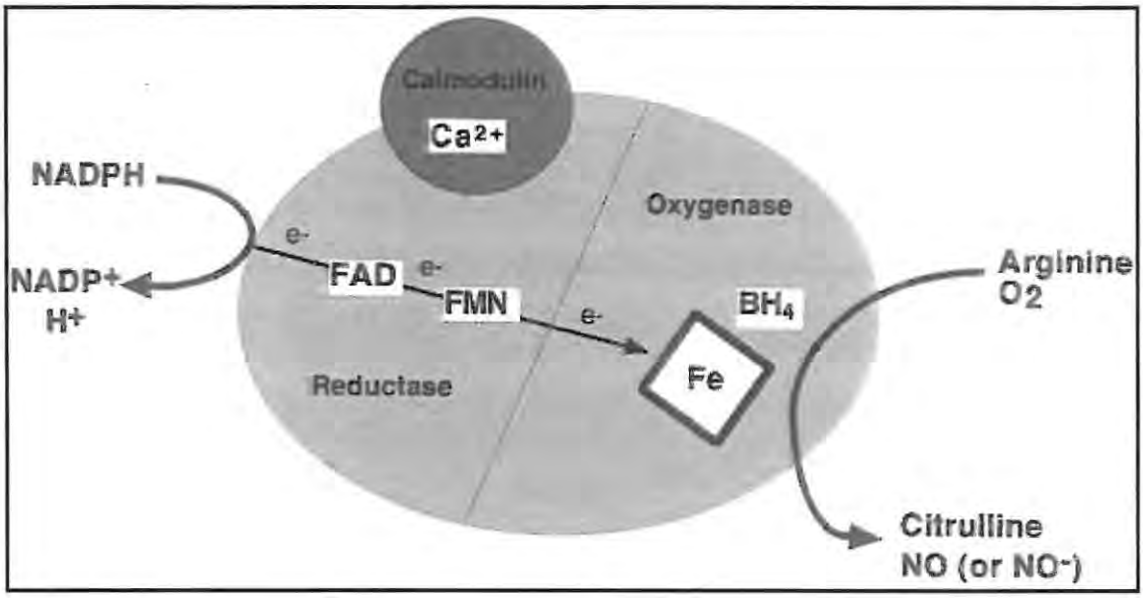


**Figure 1.9 Overall reaction catalyzed and cofactors of NOS (Knowles *et al*, 2001).**

# 1.10 Biomarkers

## 1.10.1 Introduction

Biomarkers are the key to advancing our understanding of the pathophysiology of AD, which in turn has important implications for patient diagnosis and treatment. However, biomarkers are instrumental not only in the diagnosis of AD, but also aids in following disease progression and response to treatment. Nevertheless, given the multifactorial nature of AD, it is unlikely that a single biomarker will meet the needs for clinical diagnosis. On the other hand, a panel of biomarkers may offer the appropriate sensitivity and specificity for the disease (Craig-Schapiro *et al.*, 2009). However, this limitation not withstanding, the identification of enzyme biomarkers and their concentration levels

related to their consequent substrate concentration level requirements is important in the effective biomarker design. An interesting biomarker could be the neuronal nitric oxide synthase (nNOS) which mechanistically influences Aß production and clearance in the brain and may be hypothesized as being a catalyst for fibril formation from Aß.

### 1.10.2 Neuronal nitric oxide synthase (nNOS) and its role as a potential biomarker in AD

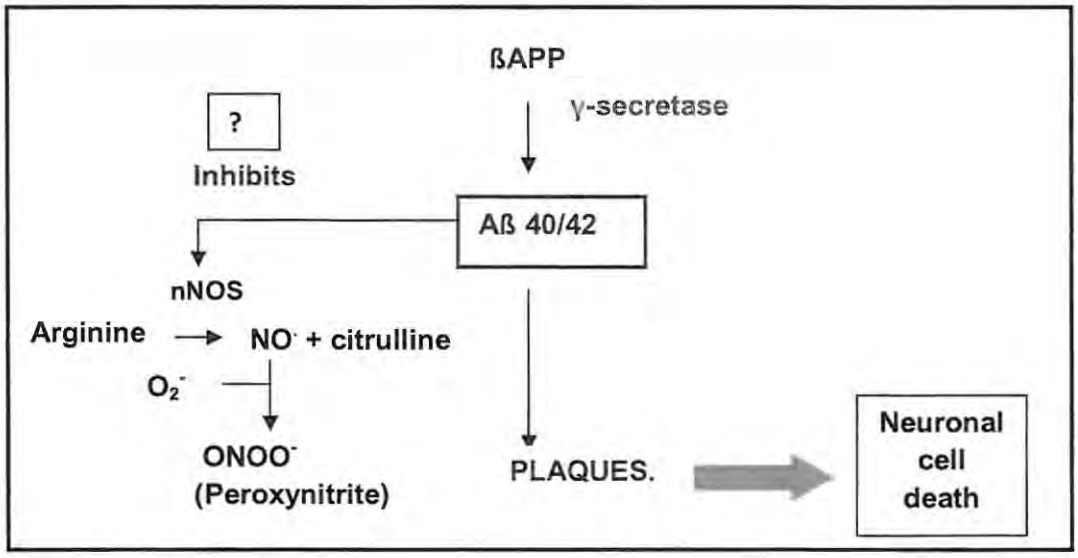


**Figure 1.10 Schematic diagram describing the role of nNOS in the amyloidogenic pathway.**

The understanding of nNOS as an enzymatic biomarker for AD is made clearer by understanding its role in the amyloidogenic pathway, considering its substrate requirements and its end metabolic products and their effect on the amyloidogenesis pathway which forms amyloid peptides. The schematic diagram (Fig. 1.10) illustrates the amyloidogenic pathway incorporating the catalysis of nNOS and its subsequent effect on the pathway.

As illustrated (Fig. 1.10), the question is; Does Aß 40/42 or Aß peptides in general inhibit nNOS? This is significant because elevated levels of arginine are found in the cerebrospinal fluid of Alzheimer patients and nNOS is an enzyme crucial in the metabolism of arginine to citrulline and nitric oxide (NO). The fact that there is a low

level of citrulline and a high level of arginine in the cerebrospinal fluid of AD patients could mean that there is a decrease in the enzyme that metabolizes this amino acid i.e., nNOS and thus reflects the possible use of nNOS as a biomarker in AD. On the other hand, when arginine levels are low and nNOS catalytic activity is high, there is excess production of NO and formation of superoxide radicals which generate reactive oxygen species (ROS) and peroxynitrite ($ONOO^-$) which are far more neurotoxic than NO (Fig. 1.10).

## 1.11 Potential inhibitors of the amyloidogenic pathway and of neuronal nitric oxide synthase (nNOS)

It is clear that there is a great need in the medical community for the ability to control and regulate the neuronal isoform of NOS, in particular, since it is this isoform that is related to AD due to its location in the brain and that it metabolizes the substrate arginine. Thus, research has been expanded to discover inhibitors and regulators of nNOS activity as it is important to find mechanistic ways to inhibit this enzyme and prevent the production of excess nitric oxide. At the same time, it is also important to regulate arginine supply within the brain and thus prevent plaque formation that ultimately leads to neuron death. The potential of blocking secretase pathways and inhibiting nNOS by chemical analogues and Aß and amino acid derivatives will now be discussed.

### 1.11.1 Inhibition of ß- and γ- secretase

Blocking the proteolytic machinery that produces Aß is a suggested strategy. This could be accomplished by either reducing the formation of APP or by inhibiting proteolysis of APP to Aß. Inhibition of ß- and γ- secretase and stimulation of a-secretase activity is suggested to be the most promising strategy for neuroprotection (Cummings, 2003). However, the generation of secretase specific protease inhibitors that penetrate the blood brain barrier is a challenge for drug discoveries. Also, the drug that blocks the function of γ- secretase might not be effective in patients developing AD due to factors other than Aß accumulation. Therefore, agents that prevent the initial stages of Aß formation (Aß nucleation) could be more effective than those that merely block the final stages (Aß

deposition) (Cummings, 2003). Certain inhibitors of γ-secretase that show a decrease in Aß production include gelatinase A, bafilomicin A, calpain inhibitor, brefeldin and $NH_4Cl$ (De Felice *et al.*, 2002). Moreover, recent studies have examined the protease inhibitor MG132 and calcium ionofore A23187 as potential inhibitors of ß-secretase. However, it is important to note that in humans ß-secretase can participate in the processing of other physiological substrates in addition to APP, and may be involved in important biological functions that could be affected by the use of inhibitors (De Felice *et al.*, 2002).

### 1.11.2 Inhibition by chemical analogues

To date, many compounds have been shown to inhibit nNOS, including mono-or di-substituted arginines, guanidines, isothioureas, amidines, thiazines, benzoxazoles, pyridines, pteridines, indazoles and imidazoles (Giacomo *et al.*, 2003). As previously mentioned, nNOS catalysis requires various cofactors including NADPH, FAD, FMN and $BH_4$. However it is the cofactor, $BH_4$ which markedly stimulates nNOS catalytic activity through enzyme stabilization (Giacomo *et al.*, 2003). In view of these considerations, the $BH_4$ site of nNOS may represent an ideal target for selective inhibitors of the enzyme. Since the imidazole nucleus possesses a pharmacophore role in nNOS inhibitory activity, research has shown that a particular form of the imidazole namely, the 1-[Aryloxy) alkyl]-1*H*-imidazole is a potential inhibitor of the enzyme (Giacomo *et al.*, 2003). This finding opens up ways for further modifications of imidazole analogues aimed at improving selective inhibition.

In addition, a certain amide compound (BN 80933 [(*S*)-*N*-{4[4-[3, 4-dihydro-6-hydroxy-2, 5,7,8-tetramethyl-2*H*-1-benzopyran-2-yl)carbonyl]-1-piperazinyl]phenyl}-2-thiophene carboximidamide]) was also found to display neuroprotective properties (Chabrier *et al.*, 1999) It displayed better efficacy as a dual inhibitor whereby its antioxidant moiety was linked to the nNOS inhibitor pharmacophore, thiopheneamidine. Other amine inhibitors include kynurenamine derivatives which also have shown significant nNOS inhibitory potential (Espinosa *et al.*, 2005).

Moreover, another group of inhibitors are arginine analogues. These include natural or synthetic arginine-rich peptides, oligopeptides or protein antagonists. For example, nNOS action can be inhibited by NPA (*N*-propyl-L-arginine) and 7-nitroindazole (Wiesinger, 2001). Potential analogue arginine inhibitors are agmatine, asymmetric $N^G$, $N^G$ – dimethyl-L-arginine (ADMA) and $N^G$-monomethyl-L-arginine (NMMA) which inhibits nNOS activity. Studies have further shown that L-arginine-containing dipeptides are also excellent substrates for nNOS. L-homoarginine and an L-arginine-containing dipeptide called L-arginine-L-aspartate are able to replace L-arginine as a substrate for the biosynthesis of NO. Thus, it seems that the active site of nNOS seems to be flexible enough to accommodate molecules different from L-arginine in size, charge and hydrophobicity. This should be considered when designing more selective inhibitors of nNOS (Wiesinger, 2001).

### 1.11.3 Beta-Amyloid peptides as inhibitors of nNOS

Recently the use of some amino acid derivatives in the selective inhibition of nNOS has being proposed (Giacomo *et al.*, 2003). Thus, since amyloid peptides are in effect composed of a specific 1-42 amino acid stretch and are surrounded by astrocytes, which also function to store reserve arginine in brain tissue which is eventually metabolized by nNOS, it would be interesting to investigate if the Aß 42 stretch inhibits nNOS such that levels of arginine in the brain can be regulated. In addition, the entire amyloidogenic pathway occurs within a neuron in the brain and this indicates a potential connection between brain arginine content, nNOS and amyloid peptide formation *in vivo*. Thus the close proximity of the amyloid peptide to nNOS also makes it a good starting point at attempting to selectively inhibit nNOS. To date, research into amyloid peptide inhibition has been limited. Thus, this fact opens up a novel research approach into the field of designing novel inhibitors of nNOS. Also, such research is significant because present research hypothesizes nNOS to be a catalyst for the formation of fibrils when amyloid peptides aggregate. The inhibition of nNOS by amyloid peptides will thereby prevent the fibrillogenesis of amyloid peptides thereby suppressing fibrilization-dependant neurotoxicity and thus slowing Alzheimer disease progression.

## 1.12 Research hypothesis

Beta-amyloid peptides (Aß) inhibit neuronal nitric oxide synthase (nNOS) and nNOS is a catalyst for fibrillogenesis by beta-amyloid peptides.

## 1.13 Research objectives

- Purifying and biochemically characterizing nNOS from bovine brain.
- Determining whether $Aß_{1-40}$, $Aß_{22-35}$, $Aß_{17-28}$, $Aß_{32-35}$ and $Aß_{25-35}$ inhibit nNOS and attempting to understand the mechanism of binding and inhibition.
- To study the formation and process of amyloid fibril formation. To understand conformational changes in nNOS during Aß binding.. To attempt computerized modeling in order to predict the suggested orientation and nature of Aß binding to the enzyme active site.
- The approach used to achieve the above objectives will be in the form of research techniques specifically applied to study the interaction between nNOS and Aß; namely:

- Congo red assay
- Turbidity assay
- Thioflavin-T assay
- Transmission electron microscopy (TEM)
- Quenching, fluorescence resonance energy transfer (FRET) and computational molecular modeling

# II

# Isolation, purification and characterization of neuronal Nitric oxide synthase (nNOS)

## 2.1 Introduction

The enzyme, nNOS, catalyses the oxidation of L-arginine to form L-citrulline and nitric oxide. Based on this catalytic mechanism and the enzymes dependence on levels of arginine in the brain, nNOS maybe an effective diagnostic marker in the onset of AD (Packer, 1994). However, before an enzyme can be applied to any biological application that could label it as a potential biomarker, it is imperative to purify and characterize it in terms of its kinetic properties. Enzyme assays are indispensable tools to determine the amount (concentration) of enzyme present after purification and to gain insight into the kinetic characteristics of the enzyme (Reymond and Sicard, 2006). Numerous assays have been used to quantify the enzymatic reaction of nNOS (Packer, 1994). In this chapter, three assays will be evaluated in quantifying nNOS activity.

1. The citrulline assay/ L-arginine conversion assay.
2. The oxyhemoglobin assay.
3. The fluorimetric assay.

Despite the numerous previous reports on the successful purification and characterization of nNOS from rat cerebella (Hiki *et al.*, 1992; Riveros-Moreno *et al.*, 1995; Zweier and Giraldez, 1998), it was imperative to conduct similar purification and characterization

steps in order to monitor the degree of purity and establish the appropriate kinetic parameters for enzyme efficiency. Bovine brain was used as a model for research into AD due to the relationship between prion proteins and amyloid peptides and their similar mechanistic approach in relation to nNOS (Kajava *et al.*, 2006). This chapter now focuses on the development of a suitable assay for nNOS as well as its isolation, purification and characterization.

# 2.2 Theory of techniques utilized

## 2.2.1 Citrulline assay

The citrulline assay, developed by Snyder and Bredt, (1990) is a chromogenic, discontinuous assay which relies on colour visibility of the citrulline product and termination of the reaction using a strong acid. The enzyme substrate, arginine, is added to the enzyme extract, incubated for several minutes, and then the reaction stopped by the addition of an EDTA-containing buffer which chelates the calcium ions required by nNOS and consequently inactivates the enzyme. The assay monitors the conversion of arginine to citrulline (Fig. 1.8; pg 14) as this conversion is stoichiometric with the enzymatic formation of NO. The citrulline assay requires equimolar amounts of NADPH and $O_2$ as well as flavin-adenine dinucleotide (FAD) or flavin mononucleotide (FMN), protoporphyrin IX heme iron (heme) and (*6R*)-tetrahydro-L-biopterin ($BH_4$); also $Ca^{2+}$/calmodulin are essential for the assay.

## 2.2.2 Oxyhemoglobin assay

The oxyhemoglobin assay measures the reaction of nitric oxide with oxyhemoglobin to yield nitrate and methemoglobin (extinction coefficient = 60 000 $M^{-1}$ $cm^{-1}$ at 401 nm) (Scheme 2.1) (Feelisch *et al.*, 1997). nNOS activity is quantified against methHb (methemoglobin) production as the reduction of oxyHb (oxyhemoglobin) which is stoichiometric with NO and occurs at a rate faster than the reaction between molecular oxygen and NO.

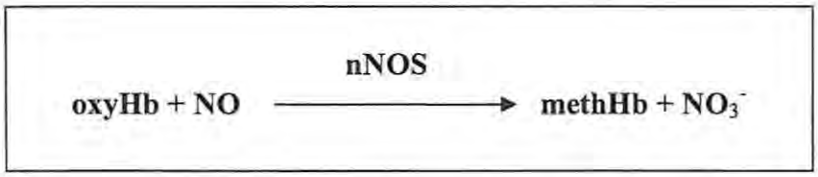


**Scheme 2.1 Schematic representation of nNOS catalysis using the oxyhemoglobin assay.**

A significant problem within this assay is an irreproducible extinction coefficient for the absorbance change at 401nm, because oxyHb has a considerable absorbance at 401nm which makes this method sensitive. In addition, concentrations of $BH_4$ (tetrahydro-L-biopterin dichloride) greater than 12 μM, cause a considerable amount of interference. Hence, even a small change in concentration of $BH_4$ can affect the assay. In addition, activity measurements can also be complicated by the occurrence of uncoupled NADPH oxidation, the products of which may include superoxide anion and/or peroxide (Packer, 1994). Nevertheless, this assay is well-suited to following activity during purification and kinetic studies of nNOS.

### 2.2.3 Fluorimetric assay

The fluorescent system utilizes a cell-permeable 4.5-diaminofluorescein diacetate (DAF-2 DA) fluorescent compound. DAF-2 DA penetrates cells rapidly, where it is hydrolyzed by intracellular esterase activity to 4,5-diaminofluorescein (DAF-2) that, in turn, reacts with NO produced by nNOS to form a fluorescent triazolofluorescein (DAF- 2T) (Fig. 2.1). The concentration of triazolofluorescein (DAF-2T) and hence NO can be measured using an excitation wavelength of 450- 495 nm and an emission wavelength of 505-550 nm. Under biological conditions, the triazole (DAF-2T) is formed from oxidative nitrosylation (Grisham and Bryan, 2007) of the intermediate DAF-2 by $NO_2$ via a one electron transfer. In this state, it can first oxidize the diamino complex to an aromatic radical which then undergoes radical-coupling to form the nitrosamine which subsequently rearranges to the fluorescent triazole (DAF-2T) (Fig. 2.1).

The advantage of diaminofluorescein (DAF-2) is that the wavelength associated with fluorescein can be used, making equipment currently used for other bioassays easily adapted to detect NO *in vitro* and *in vivo* (Grisham and Bryan, 2007). The auto-fluorescence of DAF-2, however, limits the accuracy of this method. Thus, the DAF-2 concentration should be limited in order to minimize DAF-2 auto-fluorescence (Dirsch *et*

*al.*, 2003). In addition, the method is prone to errors by redox-active compounds and reaction reagents that may react with DAF-2 and cause spectral changes that may be interpreted as NO or nNOS signals (Grisham and Bryan, 2007). Lastly, it is important to work in a dark room when handling DAF-2 and DAF-2T samples as there can be a decrease in fluorescence of samples even if exposed to light for a few minutes (Dirsch *et al.*, 2003). These problems can limit the potential of the assay to achieve maximal nNOS activity. However, the method is an alternative approach to measuring the activity of nNOS.

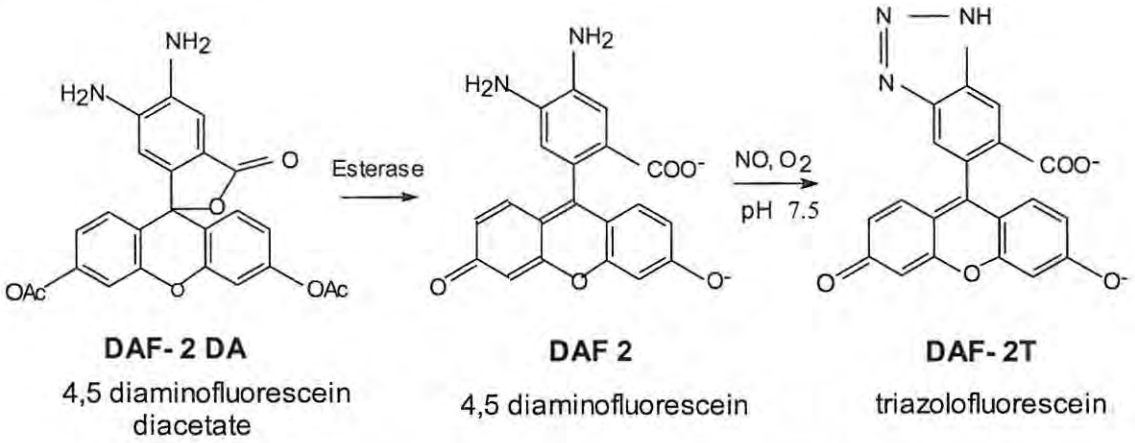


**Figure 2.1 Schematic representation of nNOS catalysis using the fluorimetric assay.**

## 2.2.4 The Bradford assay for protein

The assay is based on the immediate absorbance shift from 470 nm to 595 nm that occurs when the sulphonic acid groups of the dye, Coomassie Brilliant blue binds to the protein in acidic solution. The mechanism of dye binding can be explained by the dye existing as three absorbing species, a red cationic species $A_{470}$; a green neutral species at $A_{650}$ and a blue anionic species at $A_{595}$. Colour changes are due to successive loss of charge. Prior to protein binding, the dye molecules exist in a doubly protonated (red cationic dye form) and then upon binding of the dye to the protein, the blue anionic dye form is stabilized and detected at 595 nm. The advantage is that the colour development is rapid and the assay can be performed in 10 mins. However, interfering substances like strong bases can form a complex with the dye and hence an absorbance shift can occur above the equilibrium (Hafiz, 2005).

### 2.2.5 Poly (ethylene) glycol precipitation

Poly (ethylene) glycol (PEG) is a water-soluble, inert polymer of cross-linked dextrins that is used for fractional precipitation of proteins and other macromolecules. When mixed with protein samples, PEG increases the viscosity of the solution and reduces the solubility of proteins, thus precipitating the protein according to size (Plourde *et al.*, 1991). PEG is not influenced by the buffer conditions of the sample and unlike other organic precipitating agents like acetone or ethanol, it has little tendency to denature or otherwise interact with proteins, even at high concentrations and increased temperatures (Deutscher, 1990). Another advantage of using PEG is that it is more rapid to achieve protein equilibration than precipitation with acetone or ammonium sulphate (Deutscher, 1990). The choice of PEG concentration to use is usually determined by means of an analytical precipitation curve. The protein samples are mixed with buffered solutions containing 5-40 % (w/v) PEG and incubated at optimal temperature for 30-60 mins (Thrash *et al.*, 1991). The samples are centrifuged and the remaining protein in the supernatant is assayed. This provides an estimate of the maximum concentration of PEG that can be added without losing the protein of interest, and also the minimum concentration of PEG required to bring the protein out of solution (Deutscher, 1990). PEG is usually removed from the sample by ultrafiltration or in subsequent chromatographic steps. It is, however, worth noting that the performance of the chromatography column may be altered due to the osmotic effects of PEG (Deutscher, 1990).

### 2.2.6 Ammonium sulphate

Ammonium sulphate precipitation (salting out) is a technique used to precipitate proteins from a solution by increasing the ionic strength of the solution. The technique is reliant on the hydrophobic groups on the surface of proteins.. When the proteins are dissolved, water is forced into contact with hydrophobic groups on the proteins surface and in the process becomes ordered around the proteins. Increasing the concentration of salt ions, by the addition of ammonium sulpahte, causes water to be removed from the protein surface, exposing hydrophobic surface area. This causes the hydrophobic groups of the protein to interact leading to protein aggregation and precipitation. The technique is used to fractionate the proteins from

solution since proteins with larger or more hydrophobic portions will aggregate and precipitate before those with smaller or fewer portions of hydrophobic groups (Harris and Angal, 1994). Ammonium sulphate is the ideal salt for the process because (1) at saturation, it is of sufficiently high molarity that it causes the precipitation of most proteins; (2) it does not have a large heat of solution, so that heat generated is easily dissipated; (3) its concentrated solutions prevent or limit bacterial growth and (4) in solution it protects most proteins from denaturation. A limitation in the use of ammonium sulphate for fine fractionation of protein is that, in going from one step to the next as one increases the concentration of the salt, the purification achieved is usually only 2 to 5 times over the previous fraction. One should also note that when used with tissue homogenates and extracts, ammonium sulphate up to a concentration of 25 % saturation often yields the first cut that contains particulate matter such as ribosomes, membrane fragments, large aggregates of protein, and even denatured proteins (Deutscher, 1990).

### 2.2.7 Dialysis

This technique relies on the removal of low molecular weight solutes and buffer exchange. This method is based on the properties of a semi permeable membrane separating the protein solution from the dialysis buffer. It allows for free passage of molecules below a certain molecular weight, the so-called 'molecular weight cutoff, while macromolecules cannot penetrate the pores of the membrane. The process of dialysis is driven by the difference in concentration of the solutes on the two sides of the membrane. As the equilibrium concentration is approached, the diffusion of solutes becomes equal in both directions (Deutscher, 1990).

### 2.2.8 Ion exchange chromatography

Ion exchange chromatography is the most powerful chromatographic technique used for the separation and purification of proteins on the basis of charge (Bonnerjera *et al.*, 1986). The ion exchange technique is most frequently used for its high resolving power, its simplicity and its high capacity for a wide range of biological molecules (Amersham Biosciences, 2007). Similar to other types of liquid chromatography, ion exchange has both stationary (column packing) and mobile phases. It differs from other types of liquid

chromatography in that the stationary phase carries ionizable functional groups, fixed by chemical bonding to the stationary phase (Deutscher, 1990). There are two different types of ion exchange groups namely, the anion exchanger such as DEAE (diethylaminoethyl) and a cation exchanger such as CM (carboxymethyl) (Fig. 2.2).

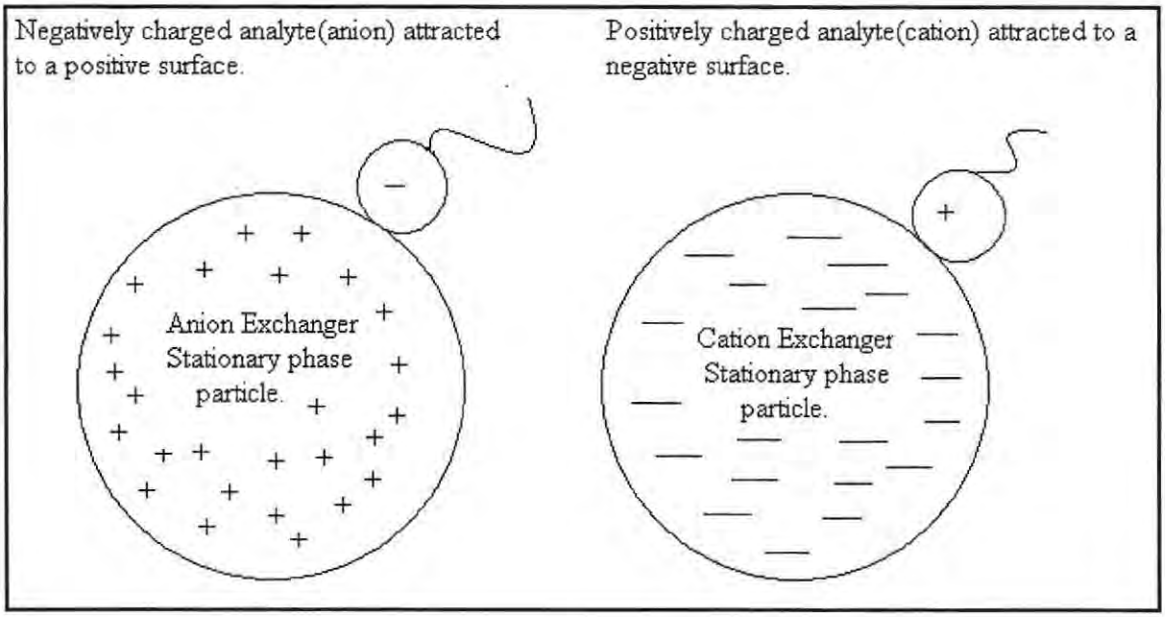


**Figure 2.2 Ion exchanger groups (Adapted from www.waters.com/waters/nav.htm, 2007).**

Anion exchangers contain a positively–charged matrix and therefore bind to negatively charged counter-ions (anions) in the ion exchange column. A cation exchanger is a negatively-charged matrix that binds to positively charged counter-ions (cations). The charges on the matrix are fixed but the counter ions are not fixed and can be displaced. The matrix used for ion exchange comes in various forms based on its characteristics and may include inorganic compounds, polysaccharides and synthetic resins (Amersham Biosciences, 2007). In principle, ion exchange separation occurs in four main steps (Amersham Biosciences, 2007).

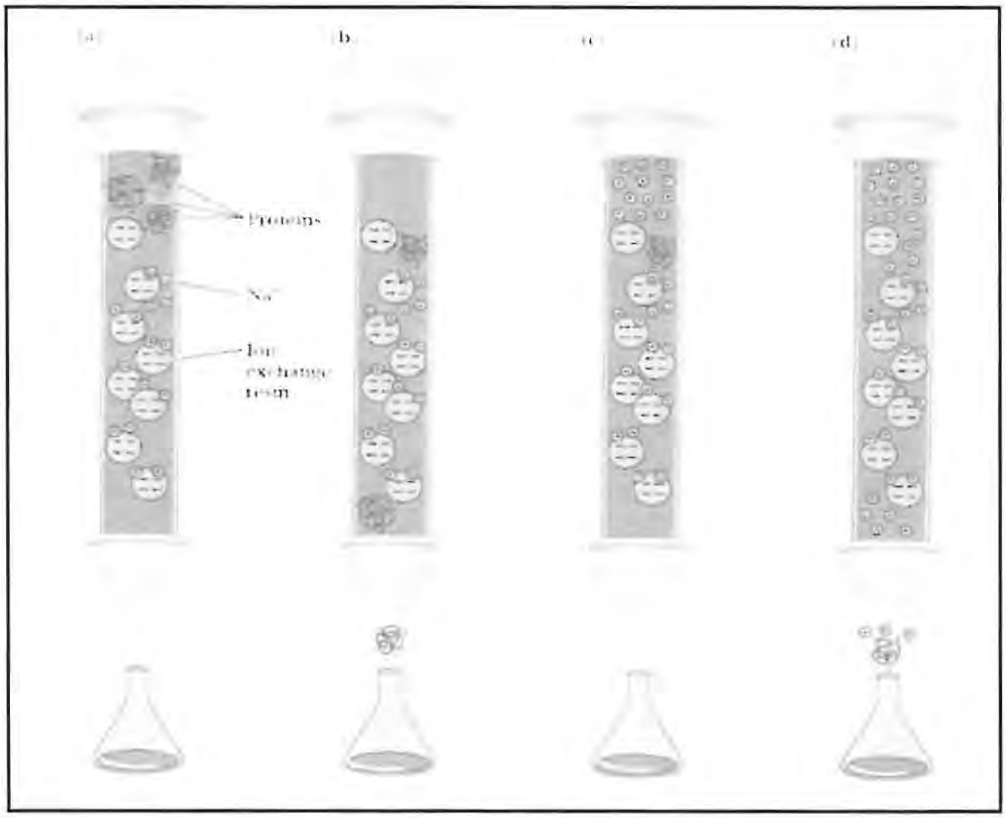

**Figure 2.3 A schematic representation of ion exchange chromatography using a cation exchanger (Source: Grisham and Garrett, 2006).**

Proteins are applied to the column Fig. 2.3 (a). In this step, the molecule of interest carrying the appropriate charge replaces the counter-ions and adsorb reversibly to the ion-exchanger matrix. The column resin is bound to $Na^+$ counter ions (small red spheres). Proteins with a net negative charge pass through the column Fig. 2.3 (b). An excess of $Na^+$ ions are added to the column Fig. 2.3 (c). The $Na^+$ ions reversibly out compete the bound proteins for the binding sites and the proteins of interest elute Fig. 2.3 (d).

## 2.2.9 Electrophoresis

Sodium dodecyl sulphate-polyacrylamide gel electrophoresis (SDS-PAGE), under denaturing conditions was used to examine the purity and determine the molecular weight of the enzyme. The electrophoresis technique is based on the migration of charged particles in an electric field (Laemmli, 1970). To enable the estimation of molecular weights, proteins are mixed with an anionic detergent (such as SDS), which binds to the

protein at a constant ratio of 1.4 g to 1 g of protein to form rod-like complexes. The lengths of these complexes vary according to the molecular weights of the individual proteins. The predominant negative charge of the SDS gives all the protein/SDS complexes an overall negative charge, with the same charge to mass ratio.

The addition of a thiol reducing agent (such as 2-mercaptoethanol) to the protein/SDS complex breaks the disulphide bonds when boiled in the presence of excess SDS (Laemmli, 1970). This disruption of disulphide bonds dissociates the individual polypeptide subunits. When a gel system is placed in the appropriate buffer preparation, the introduction of an electric field will allow complexes to migrate according to their molecular weights. The sample buffer usually contains an ionisable tracking dye that allows the run to be monitored. Once the run has reached completion, it is stained with a staining solution like Coomassie brilliant blue for a few hours and washed in an appropriate destaining solution overnight. The proteins are visible as blue bands on a clear background. Solutions containing a mixture of proteins with known molecular masses are run with the unknown samples in order to determine the relative molecular masses of the proteins of interest (Wilson and Walker, 2000).

As a precaution, SDS-PAGE only affords the separation of proteins according to their molecular weights on a preparative scale, and therefore does not allow re-use of proteins due to difficulty of removing SDS and denaturation of proteins. Native (non-denaturing) PAGE has a distinct advantage over SDS-PAGE in that it allows the recovery of biological activity of the proteins being separated (Wilson and Walker, 2000).

## 2.3 Aims

- To purify nNOS from bovine brain, employing methods of poly (ethylene) glycol precipitation, ammonium sulphate precipitation and ion exchange chromatography.
- To compare three enzyme assays; namely, citrulline, oxyhemoglobin and fluorescence.

- Determine the ammonium sulphate concentrations at which nNOS from bovine brain would precipitate, both intra-and extracellularly.
- Determining the molecular weight of nNOS, using the technique of gel electrophoresis.
- Determining kinetic parameters of nNOS and its physiological optimum pH, temperature and thermal stability.

# 2.4 Reagents and materials

## 2.4.1 Reagents

Bovine brain (approximately 370 g) was kindly donated by Rosedale abattoir (Grahamstown, South Africa). Electrophoresis reagents such as acrylamide; bis-acrylamide; bromophenol blue; *N, N, N', N'*- tetramethyl-ethylenediamine (TEMED); ammonium persulphate; ß-mercaptoethanol; Coomassie Blue commercial stain and enzyme assay reagents such as $N^a$- benzoyl-L-arginine ethyl ester hydrochloride (BAEE); DL-citrulline; calcium chloride; 4,5–diaminofluorescein diacetate; tetrahydro-L-biopterin dichloride; ß-nicotinamide adenine dinucleotide phosphate reduced tetrasodium salt; hemoglobin $A_0$ (ferrous stabilized, human); thiosemicarbazide; 2,3 butanedione monoxime; ammonium sulphate; poly (ethylene glycol) [PEG 20 000]; DEAE-Sepharose®; bovine serum albumin, Bradford reagent, ethylenediaminetetraacetic acid (EDTA), 4-(2-hydroxyethyl) piperazine-*N*'-(2-ethane-sulphonic acid monosodium salt [Hepes] and the fluorimetric assay kit were obtained from Sigma-Aldrich (South Africa).

Commercial neuronal nitric oxide synthase obtained from rat brain; dithiothreitol (DTT); Sodium dodecyl sulphate (SDS); glycerol (50 %) ; Tris (hydroxymethyl) aminomethane; phenylmethylsulphonylfluoride (PMSF); ferric chloride hexahydrate ($FeCl_3$); sodium chloride (NaCl); perchloric acid; sulphuric acid; ortho-phosphoric acid; glacial acetic acid and hydrochloric acid were obtained from Merck Chemicals (South Africa). Molecular weight markers were obtained from PEQGOLD$^{TM}$ (Erlangen, Germany). All other chemicals were of analytical grade and were obtained from readily available sources. In

all the experiments, reagents were dissolved in milli-Q water and all the experimental conditions throughout the purification were performed at 0-4 °C, except where indicated.

### 2.4.2 Materials

All the chromatographic columns, PowerPac Basic electrophoresis kit (model 300) and the fraction collector (model 2110) were purchased from Bio-Rad (South Africa). Snake skin dialysis tubing was obtained from Pierce, Rockford (Illinois, USA). Bench-top centrifuges (Epperndorf 5810R and Eppendorf MiniSpin®); self-regulated temperature water bath (model 130) and pH meter (Ionolab pH level 1) were purchased from Merck (South Africa). UV analyses were performed on a PowerWaveX$^{TM}$ microplate reader which was purchased from Bio-Tek Instruments (Vermont, USA).

## 2.5 Methods

### 2.5.1 Citrulline assay

The citrulline assay was conducted, with slight modifications, according to the protocol previously described in literature (Boyde and Rahmatullah, 1980). The reaction mixture contained benzoyl-L-arginine ethyl ester (5 mM, 10 µl), $CaCl_2$ (5 mM, 10 µl), dithiothreitol (2 mM, 10 µl) in Tris-HCl buffer (50 mM, pH 7.6, 940 µl). Chromogenic reagent was made from thiosemicarbazide (18 mM) in 2,3 butanedione monoxime solution (500 mg in 100 ml distilled water) and sulphuric: orthophosphoric acid (1:1) in the presence of ferric chloride ($FeCl_3$) (0.25 g). The reaction was started by the addition of brain extract (10 µl) in NADPH (1.0 mM, 10 µl) and allowed to incubate at 40 °C for 2 min, before being stopped with perchloric acid (5 M, 10 µl). This mixture (250 µl) was treated with chromogenic reagent (250 µl) and cooled to 22 °C for 2 min. The reduction of benzoyl-L-arginine ethyl ester was then determined spectrophotometrically at 530 nm. The citrulline extinction coefficient ($e_{530}$) was 27.3 $M^{-1}.cm^{-1}$ (Sakakibara and Yanagisawa, 2003) and activity of nNOS was determined according to equation 1. One unit of activity was defined as the amount of nNOS that produced 1 µmol of citrulline per min per ml reaction mixture.

$$\text{Enzyme activity} = \frac{\Delta A.V_T.D_f}{e.t.l.V_e} = \mu mol/ml/min \quad \text{.....Eq (1).}$$

**Equation parameters**

| | |
|---|---|
| $\Delta A$ = change in absorbance | $D_f$ = dilution factor |
| $V_T$ = total volume (ml) | e = extinction coefficient ($M^{-1}.cm^{-1}$) |
| t = time (min) | l = path length (cm) |
| $V_e$ = volume of extract (ml) | |

## 2.5.2 Oxyhemoglobin assay

The oxyhemoglobin assay was conducted, with slight modifications to the assay by Feelisch, according to the protocol previously described in literature (Feelisch *et al.*, 1997). The reaction mixture (100 µl) contained the following reagents: benzoyl-L-arginine ethyl ester (50 µM), $CaCl_2$ (1 mM), DTT (120 µM), $BH_4$ (12 µM), NADPH (100 µM) and oxyhemoglobin (3 µM, 1 mM stock solution) in Hepes buffer (50 mM, pH 7.4, 390 µl). The reaction was started by the addition of the brain extract (10 µl) and the reaction mixture was allowed to incubate at 22 °C for 2 min. Activity measurements were calculated for a change in absorbance using an extinction coefficient ($e_{410}$) of 60 000 $M^{-1}$ $cm^{-1}$ (Packer, 1994), according to equation 1; pg 32. One unit of activity was defined as the amount of nNOS that produced 1 µmol of methemoglobin per min per ml of reaction mixture.

## 2.5.3 Fluorimetric assay

The fluorimetric assay was determined by the fluorimetric assay kit according to the manufacturer's instructions. The reaction mixture contained reaction buffer (460 µl), NADPH (10 µl), arginine (10 µl) and 4,5-diaminofluorescein diacetate (DAF-2DA) (10

µl). The reaction was started by the addition of brain extract (10 µl) and was allowed to incubate at 22 °C for 2 min in the dark before the fluorescence was read at an excitation wavelength of 490 nm and an emission wavelength of 520 nm. Two controls were prepared using similar reagents with the same quantities but omitting nNOS in one control and omitting DAF-2DA in the other control. One unit of activity was defined as the amount of nNOS that produced 1 µmol of DAF-2T per min per ml of reaction mixture. One arbitrary unit (AU) of relative fluorescence is equivalent to one unit of nNOS activity.

### 2.5.4 Isolation of nNOS

Fresh bovine brain (374 g) was homogenized in Hepes buffer (50 mM, pH 7.6, 600 ml) that contained EDTA (1.0 mM), NADPH (1.0 mM), DTT (0.5 mM) and PMSF (0.43 mM) and stored as 20 ml aliquots at - 70 °C until required.

### 2.5.5 Protein determination

The protein concentration for all experiments was routinely determined according to the method of Bradford (1976). The assay was performed in a 96-well microplate. Brain extract (5 µl) was added to a single well, followed by Bradford reagent (245 µl). The reaction was performed in triplicate. The mixture was incubated at 22 °C for 10 mins. Absorbance of the solution was measured at 595 nm and the concentration of the unknown samples was determined using the slope of the straight line of a BSA standard curve.

### 2.5.6 Ammonium sulphate precipitation

Crude brain extract (20 ml) was sonicated (10 W, 30 s intervals, 4 min) followed by centrifugation (10 000 x *g*, 4 °C, 30 mins) and the cell free supernatant extract was assayed for nNOS activity and protein and then used for further analyses. Crude extract (5 ml) was precipitated using 20–50 % ammonium sulphate with stirring (4°C, 50 min) and then centrifuged (4 000 x *g*, 4 °C, 50 min) to yield a supernatant (S1) and a pellet (P1). P1 was collected and resuspended in Tris-HCl buffer (50 mM, pH 7.5, 5 ml) and

dialyzed against the same volume and concentration of buffer to remove excess salt (4 °C, 24 h). The citrulline assay and Bradford assay were performed on both P1 and S1 as described previously (2.5.1 and 2.5.5).

### 2.5.7 Poly (ethylene glycol) 20 000 precipitation

A dry matrix of poly (ethylene glycol) (25 g) was added to a different aliquot of crude extract (5 ml) and was left to stand (4 °C, 24 h). The concentrated sample volume was adjusted to total volume (5 ml) using Tris-HCl buffer (10 mM, pH 7.5) and then assayed for activity using the citrulline and Bradford assay as previously described (2.5.1 and 2.5.5).

### 2.5.8 Anion- exchange on DEAE-Sepharose®

Fresh crude brain extract (50 ml) was sonicated (10 W, 30 s intervals, 4 min) followed by centrifugation (10 000 x g, 4 °C, 30 mins) and the cell-free supernatant extract (30 ml) was assayed for nNOS activity and protein (2.5.1 and 2.5.5) and then used for ion exchange chromatography. The crude extract (30 ml), obtained after centrifugation and sonication was applied on a glass Econo-Column® (3 x 40 cm) packed with DEAE-Sepharose® anion-exchanger resin, with a bed volume (30 ml). The column was previously equilibrated with Tris-HCl buffer (50 mM, pH 7.6) and washed with the same buffer until $A_{280}$ nm was at the baseline. The adsorbed proteins were then eluted by gradient elution with NaCl (0-1 M, 500 ml) in the same buffer at a flow rate of 2 ml/min (5 ml per tube). A total of 8 fractions (5 ml) were collected, pooled, dialyzed against Tris-HCl buffer (10 mM, pH 7.6) and the concentrated sample volume was then adjusted to total volume (5 ml) using Tris-HCl buffer (10 mM, pH 7.6) and the citrulline and Bradford assay were performed as previously described (2.5.1 and 2.5.5).

### 2.5.9 Dialysis of the crude and subsequent protein samples

The protein samples were dialyzed using a snake skin dialysis tubing (10 000 Da cut-off) for the removal of unwanted small molecules. Prior to dialysis, the dialysis membrane was soaked in Tris-HCl (10 mM, pH 7.6, 5 mins). A tubing clamp was used to close one end of the dialysis tubing and the protein sample was pipetted into the tubing. The tubing

was closed off with another clamp and placed into a large beaker with Tris-HCl (10 mM, pH 7.6, 4 °C). Stirring of the buffer was carried out at the same temperature for 24 h, after which the dialysed solution was removed from the tubing. The citrulline and Bradford assay were subsequently performed as described before (2.5.1 and 2.5.5).

### 2.5.10 SDS and native PAGE analyses

The separation of proteins by SDS-PAGE was performed with a few modifications from the method of Laemmli (1970). The apparatus was assembled according to the manufacturer's instructions. The electrophoretic separation of protein products was performed at a constant voltage of 200 V. After the electrophoretic run was completed, both the stacking (5 %) and the separating (12 %) gel were routinely stained with Coomassie commercial stain. The sample was loaded at 1.3 µg total protein per well.

The procedure for native PAGE was performed with 8 % separating gel at the same constant voltage of 200 V. After electrophoresis, the protein band was sliced out, re-suspended in minimal volume of Tris-HCl buffer (20 mM, pH 6.5, 1.0 ml) and incubated with benzoyl-L-arginine ester (0.1 g). The activity was monitored using the citrulline assay as previously described (2.5.1). The sample was loaded at 1.3 µg total protein per well

### 2.5.11 Enzyme kinetics

The kinetic properties namely, the Michaelis-Menten constant ($K_m$) and the maximal enzyme velocity ($V_{max}$) were determined by varying the substrate (benzoyl-L-arginine ethyl ester, 3 ml) between 0-15 mM and calculated from the Hanes-Woolf plot using the relationship in equation 2.

$$\frac{[S]}{V} = \frac{[S]}{V_{max}} + \frac{K_m}{V_{max}} \qquad \text{.....Eq (2).}$$

where (V) is the initial velocity of the enzymatic reaction at substrate concentration (S) and enzyme activity was determined at each substrate concentration.

### 2.5.12 Effect of temperature on nNOS activity

The effect of temperature on nNOS activity was determined at various temperatures (ranging from 10 °C–100 °C) under the standard citrulline assay conditions as described in 2.5.1.

### 2.5.13 Effect of pH on nNOS activity

To determine the pH optimum, the enzyme activity was assayed at different pH values [sodium acetate (pH 3–5.5, 50 mM); Hepes (pH 6-7, 50 mM); Tris-HCl buffer (pH 7.5-9, 50 mM)] under the standard citrulline assay conditions as described in 2.5.1 at an optimum temperature of 40 °C.

### 2.5.14 Stability of enzyme activity

The temperature stability of nNOS was determined at the optimum temperature and pH (40 °C, pH 6.5). Aliquots were removed periodically at 1 h intervals and analyzed for nNOS activity for a maximum period of 12 h. nNOS activity at time zero was considered to be 100 % residual activity.

## 2.6 Results and discussion

### 2.6.1 Evaluation of three nNOS assays

#### *2.6.1.1 Citrulline assay*

The enzymatic production of citrulline was based on the Fearon reaction, in which citrulline formed a rose pink colour with 2,3 butanedione monoxime in acid solution (Archibald, 1944). The formation of the coloured product was apparently favoured by the presence of thiosemicarbazide and ferric chloride which accelerated the carbamido-diacetyl reaction catalytically (Archibald, 1944).

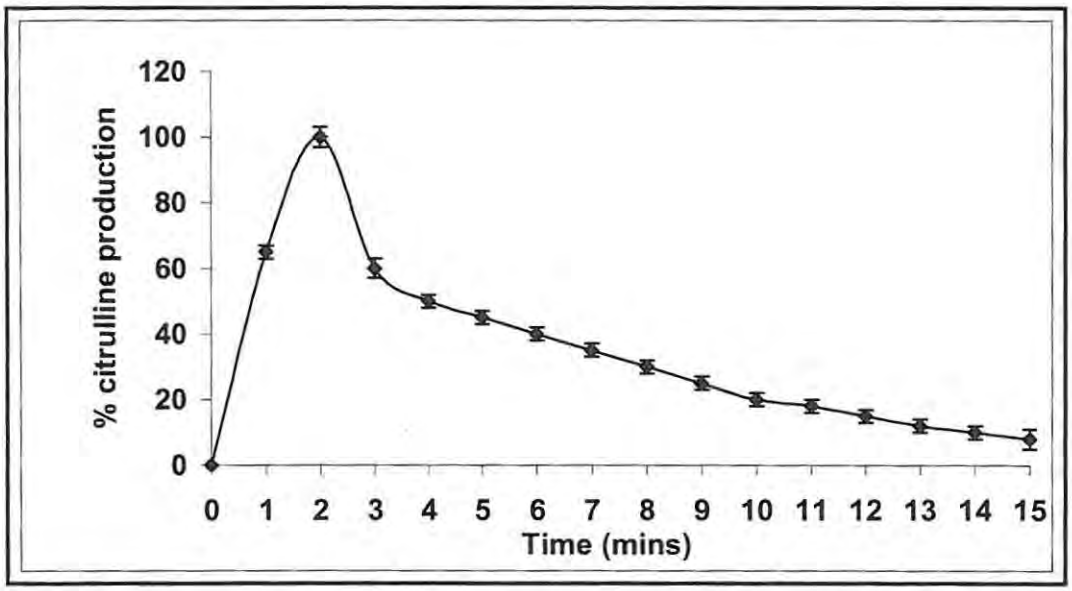


**Figure 2.4 Enzymatic progress curve representing the amount of citrulline product per unit time; values represent the mean (± S.E.M) of three trials.**

It was essential to determine the time dependant enzyme production of citrulline in order to establish a standard time parameter for subsequent enzyme activity assays (Fig. 2.4). The amount of citrulline produced per minute was relative and was inclusive of both residual brain citrulline and nNOS citrulline production expressed as a percentage (Fig. 2.4). The results (Fig 2.4) showed that 100 % citrulline production (~ 800 μM) occurred within 2 mins and it was this time frame that was used in subsequent activity assays. Since 400 μM of citrulline per min per ml was produced by nNOS, it was the enzyme catalyzed production of citrulline which was important to the assay and not so much the factor of residual citrulline present within the brain. The activity of nNOS was spectrophotometrically determined as 3.77 U/ml after 2 min according to equation 1; pg. 31. This activity was 15 times higher than the oxyhemoglobin assay and 20 times higher than the fluorimetric assay and so proved to be the best assay used. Also, the citrulline assay was faster, required less material and allowed the handling of different samples at the same time.

### *2.6.1.2 Oxyhemoglobin assay*

The activity of the enzyme was calculated according to equation 1; pg 32 and was determined as 0.25 U/ml. The assayed activity proved that although the assay was

sensitive, it was well suited for monitoring the activity of nNOS and was a simple and continuous assay. However, in view of the simplicity of the reaction and the availability of the reagents and the higher enzyme activity obtained, the citrulline assay was preferred.

### *2.6.1.3 Fluorimetric assay*

Brain extract was incubated for 1 min along with two controls. One control contained no nNOS and the other control contained no DAF-2DA. The results showed that the enzymatic reaction (reaction 1 in Fig. 2.5) yielded 0.180 RFU ˜ 0.180 U/ml. However, activity dropped to 0.015 RFU ˜ 0.015 U/ml in the first control (reaction 2 in Fig. 2.5) and dropped to approximately the same amount (0.01 RFU ˜ 0.01 U/ml) in the second control in the absence of DAF-2DA, indicating a small non-enzymatic component. The evaluation of the fluorimetric assay proved to be less sensitive than the other two because of spectral interference from reaction reagents which affected the assay performance and consequently this assay was abandoned.

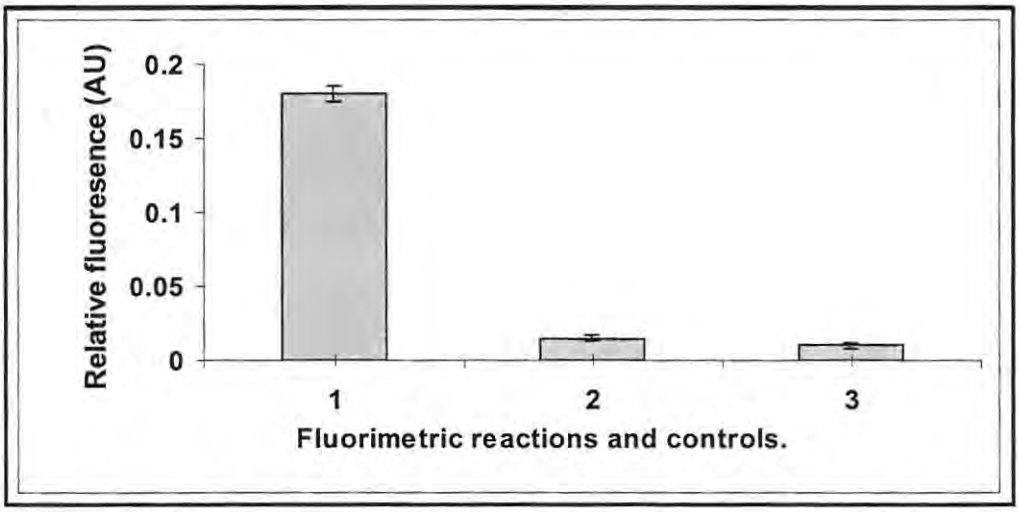


**Figure 2.5 Relative fluorescence (AU) which is equivalent to one unit of nNOS activity; values represent the mean (± S.E.M) of three trials. (1) fluorescence in presence of nNOS; (2) fluorescence of control without nNOS; (3) fluorescence of control without DAF-2DA.**

## 2.6.2 Purification of nNOS from bovine brain

**Table 2.1 Partial purification table of the nNOS sourced from bovine brain. Purification steps were not performed successively due to an attempted approach at different techniques of purification.**

| Purification step | Volume (ml) | Total protein (mg) | Total activity (U) | Specific activity (U/mg) | Yield % | Fold |
|---|---|---|---|---|---|---|
| **Crude extract** | 20 | 96.4 | 75.3 | 0.781 | 100 | 1 |
| **$(NH_4)_2SO_4$ (40 %)** | 5 | 19.9 | 14.9 | 0.749 | 20 | 1 |
| **PEG 20 000** | 5 | 19.3 | 16.3 | 0.845 | 22 | 1 |
| **DEAE-Sepharose (dialysis)** | 5 | 11.6 | 28.7 | 2.27 | 38 | 3 |

Two methods were attempted to concentrate nNOS from the crude extract i.e. $(NH_4)_2SO_4$ precipitation and PEG 20 000. Purification was further attempted using an anion exchange chromatography step on DEAE-Sepharose®. All three purification steps were performed independently. The results of the concentration and purification procedures are summarized in Table 2.1.

$(NH_4)_2SO_4$ precipitation was the first concentration step performed after sonication and centrifugation of the crude (20 ml) extract to yield S1 and P1. This was significant as S1 contained the nNOS that had been released into the extracellular fluid and P1 which was resuspended in Tris-HCl homogenization buffer (50 mM, pH 7.5) contained the intact nNOS. Protein concentration and enzyme activity assays were conducted for both the S1

and P1 in order to determine the best $(NH_4)_2SO_4$ cut required to precipitate the enzyme and extraneous protein (Fig. 2.6).

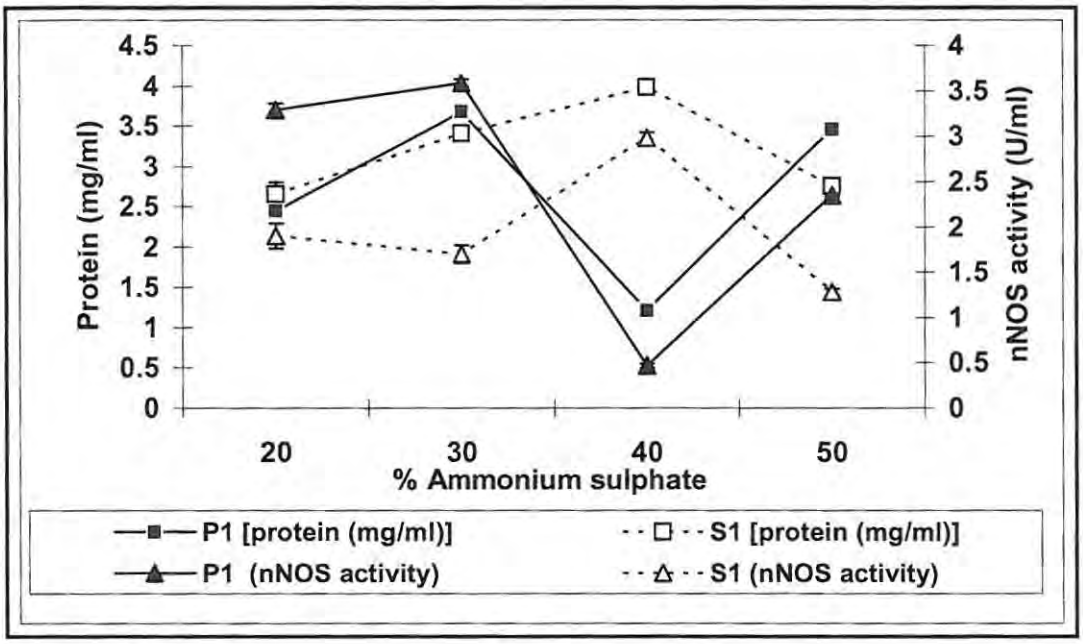


**Figure 2.6 Protein concentrations of both P1 and S1 from bovine brain extract using $(NH_4)_2SO_4$ precipitation; values represent the mean (± S.E.M) of three trials.**

The results (Fig. 2.6) showed that a low concentration of protein (3.41 mg/ml) with an enzyme activity (1.75 U/ml) was precipitated for S1 at 30 % $(NH_4)_2SO_4$. At 50 % $(NH_4)_2SO_4$ precipitation, S1 showed a lower protein concentration (2.76 mg/ml) with a similar enzyme activity (1.28 U/ml). However, the highest concentration of protein (3.98 mg/ml) and the highest enzyme activity (2.98 U/ml) was precipitated at 40 % $(NH_4)_2SO_4$ for the S1 (Fig. 2.6).

Conversely, the resuspended P1 precipitated the lowest concentration of protein (1.21 mg/ml) with the lowest enzyme activity (0.465 U/ml) at 40 % $(NH_4)_2SO_4$. At 50 % $(NH_4)_2SO_4$ precipitation, P1 showed a higher protein concentration (3.46 mg/ml) with a higher enzyme activity (2.35 U/ml). However, a similar high concentration of protein (3.68 mg/ml) with highest enzyme activity (3.59 U/ml) was precipitated for the resuspended P1 at 30 % $(NH_4)_2SO_4$ (Fig. 2.6).

It is clear from the results that the amount of nNOS was highest in the S1 and was effectively precipitated at 40 % $(NH_4)_2SO_4$. Nevertheless the enzyme, isolated using

$(NH_4)_2SO_4$ showed a similar specific activity (0.749 U/mg) to that of the 20 ml crude extract (0.781 U/mg) and produced a 20 % yield with a one-fold purification indicating that this step was unsuccessful in concentrating nNOS (Table 2.1). Hence, a second purification step involving PEG 20 000 was performed but also proved to be unsuccessful in concentrating nNOS. Although a fairly high specific activity (0.845 U/mg) was obtained compared to $(NH_4)_2SO_4$, PEG 20 000 produced a similar yield of 22 % and a similar purification fold increase (Table 2.1). Thus, these two techniques produced a one-fold purification and hence were abandoned in favor of ion exchange chromatography by DEAE-sepharose.

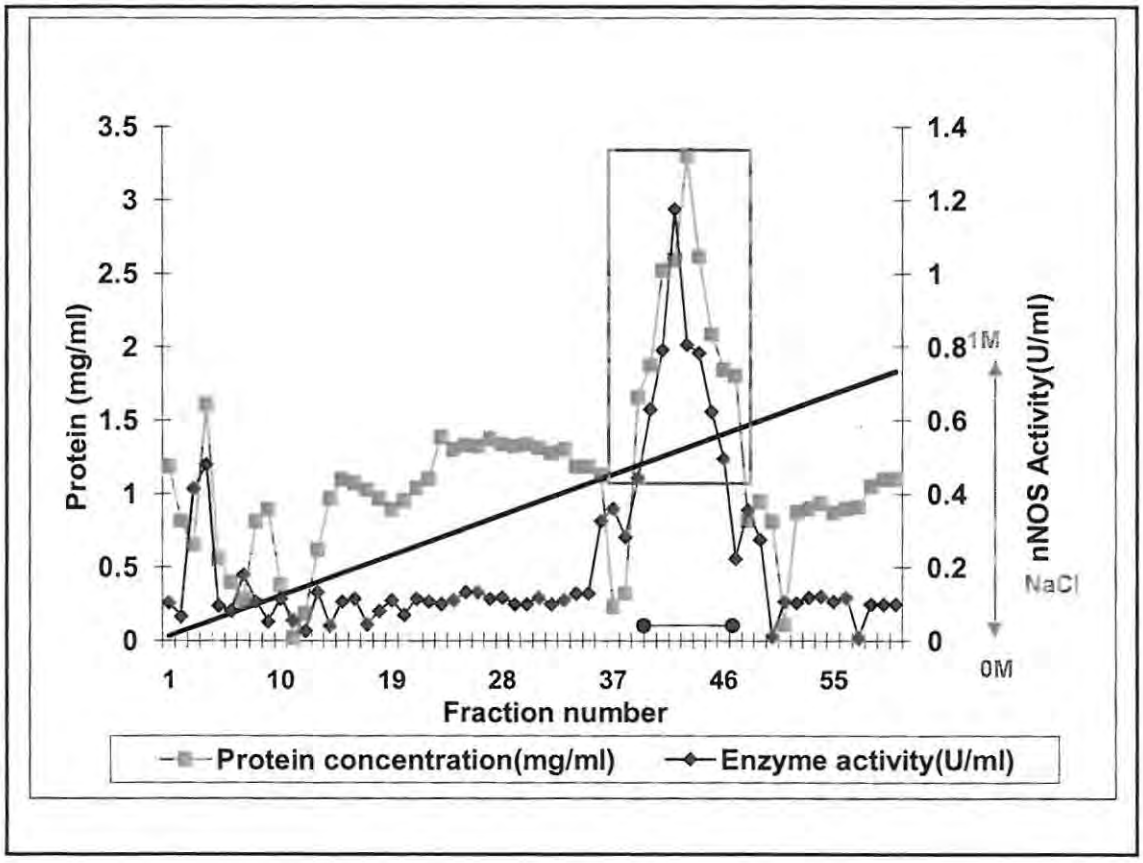


**Figure 2.7 Elution profile of DEAE-Sepharose ion-exchange chromatography. Proteins eluted with linear NaCl gradient (0-1 M) in Tris-HCl buffer (50 mM, pH 7.6); Flow rate, 2 ml/min (5 ml per tube). Fractions 39-46 were pooled.**

A fresh batch of crude extract (20 ml) was subjected to a one-step anion exchange chromatographic procedure after sonication and centrifugation. Eight active fractions (39-46) were eluted with approximately 0.75 M NaCl (Fig. 2.7). These undialyzed eight fractions were pooled and assayed using the citrulline and Bradford assay as described before (2.5.1 and 2.5.5). However, the specific activity of the undialyzed pooled fractions was very low (0.313 U/mg) and thus produced a very low yield (0.39 %) and a fold of 0.4 (values not shown on table 2.1), indicating that no enzyme activity was retained. Hence, the 40 ml fraction was dialyzed and reconstituted in Tris-HCl buffer (10 mM, pH 7.5, 5 ml) and assayed using the citrulline and Bradford assay as described before (2.5.1 and 2.5.5). Results showed a seven times greater specific activity (2.27 U/mg) than that prior to dialysis. Thus, this attempt at purification was only successful after dialysis was performed on the pooled fractions as a high amount of extraneous protein was removed by anion exchange chromatography resulting in a 38 % yield and a three-fold purification which testified to the fact that nNOS was purified partially.

### 2.6.3 Confirmation of purity and molecular weight: SDS-and native PAGE.

A pure protein should give a single band on an SDS-polyacrylamide gel, unless the molecule is made up of two or more subunits of different molecular mass. Under reducing conditions, using SDS, the protein was resolved into two subunit components of 95 and 130kDa, respectively. This indicated an overall molecular weight of 225 kDa which was similar to values reported earlier. Packer, (1994) and Rosazza and Chen, (1996) both reported a molecular mass for nNOS of 230 kDa which comprised of subunits of molecular mass 130-155 kDa.

Native-PAGE revealed a single subunit for the purification (DEAE-Sepharose) due to the use of non-denaturing conditions (Fig. 2.9). The single band from DEAE-Sepharose was cut from the gel and tested for enzyme activity (5 U/ml). Thus, native-PAGE was successful in detecting nNOS on the basis of its biological activity.

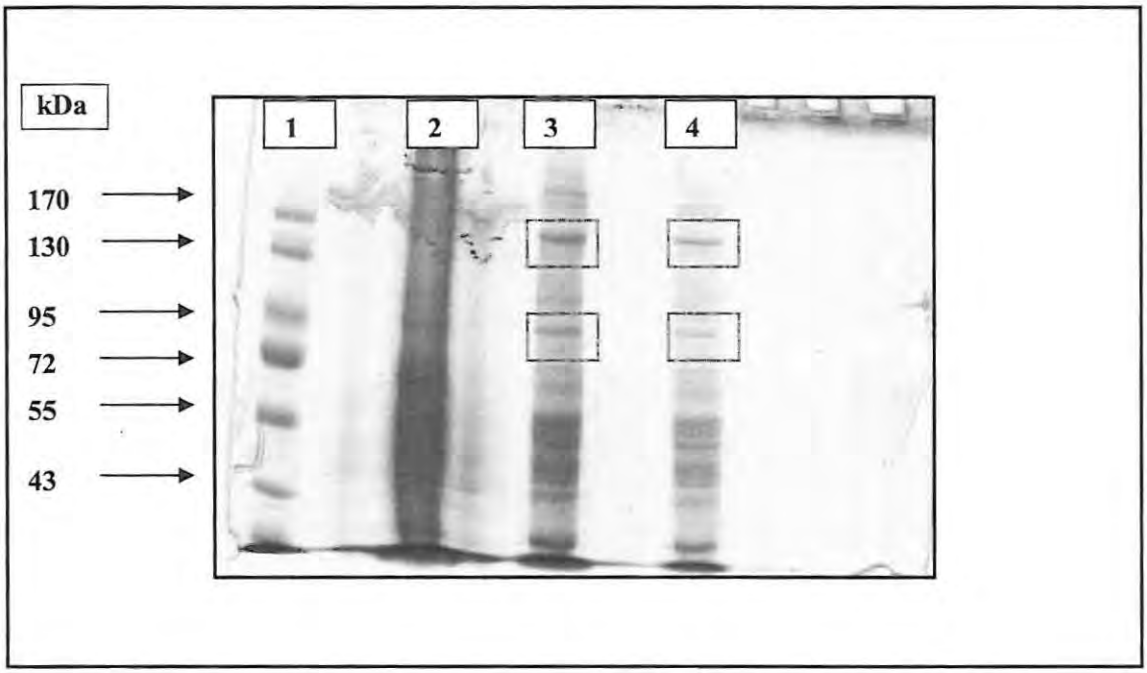


**Figure 2.8 SDS-PAGE analyses of the purified nNOS from bovine brain. Lane 1, molecular weight markers; Lane 2, crude brain extract; Lane 3 and Lane 4, separation of purified protein products using DEAE Sepharose. The stacking gel concentration was 5 % and the separating gel was 12 %. The gel was stained with Coomassie Blue commercial stain and destained with acetic acid: methanol: water (1:1:8, v/v).**

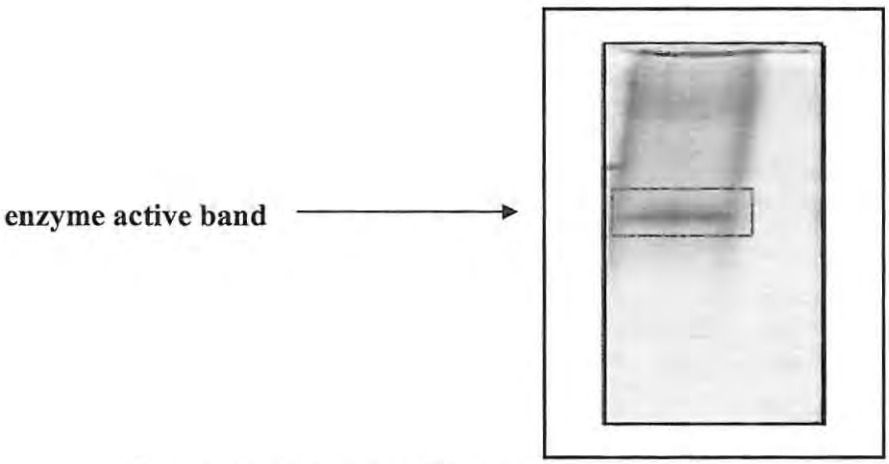


**Figure 2.9 Native-PAGE analysis of the DEAE Sepharose purified nNOS from bovine brain using a separating gel of 12 %.**

### 2.6.4 Kinetic behaviour of nNOS in the presence of benzoyl arginine ethyl ester.

The parameters $K_M$ and $V_{max}$ were calculated from the intercept and slope of the straight line of the Hanes-Woolf plot (Fig. 2.10), respectively The results showed that for benzoyl arginine hydrolysis, the $V_{max}$ and $K_M$ were 0.332 μmol.min$^{-1}$ and 70 μM, respectively. The turnover number ($k_{cat}$) and the catalytic efficiency ($k_{cat}/K_m$), calculated using equations 3 and 4 and were found to be 50.95 min$^{-1}$ and 0.73 min$^{-1}$.μM$^{-1}$, respectively. The total amount of enzyme [$E_t$] was 0.0065 μmol.

$$k_{cat} = \frac{V_{max}}{[E_t]} \quad \text{.....Eq (3).}$$

Where $V_{max}$ is the maximum velocity of the enzyme

$$\text{Catalytic efficiency} = \frac{k_{cat}}{K_M} \quad \text{.....Eq (4).}$$

where $K_M$ is the Michaelis-Menten constant.

Interestingly, the kinetic constant $K_M$ (70 μM) indicated a lower affinity for benzoyl arginine as opposed to other reported values (11 μM; 2 μM; 3.2 μM; 1.5 μM) for nNOS (Riveros-Moreno *et al.*, 1995; Bredt and Snyder, 1990; Giraldez and Zweier, 1998; Hiki *et al.*, 1992). It must be noted, however, that these reported $K_M$ values from literature were from a highly purified enzyme preparation while present findings was for the commercially purified form of nNOS. Also, the $V_{max}$ of the commercially purified nNOS was found to be 0.332 μmol.min$^{-1}$ which was lower than that of 1 μmol.min$^{-1}$ reported by Snyder and Bredt , (1990).

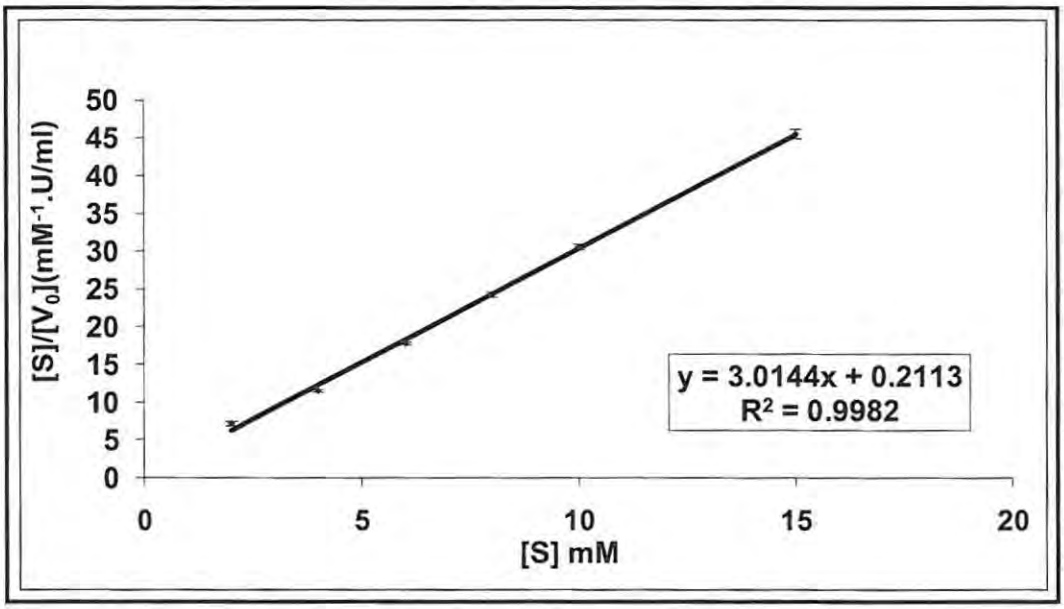


**Figure 2.10 Hanes-Woolf plot for the determination of kinetic parameters ($V_{max}$ and $K_M$) of nNOS from bovine brain; values represent the mean (± S.E.M) of three trials.**

## 2.6.5 Physico-chemical properties of nNOS

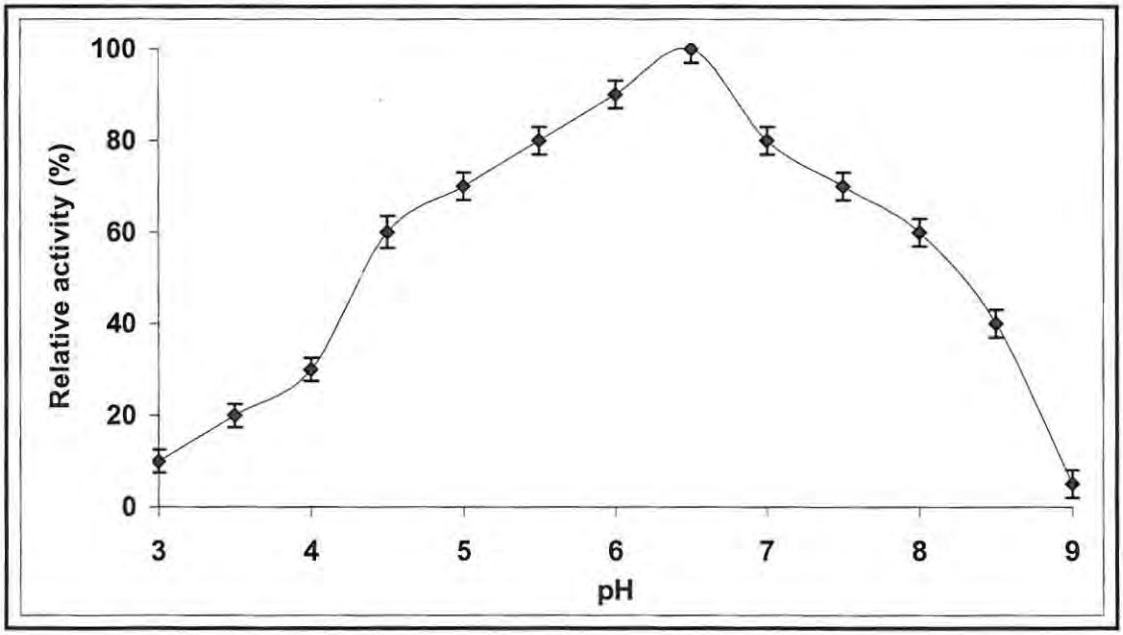


**Figure 2.11 pH profile of the purified nNOS from bovine brain; values represent the mean (± S.E.M) of three trials. 100 % relative activity = 5 U/ml.**

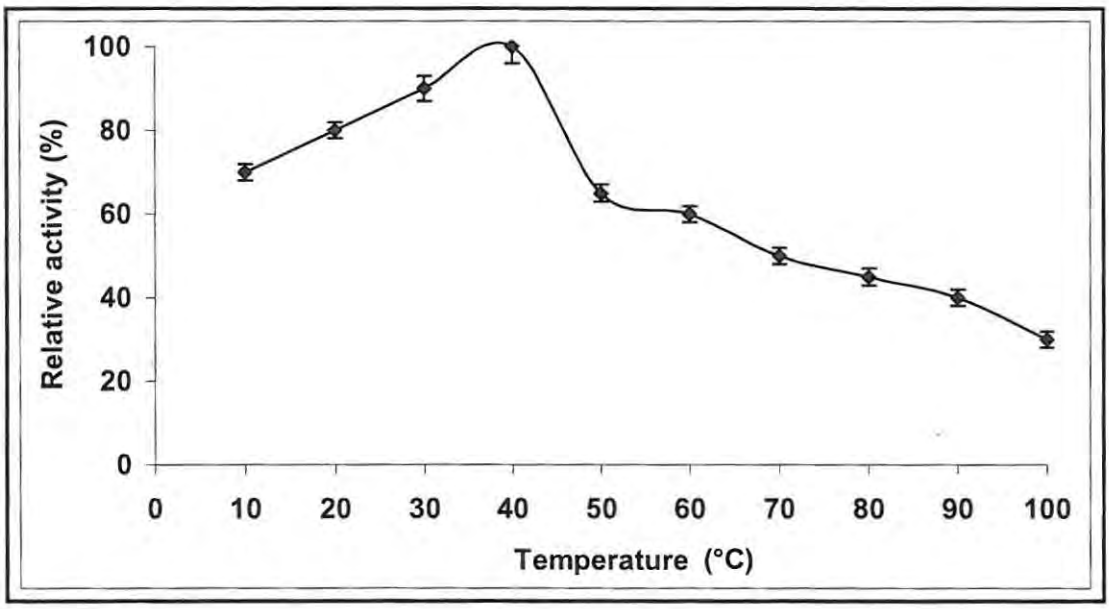


**Figure 2.12 Temperature profile of the purified nNOS from bovine brain; values represent the mean (± S.E.M) of three trials. 100 % activity = 5 U/ml.**

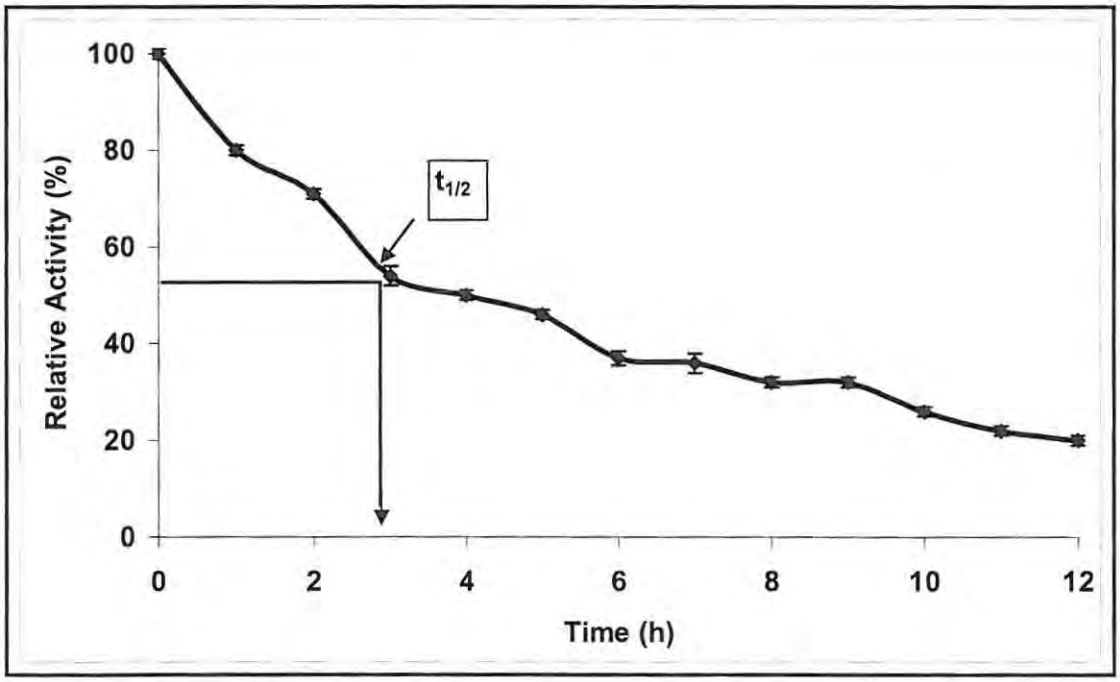


**Figure 2.13 Temperature stability of the purified nNOS from bovine brain; values represent the mean (± S.E.M) of three trials.** $t_{½}$ = 3 h; **100 % activity = 5 U/ml.**

The temperature and pH optima were determined at various ranges under the conditions as previously described in 2.5.12 and 2.5.13. The enzyme showed a 40 % decrease in

activity between pH 6.5 and 4.5 and 6.5 and 8 but rapidly lost its activity beyond these extremes. Thus, the pH optimum of nNOS was found to be 6.5 (Fig. 2.11), which was similar that of 6.8 reported by Riveros-Moreno *et al.*, (1995). Based on the temperature profile (Fig. 2.12), the enzyme showed 30 % decrease in activity between 40 °C and 10 °C and 40 °C and 70 °C, but its activity was lower beyond these temperature ranges. Thus, nNOS showed an optimum of 100 % activity (5 U/ml) at 40 °C with a half life of approximately 3 h (Fig. 2.13). This optimum temperature was comparable to a reported value of 37 °C for nNOS (Hiki *et al.*, 1992).

## 2.7 Conclusion

The citrulline assay was the assay method of choice due to it being faster, economical, reliable and produced higher enzyme activity results. It was also concluded that nNOS secreted into the extracellular fluid was predominant as S1 exhibited the highest protein concentration (3.98 mg/ml) and the highest enzyme activity (2.98 U/ml) after 40 % $(NH_4)_2SO_4$ precipitation. Purification results proved that it was very difficult to purify nNOS. According to characterization, the enzyme had a half life of 3 h (Fig. 2.13) indicating that the enzyme was relatively stable, but lost its stability at each purification step. The purification techniques; namely, $(NH_4)_2SO_4$ precipitation and PEG 20 000 precipitation were attempted but were unsuccessful in concentrating the enzyme. These techniques produced no increase in fold purification with a yield of 20-22 % with no change in specific activity (0.749 and 0.845 U/mg, respectively) compared to the crude (0.781 U/mg). The time involved in stirring, centrifugation and dialysis for these techniques was longer than the half life of 3 h, e.g., dialysis involved a 24 h period which could have resulted in loss of activity. According to the thermal stability profile of nNOS (Fig. 2.13), the enzyme lost 60 % of its activity in the first 6 h. Thus, it was concluded that hardly any activity remained after 24 h.

In addition, the eight fractions collected from anion exchange on DEAE Sepharose (Fig. 2.7), prior to dialysis, had a very low specific activity (0.313 U/mg) with no fold increase in purification and a 0.39 % yield. According to Fig. 2.7, the first 40 fractions were eluted at a flow rate of 2ml/min indicating that the enzyme was still bound to the column and

possibly lost 40 % of its activity in the first 100 min according to the thermal stability profile of nNOS (Fig. 2.13), thus lowering the specific activity of the enzyme considerably. A high amount of total protein (92.5 mg) was due to a high amount of extraneous protein in the crude extract and this also lowered the specific activity of the enzyme while producing a total activity (28.7 U). However, after dialysis was performed on the 40 ml pooled fraction, a lower amount of total protein (11.6 mg) (Table 2.1) was calculated suggesting that nearly 80 mg of unwanted protein was removed by the technique of dialysis while still retaining the total activity (28.7 U). Hence, DEAE ion exchange was successful in isolating the enzyme containing very high specific activity (2.27 U/mg) compared to $(NH_4)_2SO_4$ (0.749 U/mg) and PEG 20 000 (0.845 U/mg) resulting in a three fold purification. According to the enzyme kinetic data, the catalytic behaviour of the purified nNOS obeyed Michaelis-Menten kinetics with $V_{max}$ and $K_M$ values estimated from the Hanes-Woolf plot of 0.332 $\mu mol.min^{-1}$ and 70 $\mu M$, respectively. The enzyme retained > 80 % optimal activity between pH 5.5 and 6.5 and its optimal temperature was 40 °C. The relative stability of nNOS and its high catalytic activity made it a suitable biocatalyst for benzoyl-L-arginine ethyl ester under controlled reaction conditions.

# III

# Inhibition studies of nNOS by ß-amyloid peptide

## 3.1 Introduction

Inhibitors are substances which decrease the rate of an enzyme-catalyzed reaction when combined directly to the enzyme. Reversible inhibitors bind to an enzyme in a non-covalent interaction and can be removed by dialysis to restore full enzyme activity. Irreversible inhibitors, on the other hand, bind to the enzyme by covalent interaction and cannot be removed from the enzyme by dialysis (Palmer, 1995). Reversible inhibitors rapidly form an equilibrium system with the enzyme to show a definite degree of inhibition (depending on the concentration of enzyme, inhibitor and substrate) which remains constant over a period when initial velocity studies are normally carried out (Palmer, 1995). Moreover, reversible inhibition includes competitive inhibition, uncompetitive inhibition and noncompetitive inhibition. The competitive inhibitors specifically bind at the enzyme's catalytic site, where it competes with substrate for binding in a dynamic equilibrium–like process; the inhibition can be reversed by excess substrate. The uncompetitive inhibitors bind only to the enzyme-substrate complex at locations other than the catalytic site. Substrate binding modifies the enzyme structure, making the inhibitor-binding site available; this type of inhibition cannot be reversed by excess substrate. Finally, the non-competitive inhibitor binds to the enzyme or enzyme-substrate complex other than at the enzymes catalytic site. Substrate binding is unaltered but the enzyme-substrate-inhibitor (ESI) complex cannot form products; the inhibition cannot be reversed by excess substrate (Palmer, 1995).

This chapter aims to define the effect of $A\beta_{1-40}$ and shorter peptide fragments on the enzymatic activity of nNOS and the type of inhibition which may result. A previous study has shown that Aß and excess arginine accumulation occurs within neurons found in the brain of an AD patient (Cantoni *et al.*, 2002). In addition, Aß found outside the neuron have the ability to be internalized and thus also contribute to Aß accumulation in the neuron (Cantoni *et al.*, 2002). Thus, it is clear that high levels of arginine can be attributed to low nNOS catalytic activity within the neuron, which is also the site for Aß production from APP cleavage. Hence, it is significant to investigate whether these Aß peptides have the potential to inhibit nNOS and thus regulate the levels of nNOS which in consequence will lower levels of arginine. This should imply then that Aß peptides are influential in altering the levels of nNOS found in the brain which may result in the enzyme being a potential biomarker in AD.

# 3.2 Aims

- To determine whether $A\beta_{1-40}$, $A\beta_{22-35}$, $A\beta_{17-28}$, $A\beta_{32-35}$ and $A\beta_{25-35}$ inhibit nNOS and thus calculate the inhibition constant ($K_i$).
- To determine the effect of inhibition of nNOS by Aß relative to both substrate concentration and time dependent factors.

# 3.3 Reagents and materials

## 3.3.1 Reagents

Commercial neuronal nitric oxide synthase obtained from rat brain; DTT; PMSF; $FeCl_3$; NaCl; Tris (hydroxymethyl) aminomethane; perchloric acid; sulphuric acid; ortho-phosphoric acid; glacial acetic acid and hydrochloric acid were obtained from Merck Chemicals (South Africa). Amyloid peptides ($A\beta_{1-40}$, $A\beta_{22-35}$, $A\beta_{17-28}$, $A\beta_{32-35}$ and $A\beta_{25-35}$) were obtained from Sigma Aldrich (South Africa). All other chemicals were of analytical grade and were obtained from readily available sources. In all the experiments, reagents were dissolved in milli-Q water and all the experimental conditions throughout the purification, were performed at 0-4 °C, except where indicated.

### 3.3.2 Materials

UV analyses were performed on a PowerWaveX$^{TM}$ microplate reader which was purchased from Bio-Tek Instruments (Vermont, USA).

## 3.4 Methods

### 3.4.1 Substrate dependent inhibition of nNOS by Aß

Partially purified nNOS (5 µl) in Tris-HCl buffer (50 mM, pH 7.6, 76 µl) was treated with amyloid peptides $Aß_{1-40}$, $Aß_{22-35}$, $Aß_{17-28}$, $Aß_{32-35}$ and $Aß_{25-35}$ (0, 1 and 2 nM, 5 µl) in the presence of varying amounts of the substrate benzoyl arginine ethyl ester (0-15 mM, 8 µl) in the presence of chromogenic reagent (100 µl) to investigate the effect of substrate dependant inhibition on nNOS.

### 3.4.2 Time dependent inhibition nNOS by Aß

To further investigate their role in time dependent inhibition, $Aß_{1-40}$, $Aß_{22-35}$, $Aß_{17-28}$, $Aß_{32-35}$ and $Aß_{25-35}$ (1 nM, 2 nM ,5 µl each) were incubated with nNOS (200 µM, 5 µl) in Tris-HCl buffer (50 mM, pH 7.6, 76 µl) in the presence of the substrate benzoyl arginine ethyl ester (8 mM, 8 µl). The citrulline assay was performed as described previously (2.5.1). Absorbance was read at 530 nm at 2 mins intervals for duration of 30 mins. The value of $K_i$ (inhibitor constant) for $Aß_{1-40}$, $Aß_{22-35}$, $Aß_{17-28}$, $Aß_{32-35}$ and $Aß_{25-35}$ was calculated using equation 5.

$$K_i = \frac{[Aß.]\ V_{max}^{app}}{V_{max} - V_{max}^{app}} \quad \text{..... Eq (5).}$$

where **[Aß]** = concentration of amyloid peptide; $V_{max}^{app}$ = apparent maximum velocity in the presence of Aß.

# 3.5 Results and discussion

## 3.5.1 Substrate dependent inhibition of nNOS by ß-amyloid peptides.

### *3.5.1.1 Determination of $K_i$ for $A\beta_{1-40}$*

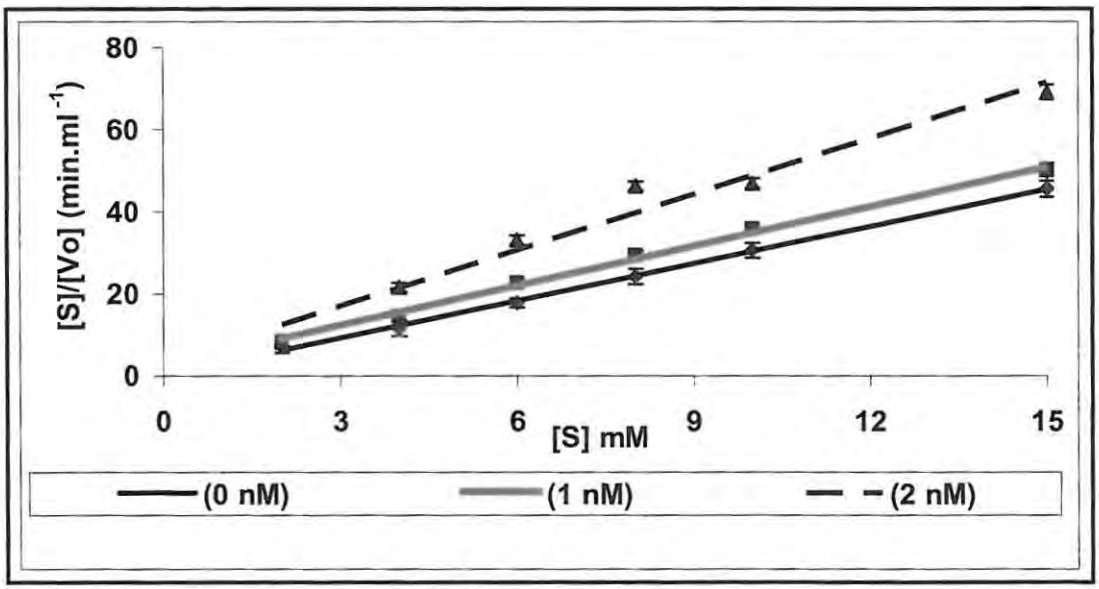


**Figure 3.1 Hanes-Woolf plot of Aß$_{1-40}$ (0,1 and 2 nM) in the presence of nNOS from bovine brain; values represent the mean (± S.E.M) of three trials.**

### *3.5.1.2 Determination of $K_i$ for $A\beta_{22-35}$*

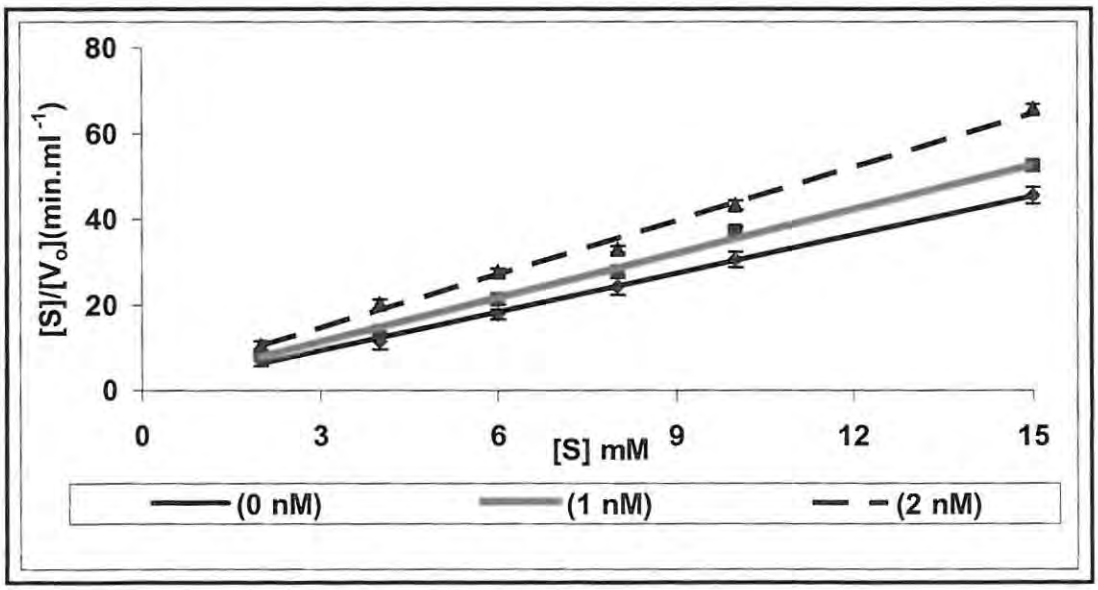


**Figure 3.2 Hanes-Woolf plot of Aß$_{22-35}$ (0,1 and 2 nM) in the presence of nNOS from bovine brain; values represent the mean (± S.E.M) of three trials.**

*3.5.1.3 Determination of $K_i$ for $A\beta_{17-28}$*

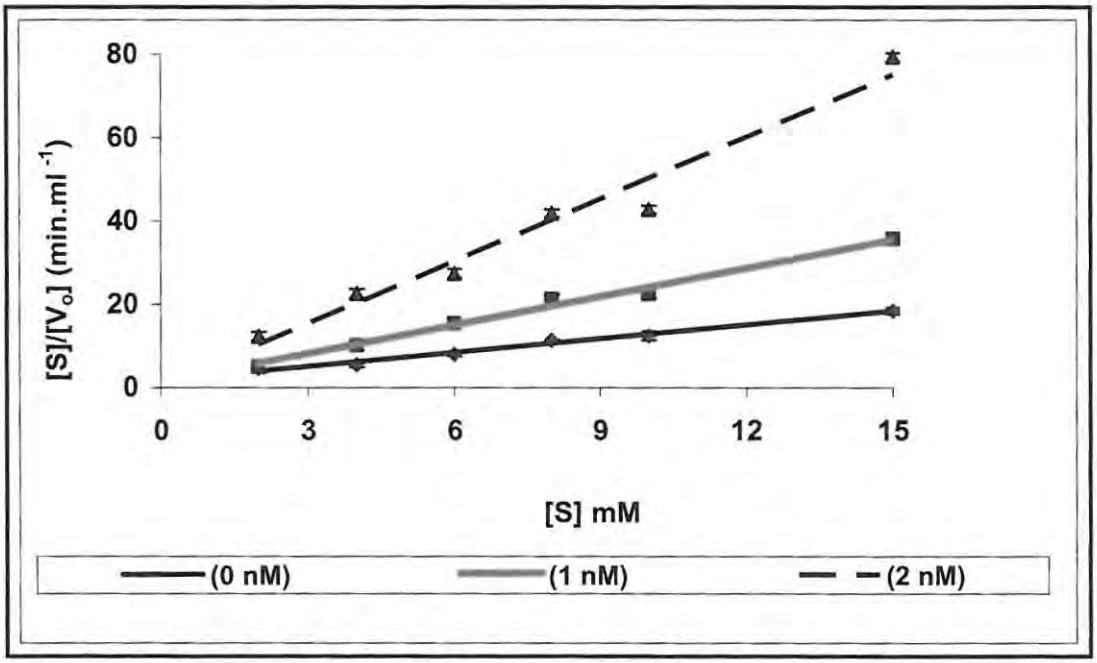


**Figure 3.3 Hanes-Woolf plot of $A\beta_{17-28}$ (0,1 and 2 nM) in the presence of nNOS from bovine brain; values represent the mean (± S.E.M) of three trials.**

*3.5.1.4 Determination of $K_i$ for $A\beta_{32-35}$*

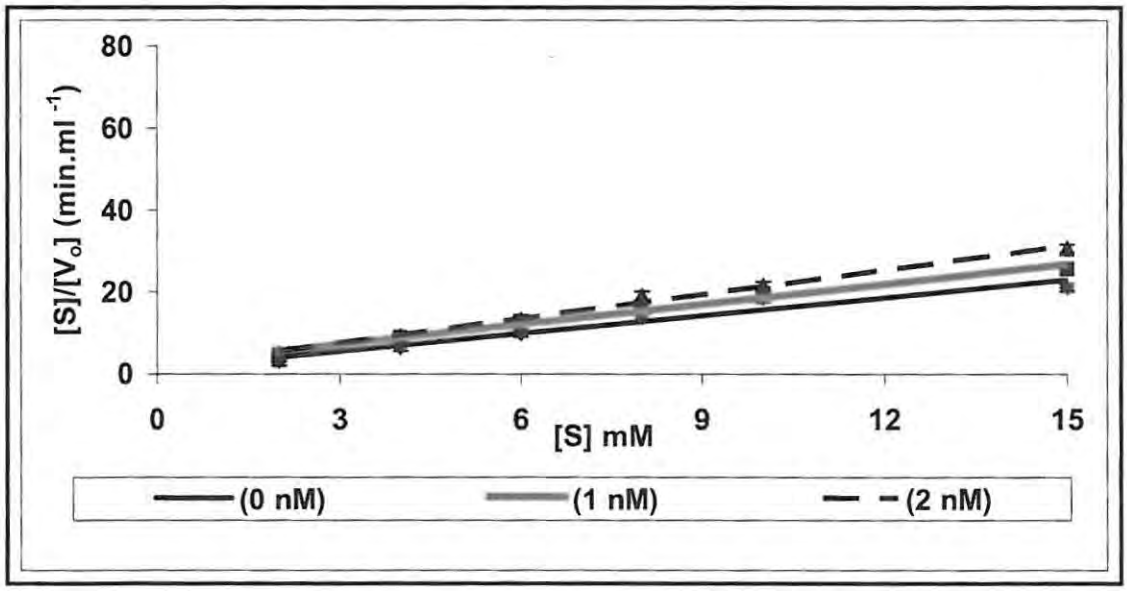


**Figure 3.4 Hanes-Woolf plot of $A\beta_{32-35}$ (0,1 and 2 nM) in the presence of nNOS from bovine brain; values represent the mean (± S.E.M) of three trials.**

### *3.5.1.5 Determination of $K_i$ for $A\beta_{25-35}$*

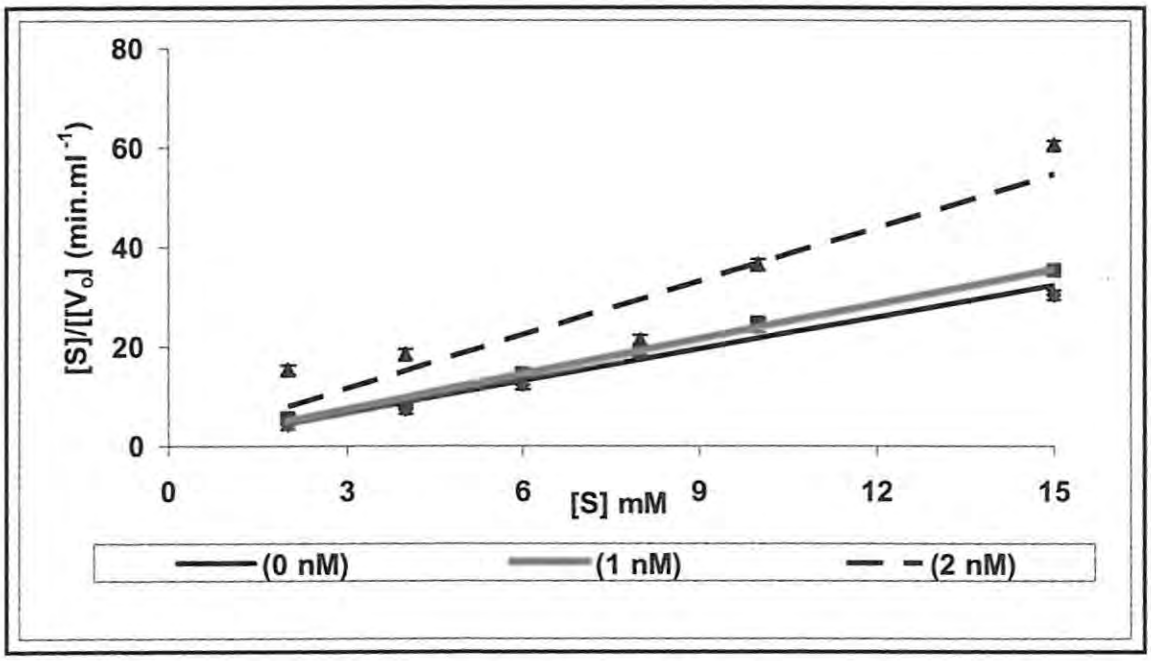


**Figure 3.5 Hanes-Woolf plot of $A\beta_{25-35}$ (0,1 and 2 nM) in the presence of nNOS from bovine brain; values represent the mean (± S.E.M) of three trials.**

It was shown that all the amyloid peptides ($A\beta_{1-40}$, $A\beta_{22-35}$, $A\beta_{17-28}$, $A\beta_{32-35}$ and $A\beta_{25-35}$) competitively inhibited nNOS at both 1 and 2 nM, respectively. The degree of inhibition was measured by the parameter $K_i$, the inhibitor constant which demonstrated the binding affinity of enzyme for inhibitor (Palmer, 1995). Results showed that $A\beta_{17-28}$ inhibited nNOS to a greater degree as reflected by its low $K_i$ value of 1.92 μM compared to the higher $K_i$ values of $A\beta_{1-40}$, $A\beta_{22-35}$, and $A\beta_{25-35}$ and $A\beta_{32-35}$ (14.4 μM; 7.4 μM ; 10 μM and 8.8 μM) (Table 3.1).

**Table 3.1 Table reflecting relative $K_i$ values for beta-amyloid peptides**

| **Aß** | 1-40 | 22-35 | 17-28 | 32-35 | 25-35 |
|---|---|---|---|---|---|
| **$K_i$ (μM)** | 14.4 | 7.4 | 1.92 | 8.8 | 10 |

### 3.5.2 Time dependent inhibition of nNOS by ß-amyloid peptides.*3.5.2.1 Inhibition of nNOS by $A\beta_{1-40}$*

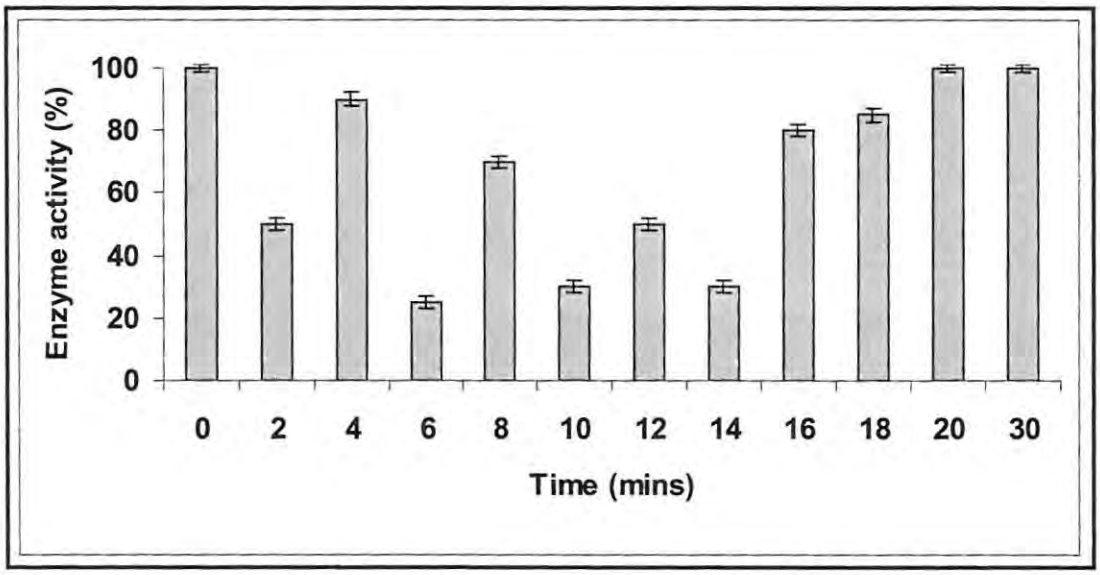


**Figure 3.6 Effect of $A\beta_{1-40}$ on nNOS activity; values represent the mean (± S.E.M) of three trials. Enzyme activity at 100 % = 5 U/ml**

*3.5.2.2 Inhibition of nNOS by $A\beta_{22-35}$*

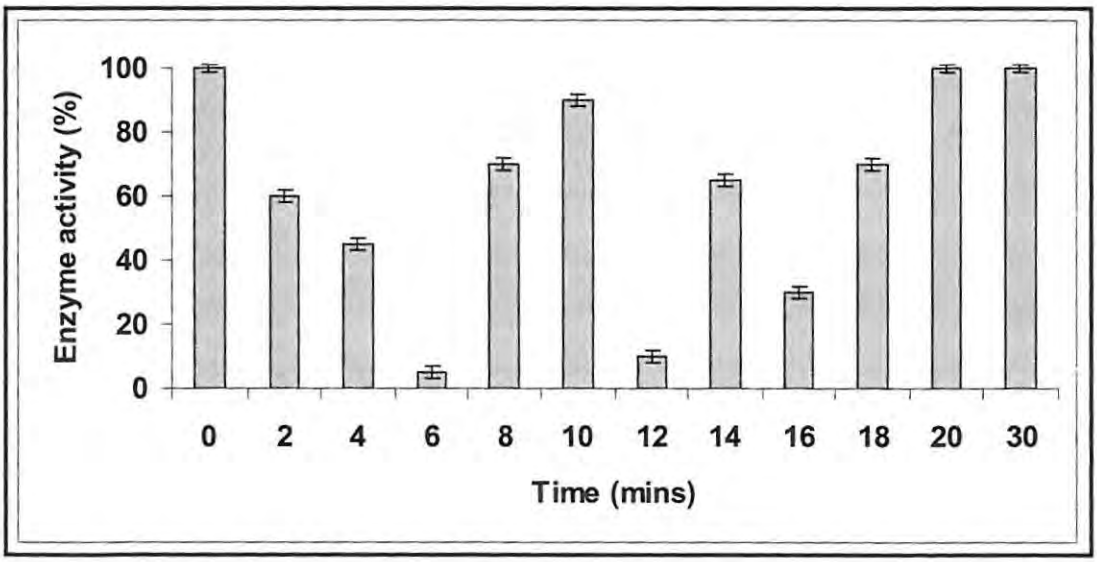


**Figure 3.7 Effect of $A\beta_{22-35}$ on nNOS activity; values represent the mean (± S.E.M) of three trials. Enzyme activity at 100 % = 5 U/ml***3.5.2.3 Inhibition of nNOS by $A\beta_{17-28}$*

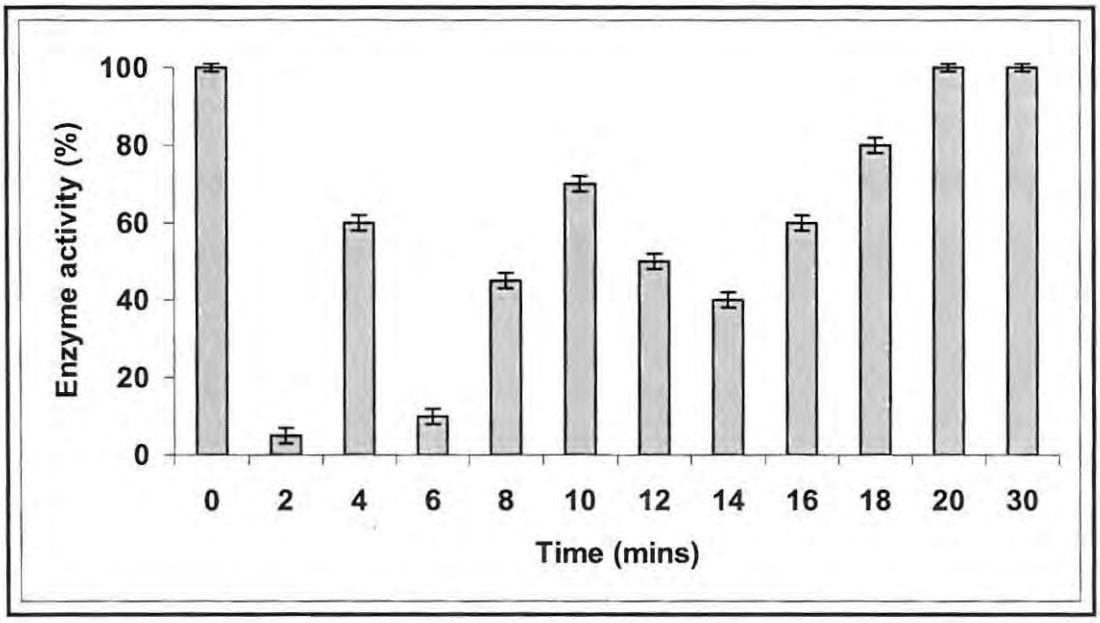


**Figure 3.8 Effect of $A\beta_{17-28}$ on nNOS activity; values represent the mean (± S.E.M) of three trials. Enzyme activity at 100 % = 5 U/ml**

### *3.5.2.4 Inhibition of nNOS by $A\beta_{32-35}$*

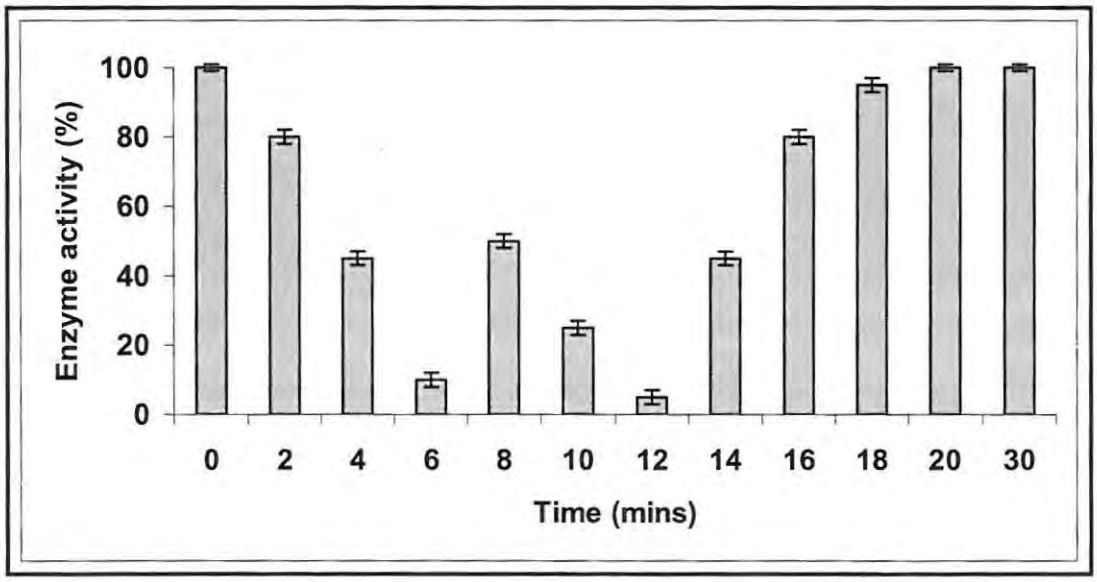


**Figure 3.9 Effect of $A\beta_{32-35}$ on nNOS activity; values represent the mean (± S.E.M) of three trials. Enzyme activity at 100 % = 5 U/ml**

### *3.5.2.5 Inhibition of nNOS by $A\beta_{25-35}$*

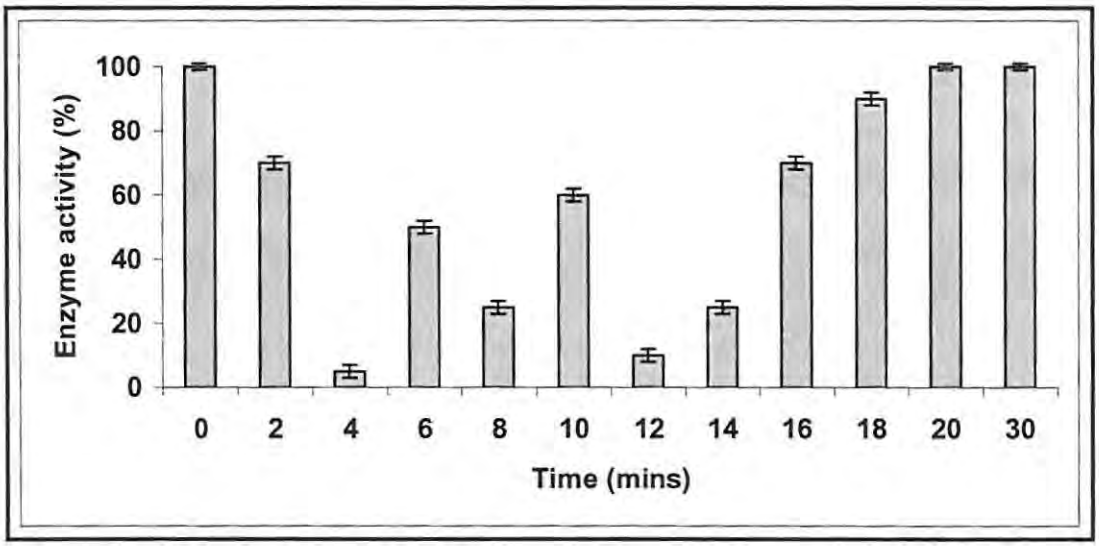


**Figure 3.10 Effect of $A\beta_{25-35}$ on nNOS activity; values represent the mean (± S.E.M) of three trials. Enzyme activity at 100 % = 5 U/ml**

All the various Aß peptides showed 100 % activity at time 0 which then steadily dropped at a rate of 55-90 % within 6 mins and thereafter enzyme activity continued to fluctuate for 18 min after which activity was restored to 100 % and remained constant with time for 30 min (Fig. 3.6-Fig. 3.10). The decrease in enzyme activity was an indication of the inhibition of nNOS by the amyloid peptides. Results for $A\beta_{22-35}$ (Fig. 3.7) and $A\beta_{32-35}$ (Fig.3.9) fitted the inhibition trend the best showing a successive drop in the activity of the enzyme by more or less the same percent within a 2 min time frame for 6 min. The other peptides,however, showed a slight fluctuation in this inhibition trend within the same time frame. In addition, $A\beta_{17-28}$ (Fig. 3.8) and $A\beta_{25-35}$ (Fig. 3.10) both showed an approximate 90 % decrease in enzyme activity within the shortest time frames of 2 and 4 min, respectively. This reveals that $A\beta_{17-28}$ inhibited nNOS rapidly and this correlates with the finding that $A\beta_{17-28}$ had the tightest binding affinity to the enzyme as earlier revealed by its lowest $K_i$ value of 1.92 µM. Thus, a tighter binding affinity may have somewhat influenced a fast inhibitory affect by $A\beta_{17-28}$ on nNOS.

Moreover, the characteristic inhibition observed was due to the association of both peptide–enzyme complexes. As the peptide was bound to nNOS, it inhibited the activity of the enzyme and the fluctuations in the activity of nNOS over time were due to the possible association between peptide and enzyme which resulted in inhibition and dissociation which resulted in decreased inhibition (Scheme. 3.1). It was also noted (Fig 3.6-3.10), that after an interval of time the enzyme activity was restored to

the original value of activity due to a similar dissociation of peptide from the enzyme. This suggested that the Aß was in a form that was no longer able to bind to the enzyme. It was speculation at this point but it was suspected that Aß had formed soluble fibrils. If this were in fact true, then it pointed towards the enzyme (nNOS) as a catalyst for fibril formation in a process called fibrillogenesis.

| **Association (inhibition)** ⟷ **Dissociation (restoring of activity)** |
|---|

**Scheme 3.1 The process of inhibition as described by shifts in equilibrium between association and dissociation between Aß and nNOS (Evans *et al.*; 1995).**

# 3.6 Conclusion

All Aß peptides inhibited nNOS successively but $A\beta_{17\text{-}28}$ was shown to inhibit the activity of nNOS to a greater extent due to its much lower $K_i$ value of 1.92 μM within 2 min, compared to other Aß peptides. The time dependent inhibition by Aß described the existence of an association vs. dissociation equilibrium between peptide and enzyme and helped to explain the fluctuations in enzyme activity subject to the rate of inhibition with the restoration of activity being indicative of probable fibrillogenesis. Finally, the possible process of fibrillogenesis alluded to the role of nNOS as an amyloidogenic catalyst. In addition, Congo red, turbidity and thioflavin-T assays were spectroscopic and spectrofluorimetric dye techniques employed in the detection of soluble and insoluble amyloid fibrils while transmission electron microscopy (TEM) was further used to visualize the morphology of insoluble fibrils as is the subject of chapter 4.

# IV

# Fibrillogenesis: Congo red; turbidity; thioflavin-T assays and transmission electron microscopy studies.

## 4.1 Introduction

Alzheimer's is an age related neurodegenerative disease associated with the accumulation of amyloid fibrils in the brain. Some amyloid fibrils may arise from cytosolic proteins, while others are derived from secretary or extracellular proteins. This suggests that both cytosolic and extracellular compartments within the brain are sites for fibril mediated toxicity. The plasma membrane is the interface between these two compartments and membrane permeabilization by amyloid fibrils is said to be the key toxicity factor in AD (Glabe, 2006). Membrane perturbation caused by fibrils may in turn initiate a series of downstream pathological events such as altered transmembrane signaling processes and the production of reactive oxygen species which disrupts normal neuronal function (Glabe, 2006). Moreover, amyloid fibrils accumulate in neurodegenerative diseases as a consequence of the intermolecular hydrogen bonding of extended polypeptide strands. The initiating event is protein mis-folding or denaturation, which results in aggregate formation in an infinitely propagating fashion (Glabe, 2006). The formation of fibrils (resulting from Aß aggregation) is called fibrillogenesis and the protein components of these amyloid fibrils vary widely. However, previous studies have shown that fibril formation is likely to progress via the consistent stacking of beta-sheet monomers. The

twisting of the beta-sheets is likely to continue to propagate as a helical twist as the sheets stack on top of each other (Howlett *et al.*, 1995).

There are two aspects of amyloid fibril formation that can be characterized *in vitro;* namely, the determination of the structure of the fibril and the process of fibril formation (i.e., mechanism and kinetics). Both processes begin with the characterization of the component peptide or protein by traditional techniques used to study protein structure (Nilsson, 2004). Firstly, the peptide molecule is usually maintained in its monomeric form. Once information about the initial secondary structure is known, the protein is subjected to conditions to promote aggregation into amyloid fibrils. The exact conditions are highly variable and sample dependent. Secondly, once conditions that promote fibril formation are established, the kinetics of the process is examined by assaying the solution for fibrils at specific time intervals (Nilsson, 2004). In addition, fibrils are known to exist in a soluble and an insoluble form with the latter being defined as a mature amyloid fibril. The most common techniques to identify the presence of fibrils are: Congo red and turbidity binding assays, thioflavin-T (ThT) fluorescence assay and transmission electron microscopy (TEM).

# 4.2 Theory of techniques utilized

## 4.2.1 Congo red assay

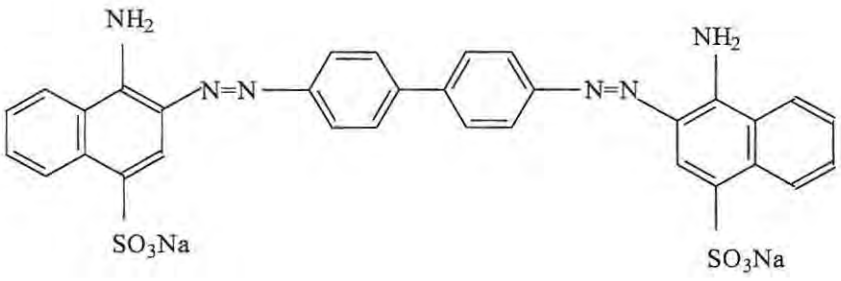


**Figure 4.1 Chemical structure of Congo red.**

Congo red was the first direct dye to be identified in 1884 and was synthesized by coupling 4-sulfo-1-naphthylamine with bisdiazotized benzidine (Klunk *et al.*, 1989). Structurally, Congo red is a diazo dye (containing two –N=N- functionalities) as well as containing two naphthalenesulphonic acid groups (Fig. 4.1). In addition, Congo red avidly stains amyloid proteins, which are thought to play a central role in Alzheimer's disease (Fig. 4.2). Moreover, Congo red staining is relatively specific and has been of interest for two reasons. Firstly, Congo red is widely used to visualize amyloid in pathological specimens. Secondly, the binding of Congo red to amyloid has been used to gain insights into the macromolecular structure of amyloid proteins (Klunk *et al.*, 1989).

**Figure 4.2 Amyloid protein stained with Congo Red (www.britannica.com).**

DeLellis and colleagues first demonstrated that binding of Congo red to amyloid fibrils was dependant on the secondary conformation of the amyloid, i.e., the beta-pleated sheet (DeLellis *et al.*, 1968). Studies have revealed that Congo red may be bound to amyloid by being partially entrapped and partially bound in 'channels' within these beta-pleated sheets by non-specific close-range forces similar to the binding of thioflavin-T (Cooper, 1974).

In addition, Congo red has several functional groups that could interact with amyloid fibrils by: (1) hydrogen bonding with the primary amino groups acting as H-bond donors; (2) ionic interactions via the sulphonic acid group (Fig. 4.3); (3) hydrophobic interactions

between the aromatic rings and the fibrils; (4) steric intercalation of the dye between ß sheets, or (5) a combination of these interactions (Nilsson, 2004).

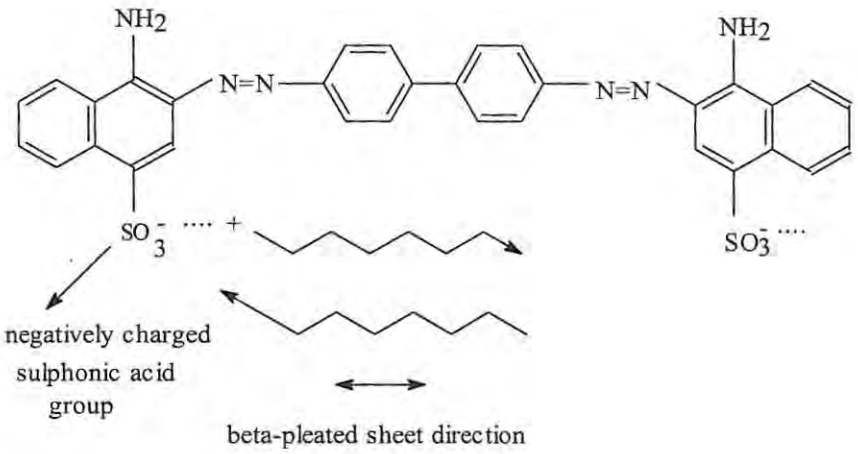


**Figure 4.3 Ionic interaction mechanism between the negatively charged sulphonic acid groups on the Congo red molecule and the positive charge on beta-pleated peptide molecule.**

## 4.2.2 Turbidimetry

Turbidimetric methods have been previously applied to determine precipitated protein aggregates (Drake *et al.*, 2004) that cause the solution to become turbid/cloudy. The induced aggregation may result from soluble/insoluble interactions whereby soluble peptides precipitate out to form insoluble peptide aggregates. For the purpose of this technique, soluble aggregates refer to those aggregates that are not visible as discrete particles by transmission electron microscopy and are not removed by filtration. Conversely, insoluble aggregates may be removed by filtration and are often visible by transmission electron microscopy (Cromwell *et al.*, 2006). Aggregation may also be induced via dipole-dipole interactions or the hydrophobic effect. Exposure of hydrophobic surfaces leads to the formation of aggregates in many proteins and may cause extensive precipitation. Small perturbations in protein structure may expose hydrophobic surfaces that lead to aggregation (Cromwell *et al.*, 2006).

In turbidimetry, the apparent absorption of radiation by the protein suspension is measured. When light radiation passes through a transparent medium, a distinct radiation phenomena occurs in which the light is scattered by the suspended particles. This scattering is due to reflection and refraction and gives rise to the Tyndall effect with the Tyndall ratio being the ratio of Tyndall intensity to that of the incident radiation (Wilson and Walker, 2000). Turbidity measurements are dependent on the particle size, concentration, nature of the sample, refractive index of the solvent, incident light wavelength and radial distribution of light scattering (light scattering angle and distance between sample and detector) (Drake *et al.*, 2004). Furthermore, different solvent systems such as trifluoroacetic acid (TFA), dimethylsulfoxide (DMSO), are usually used to induce aggregation of beta-amyloid peptides (Wang *et al.*, 2006). In this chapter, the extent of aggregation of various beta amyloid peptides in DMSO in the presence of nNOS was determined as a function of time. The absorbance or turbidity of the solution was measured and used as an indication of the degree of aggregation.

### 4.2.3 Thioflavin-T (ThT) assay

Thioflavin-T (ThT) is a commonly used non-covalent dye which, like Congo red, has also been used extensively for detecting the presence of amyloid fibrils and their rates of formation (Krebs *et al.*, 2005). It has a three-ring structure; the conjugated benzothiazol and aminobenzol rings which are arranged in an almost planar orientation (~ 30 °) in a minimum energy conformation (Fig. 4.4).

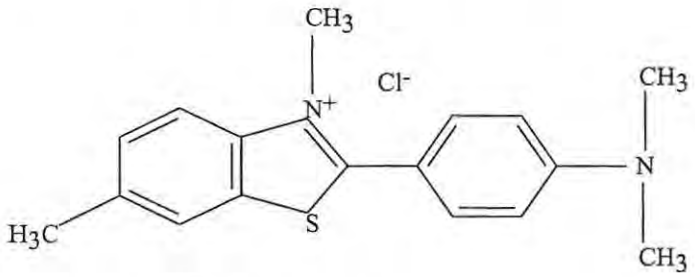


**Figure 4.4 Chemical structure of thioflavin-T.**

During excitation, the rings rotate in order to obtain the most stable exited state conformation (~ 90 °), which has low fluorescence efficiency. Polar solvents and viscosity

can affect the reorientation of the rings and ThT fluorescence. The binding to amyloid fibril probably stabilizes the planar form of the molecule and leads to a 10–500 fold increase in ThT fluorescence intensity (Fink and Munishkina, 2007). Interestingly, ThT has two excitation wavelengths (~ 335 nm and ~ 430 nm) and two corresponding emission wavelengths (~ 425–455 nm and 483 nm) which correspond to two conformations of the ThT molecule (planar and twisted) (Fink and Munishkina, 2007).

In addition, the binding of thioflavin-T to amyloid fibrils is similar to the Congo-red binding mechanism as both mechanisms are related to the ß-sheet structure of amyloid fibrils (Krebs *et al.*, 2005). These ß-sheets form 'channels' and thioflavin-T most likely sits within the fibril 'channels' surrounded by side chains, the close proximity which is likely to result in steric interactions between them. These interactions could ensure that the dye molecule remains in a flat conformation even when excited by the absorbance of a photon of light (Krebs *et al.*, 2005). By maintaining such a conformation in the excited state, the fluorescence yield is greatly enhanced and it is this enhancement that has allowed the use of thioflavin-T as a diagnostic dye for the determination of concentration of amyloid fibrils.

### 4.2.4 Transmission electron microscopy (TEM)

Transmission electron microscopy is a technique whereby a beam of electrons is transmitted through an ultra thin specimen, interacting with the specimen as it passes through. An image is formed from the interaction of the electrons transmitted through the specimen. The image is then magnified and focused onto an imaging device such as a fluorescent screen or phosphor screen (Fig. 4.5) (http://www.unl.edu). A more technical explanation of how a typical TEM works is as follows:

1. The "virtual source" at the top represents the electron gun, producing a stream of monochromatic electrons.

2. This stream is focused to a small, thin, coherent beam by the use of condenser lenses 1 and 2 (Fig. 4.5). The first lens (usually controlled by the "spot size knob") largely determines the "spot size"; the general size range of the final spot that strikes the sample. The second lens (usually controlled by the "intensity or

brightness knob") actually changes the size of the spot on the sample; changing it from a wide dispersed spot to a pinpoint beam.

3. The beam is restricted by the condenser aperture (Fig. 4.5), knocking out high angle electrons.
4. The beam strikes the specimen and parts of it are transmitted.
5. This transmitted portion is focused by the objective lens into an image.
6. The image is passed down the column through the intermediate and projector lenses, being enlarged all the way.
7. The image strikes the phosphor image screen and light is generated, allowing the user to see the image.

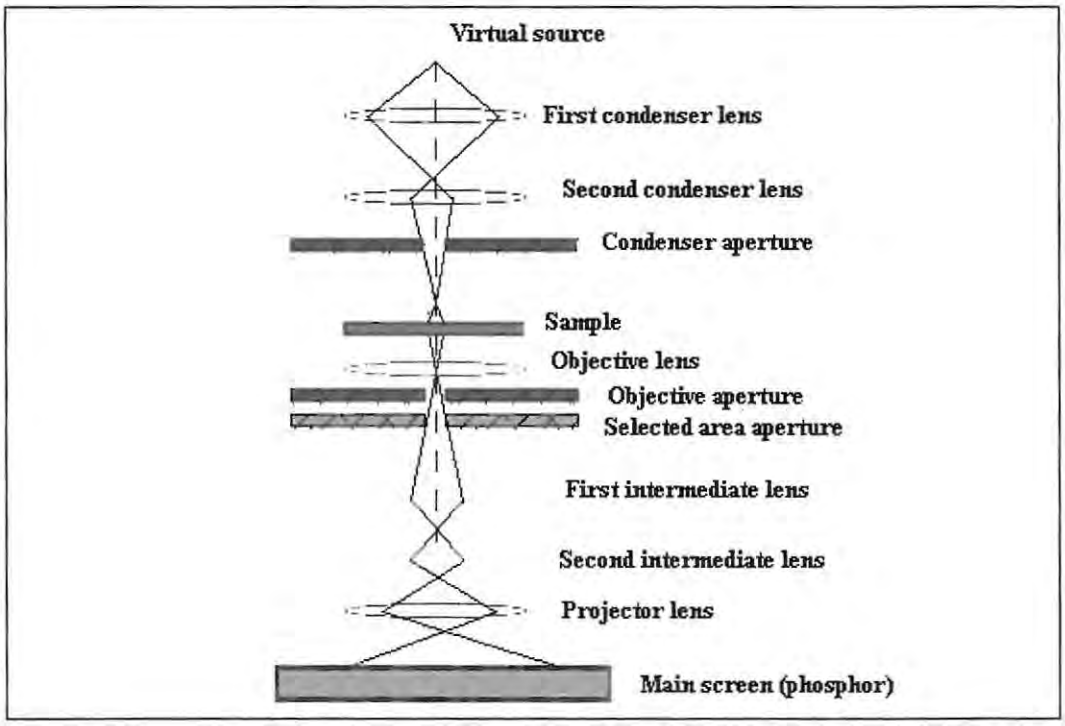


**Figure 4.5 A diagram depicting the important components in a transmission electron microscope that are responsible for its function** (http://www.unl.edu).

The darker areas of the image represent those areas of the sample that fewer electrons were transmitted through (they are thicker or denser). The lighter areas of the image represent those areas of the sample that more electrons were transmitted through (they are thinner or less dense).

# 4.3 Aims

- To use the techniques of turbidity measurement and Congo-red assay to distinguish between both soluble and insoluble fibril forms and to quantify both forms.
- The use of a fluorescent technique such as the thioflavin-T (ThT) assay to quantify the production of amyloid fibrils.
- To use transmission electron microscopy (TEM) to visually examine the morphology (shape and size) of amyloid fibrils.

# 4.4 Reagents and materials

## 4.4.1 Reagents

Amyloid peptides $A\beta_{1-40}$, $A\beta_{22-35}$, $A\beta_{17-28}$, $A\beta_{32-35}$ and $A\beta_{25-35}$; $N^a$-benzoyl-L-arginine ethyl ester hydrochloride (BAEE); DL-citrulline; calcium chloride; 2,3-butanedione monoxime, thiosemicarbazide and Congo red were obtained from Sigma-Aldrich (South Africa). Commercial neuronal nitric oxide synthase obtained from rat brain; DTT; thioflavin-T (ThT); fluorescein, Tris (hydroxymethyl) aminomethane; perchloric acid; sulphuric acid; ortho-phosphoric acid; glacial acetic acid; hydrochloric acid; PMSF and $FeCl_3$ were obtained from Merck Chemicals (South Africa). Uranyl acetate (UA) was obtained from Advanced Laboratory solutions. All other chemicals were of analytical grade and were obtained from readily available sources. In all the experiments, reagents were dissolved in Milli-Q water and all the experimental conditions throughout the purification, except where indicated, were performed at 0-4 °C.

### 4.4.2 Materials

A self-regulated temperature water bath (Model 130); dry heating mantle; pH meter (Ionolab) was purchased from Sigma Aldrich (South Africa). Absorbance spectroscopy was performed on a PowerWave 96 microplate spectrophotometer purchased from Bio-Tek instruments. A fluorescence spectrophotometer (model F-2500, 230 V, 1.8 A, 50/60 Hz), obtained from Hitachi® was used to conduct fluorescence spectroscopy. Transmission electron microscopy (TEM) analysis and imagery were performed on a JEOL JEM-1210 transmission electron microscope at 100 kV. Carbon nickel grids (200-400 mesh spacing) were obtained from Wirsam Scientific and Precision.

## 4.5 Methods

### 4.5.1 Congo red binding assay

The Congo red binding assay method was performed as previously described (Klunk *et al.*, 1989) with slight modifications. Congo red solution (12.5 µM) was prepared in Tris-saline buffer (100 mM Tris-Cl, pH 7.4, containing 150 mM NaCl, and then mixed with 1:5 v/v amyloid peptides $A\beta_{1-40}$, $A\beta_{22-35}$, $A\beta_{17-28}$, $A\beta_{32-35}$ and $A\beta_{25-35}$ (100 µM) with Congo red solution in the presence of nNOS (5 µl). The amount of Aß fibril ($A\beta_{FIB}$) was calculated according to equation 6.

$$[A\beta_{FIB}] = \left[\frac{A_{540}}{25\,295}\right] - \left[\frac{A_{480}}{46\,306}\right] \quad \text{..... Eq (6).}$$

where $A_{540}$ is the total absorbance of the Congo red-Aß mixtures at 540 nm and $A_{480}$ is the absorbance of the Congo red at 480 nm. The values 25 295 and 46 306 are the extinction coefficients of the Congo red-Aß complex and the Congo red alone, in units of

$ml.\mu mol^{-1}$ respectively. Controls were prepared by replacing the enzyme with Tris-HCl buffer still containing Aß.

### 4.5.2 Turbidity assay.

The turbidity assay method was performed as previously described, with slight modifications to the procedure (Evans *et al.*, 1995). Aliquots of each Aß peptide dissolved in DMSO were added to Tris-HCl buffer (10 mM, pH 7.4, 190 µl) and nNOS (5 µl) to give a final concentration of 5 nM in the cuvette. Controls were prepared in a similar way as to the Congo red assay by replacing the nNOS enzyme with an equivalent amount of Tris-HCl buffer containing Aß. Aggregation was measured by turbidity at 400 nm vs. a blank buffer.

### 4.5.3 Thioflavin- T (ThT) assay

Thioflavin-T (ThT) was used to indicate the presence of Aß fibrils using a modified version of that previously reported (LeVine, 1993). nNOS (5 µl) was added to a reaction mixture containing ThT (2 µl, 3.14 mM) and NaOH (200 µl, 10 mM) in Tris HCl buffer (pH 7.6, 100 mM) and NaOH (10 mM) in a final volume of 1.0 ml. Increasing concentrations of Aß peptides were added, incubated for 30 min at 22 °C and the shift in fluorescence was monitored at an excitation wavelength of 440 nm and an emission wavelength of 482 nm. A solution of Aß-Tris HCl buffer without ThT was used as a control. The fluorescence intensity above the control was indicative of fibril formation.

### 4.5.4 Transmission electron microscopy (TEM)

A 10 µl sample of either amyloid peptide alone or those that had been challenged with nNOS was placed onto a carbon-coated copper grid, excess liquid removed by carefully blotting with filter paper and then the sample was negatively stained with uranyl acetate (2 %, 30 sec), washed twice in deionised water, blotted dry with filter paper and viewed within the first 30 min and then after a further 24 h using a JEOL JEM-1210 TEM at an acceleration voltage of 100 kV.

## 4.6 Results and discussion

### 4.6.1 Congo red assay

For all beta-amyloid peptides tested, the concentration of fibrils was quantified according to equation 6; pg 67. All controls of the various Aß in the absence of nNOS showed no change in absorbance over the 24 h aggregation period, thus concluding that the peptide itself did not form fibrils. From the results (Fig. 4.6-Fig. 4.10), 80 % soluble fibrils were formed from $Aß_{1-40}$; $Aß_{17-28}$; $Aß_{25-35}$ and $Aß_{32-35}$ while 70 % soluble fibrils were formed from $Aß_{22-35}$ within 0.5 h of incubation with nNOS. These results substantiate the findings of supposed fibril formation within 30 min (chapter 3). Moreover, the percentage rate of soluble Aß peptide disappearance as detected by the Congo red assay was reflective of insoluble fibril formation as was later detected by the technique of turbidity. With $Aß_{1-40}$ there was a 10-15 % rate of soluble fibril decrease within 96 h. Surprisingly, after 96 h there was an increase in soluble fibrils that eventually decreased by a rate of 10-25 % and remained constant thereafter (Fig. 4.6).

With $Aß_{22-35}$ the amount of soluble fibrils remained at 68 % up to 48 h and then decreased by a further 18 % within 72 h with the amount of soluble fibrils continuing to decrease at a rate of 35-40 % from 72 h to 144 h. There was a surprising increase in soluble fibrils after 168 h which continued to decrease at a 10-20 % rate thereafter (Fig. 4.7). $Aß_{17-28}$ showed a similar trend to $Aß_{1-40}$ except that the fibrils decreased at a rate of 15 % within 48 h and then surprisingly peaked after 72 h and dropped again to 60 % of soluble fibrils. Surprisingly it was after 120 h that the percentage of soluble fibrils increased to 80 % that eventually decreased with time to 10-15 % after 10 days (Fig. 4.8). With respect to $Aß_{25-35}$ (Fig. 4.9) and $Aß_{32-35}$ (Fig. 4.10), similar fluctuations in soluble fibrils was also observed between 48 and 144 h which gradually decreased to 35 % and 20 % after 168 h, respectively and remained constant thereafter with time after a period of 10 days.

*4.6.1.1 Quantification of soluble fibrils produced by $A\beta_{1-40}$*

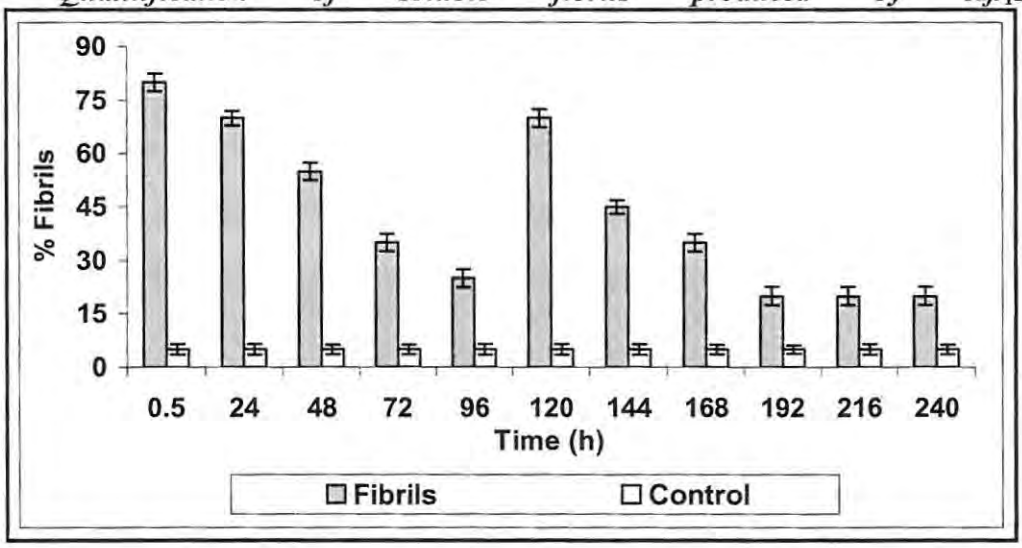


**Figure 4.6 Congo red assay of the percent soluble fibrils formed with respect to time from the incubation of nNOS with $A\beta_{1-40}$; values represent the mean (± S.E.M) of three trials.**

*4.6.1.2 Quantification of soluble fibrils produced by $A\beta_{22-35}$*

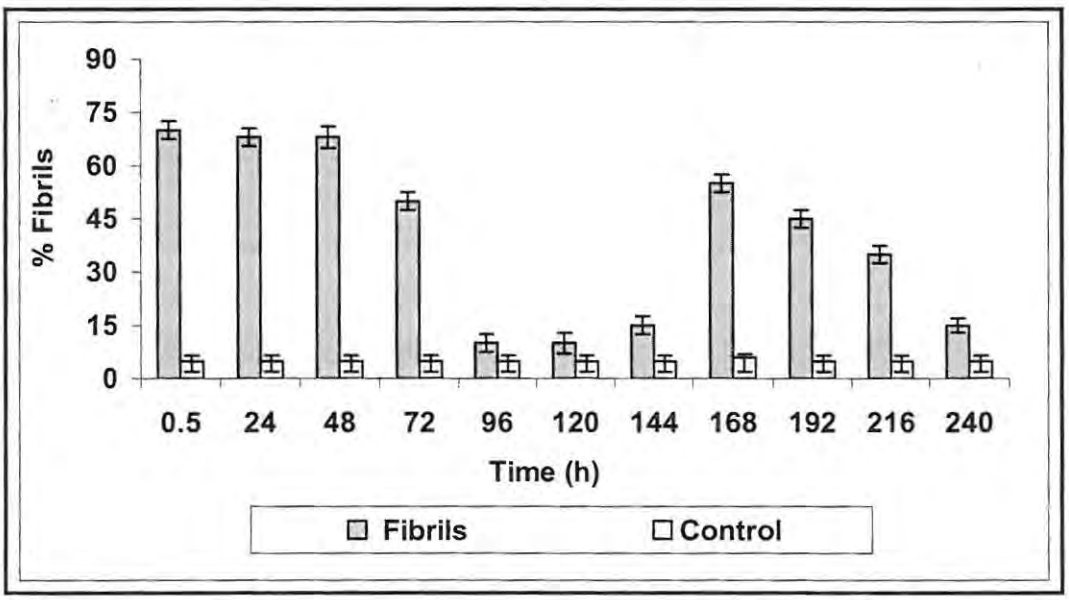


**Figure 4.7 Congo red assay of the percent soluble fibrils formed with respect to time from the incubation of nNOS with $A\beta_{22-35}$; values represent the mean (± S.E.M) of three trials.**

*4.6.1.3 Quantification of soluble fibrils produced by $A\beta_{17-28}$*

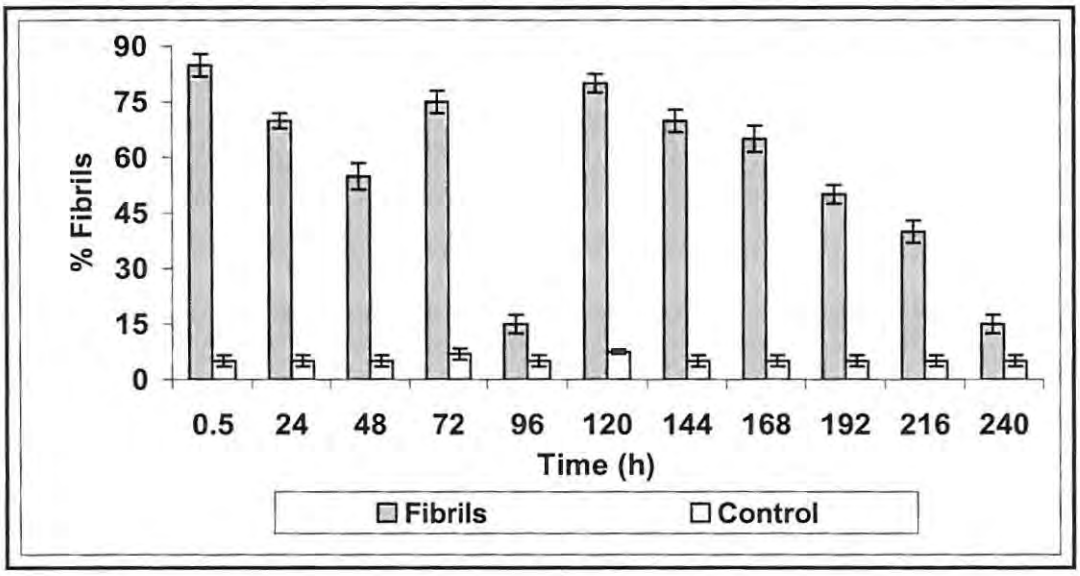


**Figure 4.8 Congo red assay of the percent soluble fibrils formed with respect to time from the incubation of nNOS with $A\beta_{17-28}$; values represent the mean (± S.E.M) of three trials.**

### *4.6.1.4 Quantification of soluble fibrils produced by $A\beta_{25-35}$*

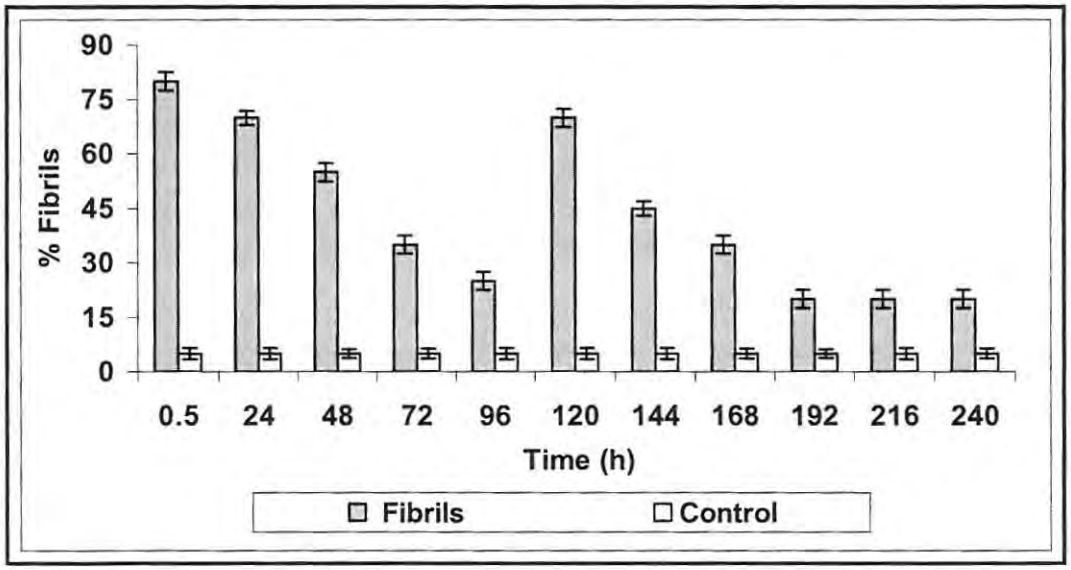


**Figure 4.9 Congo red assay of the percent soluble fibrils formed with respect to time from the incubation of nNOS with $A\beta_{25-35}$; values represent the mean (± S.E.M) of three trials.**

### *4.6.1.5 Quantification of soluble fibrils produced by $A\beta_{32-35}$*

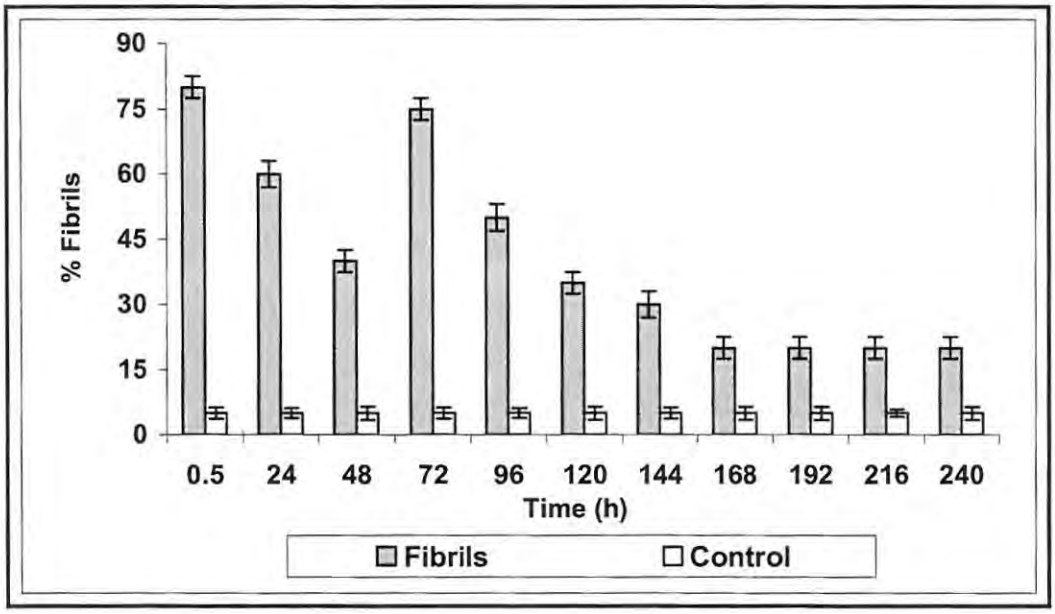


**Figure 4.10 Congo red assay of the percent soluble fibrils formed with respect to time from the incubation of nNOS with Aß$_{32-35}$; values represent the mean (± S.E.M) of three trials.**

## 4.6.2 Turbidity assay

### *4.6.2.1 Quantification of insoluble fibrils produced by Aß$_{1-40}$*

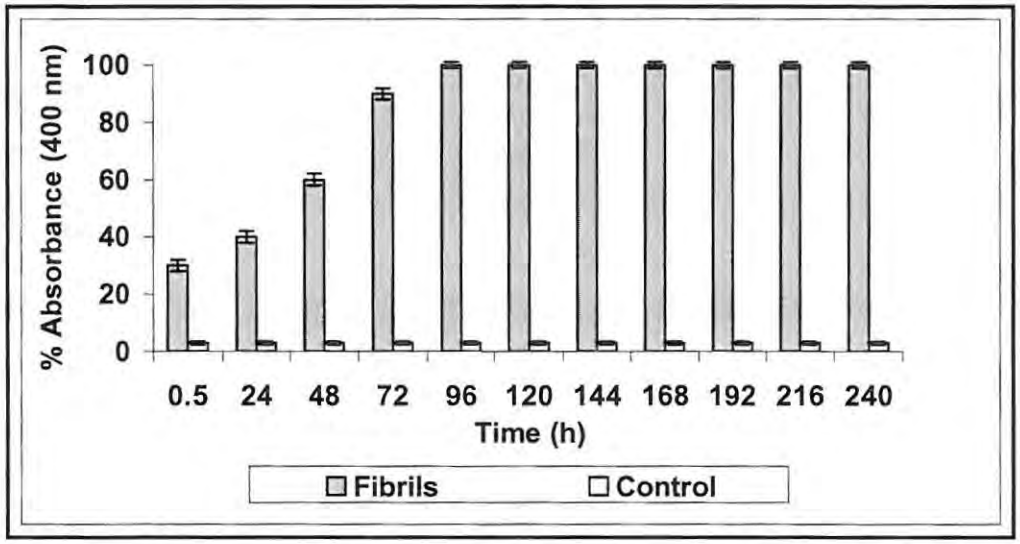


**Figure 4.11 Turbidimetric assay of the percent of insoluble fibrils formed with respect to time from the incubation of nNOS with Aß$_{1-40}$; values represent the mean (± S.E.M) of three trials.**

### *4.6.2.2 Quantification of insoluble fibrils produced by Aß$_{22-35}$*

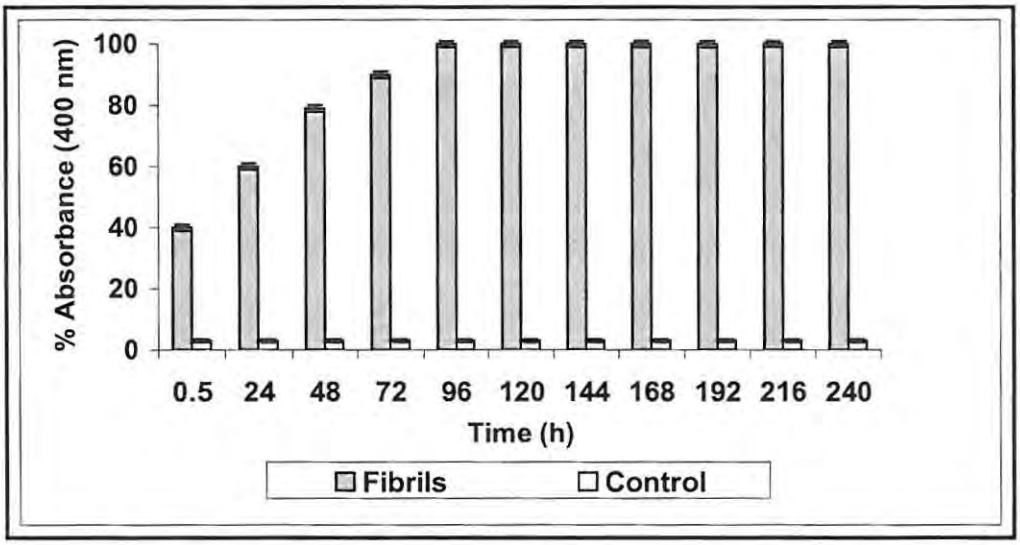


**Figure 4.12 Turbidimetric assay of the percent of insoluble fibrils formed with respect to time from the incubation of nNOS with $A\beta_{22-35}$; values represent the mean (± S.E.M) of three trials.**

### *4.6.2.3 Quantification of insoluble fibrils produced by $A\beta_{17-28}$*

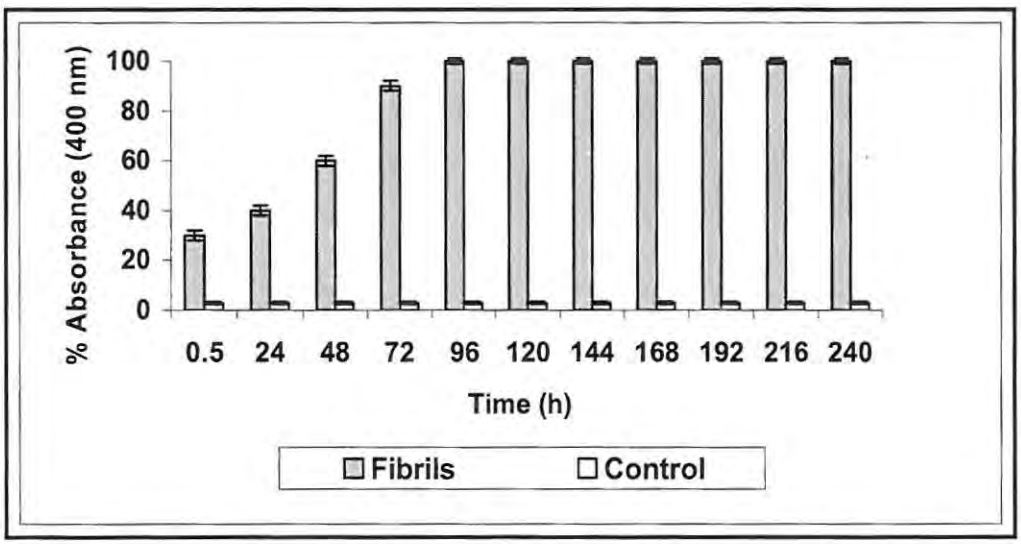


**Figure 4.13 Turbidimetric assay of the percent of insoluble fibrils formed with respect to time from the incubation of nNOS with $A\beta_{17-28}$; values represent the mean (± S.E.M) of three trials.**

### *4.6.2.4 Quantification of insoluble fibrils produced by $A\beta_{25-35}$*

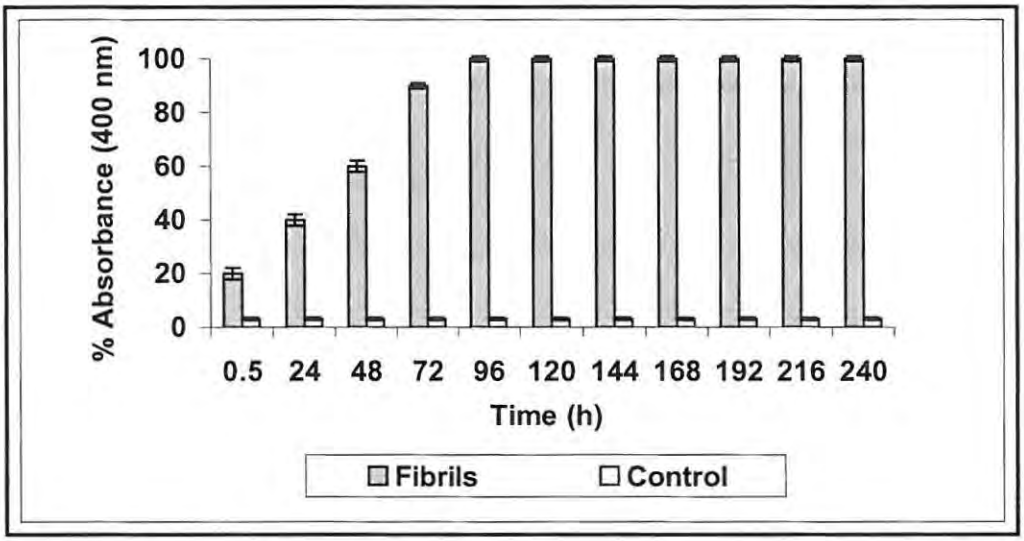


**Figure 4.14 Turbidimetric assay of the percent of insoluble fibrils formed with respect to time from the incubation of nNOS with $A\beta_{25-35}$; values represent the mean (± S.E.M) of three trials.**

### *4.6.2.5 Quantification of insoluble fibrils produced by $A\beta_{32-35}$*

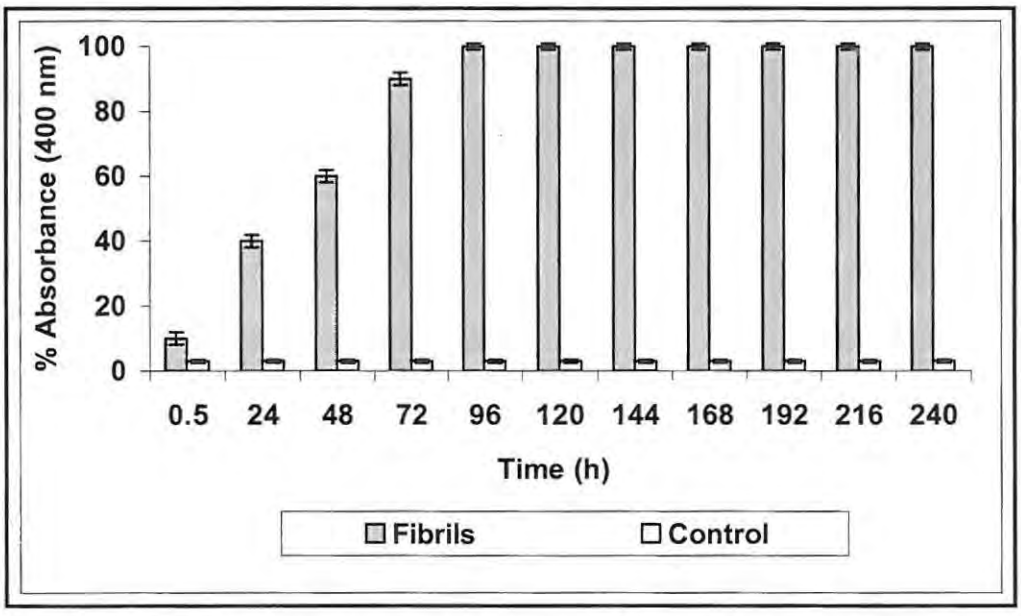


**Figure 4.15 Turbidimetric assay of the percent of insoluble fibrils formed with respect to time from the incubation of nNOS with $A\beta_{32-35}$; values represent the mean (± S.E.M) of three trials.**

The extent of aggregation of each peptide was determined with the formation of insoluble fibrils as determined by turbidity as a function of time. The bar graphs above (Fig. 4.11-Fig. 4.15) reflected the difference in behavior of the different peptide aggregations as portrayed by the response curves of $A\beta_{1-40}$, $A\beta_{22-35}$, $A\beta_{17-28}$, $A\beta_{32-35}$ and $A\beta_{25-35}$. Turbidity was directly related to absorbance at 400 nm. All controls for the various Aß in the absence of nNOS showed little or no turbidity. Thus, it was concluded that the amyloid peptide on its own did not produce insoluble fibrils and this correlated with the control results from the Congo red assay. From the turbidimetric results, the various Aß peptides produced an initial 10-40 % amount of soluble fibrils within 0.5 h that once again correlated with the supposed formation of fibrils within 30 min (chapter 3). All amyloid peptides (Fig. 4.11-Fig. 4.15) demonstrated a 10 % increase in insoluble fibril formation from 72 h to 96 h which more or less correlated with soluble fibril decrease as obtained from the Congo red results (4.6.1). After 96 h the amount of insoluble fibrils reached 100 % for all Aß peptides and remained constant thereafter with time after a period of 10 days.

The turbidity and Congo red results could be explained mechanistically using the 'seeding' and micelle effect (Caflisch and Pellarin, 2006). According to literature, fibril formation is nucleation dependent and starts from the formation of a monomer which exists in a ß-state and then proceeds into an oligomer (aggregation of monomers) (Caflisch and Pellarin, 2006). During this process, two pathways of fibril nucleation are proposed. (1) fibril nucleation on seeds; (2) nucleation within micelles, whose presence is postulated provided that the peptide concentration (C) exceeds the critical micelle concentration ($c^*$). Micelles are in fast equilibrium with free monomers at concentration ($c^*$). Moreover, nuclei are spontaneously formed out of micelles and fibrils grow by binding monomers to fibril ends with the rate proportional to the concentration of free monomers (Lomakin *et al.*, 1997). There is a dynamic equilibrium which also exists between monomers and micelles which suggests that, despite their ordered arrangement, fibrils are dynamic assemblies.

Thus based on literature, the process of nucleation in the turbidity and Congo red assays were simply the aggregation of monomers in the ß-state referred to as the nucleus. This was the first step in fibril formation. Within 0.5 h it was reasoned that the concentration of amyloid peptide (C) was below a certain critical concentration (c*) so that fibrils grew on 'seeds' initially present in solution and as the amount of fibrils increased above a certain critical concentration (c*), micelles began to form in solution which were in equilibrium with soluble Aß monomers. The micelles which formed in solution provided domains of high local protein concentration in which fibril nuclei formed. This was the start of the aggregation process monitored by turbidity. Once the aggregation process began and a critical nucleus was formed, the soluble fibrils detected by Congo red assay, now precipitated out of solution to form insoluble fibrils that were detected by turbidity.

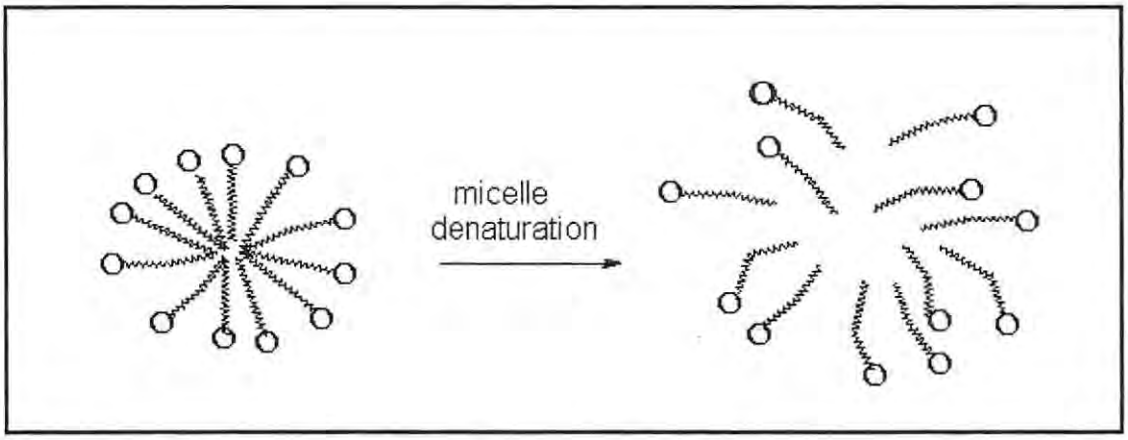


**Figure 4.16 Micelle denaturation model explaining the unexpected increase in soluble fibrils, as detected by the Congo red assay (Chasman, 2003).**

Moreover, the Congo red assay results (4.6.1) have shown a general trend in soluble fibril 'disappearance' with time. The surprising increase in soluble fibrils from the Congo red assay results could further be explained using the model of micelle denaturation (Fig. 4.16) developed by Chasman (2003). Based on the model, it can be suggested that with increased amount of fibrils, there were more micelles in solution which could have resulted in structural disorganization called micelle denaturation. This makes sense because studies in chapter 3 demonstrated the probable chance of fibrils forming rapidly within a few minutes (30 min). The micelles reached a point of saturation due to increasing soluble fibril formation which made them redissolve into solution. This

process destroyed the primary nucleus of peptide aggregation and thus increased the number of soluble fibrils in solution as revealed in the Congo red assay results. It has been suggested that these soluble amyloid oligomers may represent the primary toxic mechanism of amyloid pathogenesis, rather than the mature aggregates (Glabe, 2006).

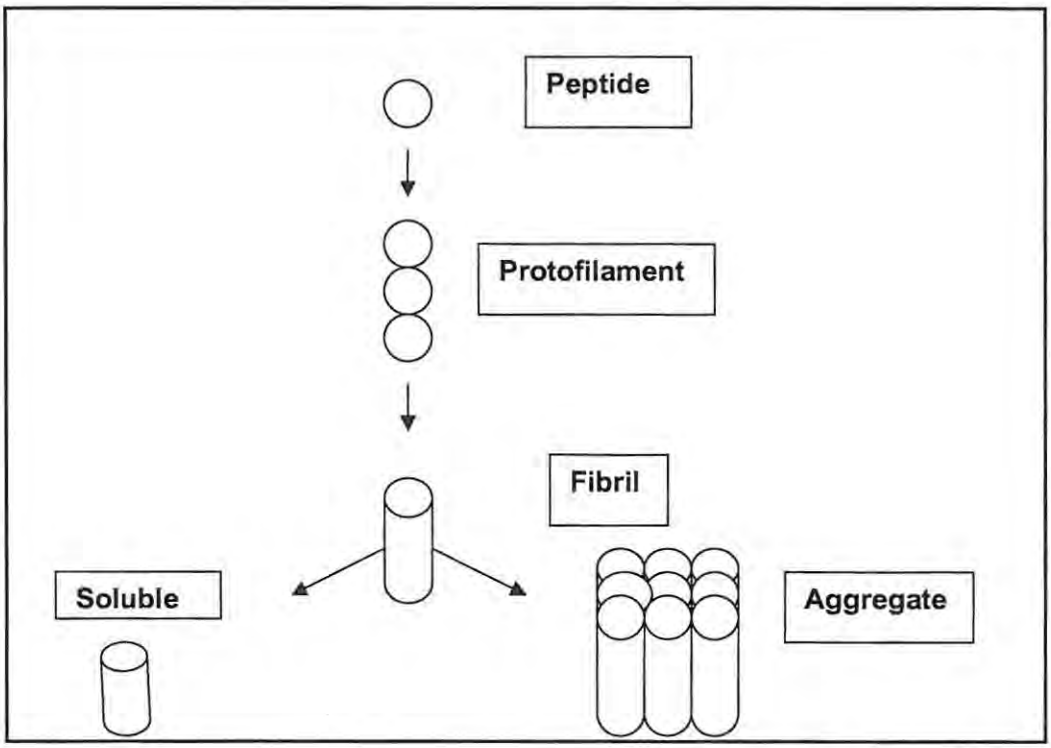


**Figure 4.17 Assembly process observed during amyloid fibril formation (Nilsson, 2004).**

With time the amount of soluble fibrils decreased as they precipitated out of solution to form aggregates which was monitored by the turbidity assay (4.6.2). These aggregates seemed to be the final step in the process of fibril formation as they remained insoluble over some time and did not redissolve into soluble fibrils. The possible existence of 'seed' aggregates could possibly explain the turbidity results obtained for $A\beta_{1-40}$, $A\beta_{22-35}$, $A\beta_{17-28}$, $A\beta_{32-35}$ and $A\beta_{25-35}$. The bar graphs from the turbidity assay (Fig. 4.11-Fig. 4.15) showed a sudden increase in turbidity over time which remained constant due to the formation of aggregates. This sudden increase in turbidity was the result of possible pre-fibril species which are associated with a spontaneous self-association of monomers into large fibrils. Literature (Wang *et al.*, 2006) supported this finding as it has been found that 'seeding' is a relatively fast process which apparently eliminates the requirement of

nuclei formation resulting in spontaneous formation of insoluble fibrils over time. Moreover, the pH of 7.4 was fairly adequate for fibril formation as literature showed that pH optimum for aggregation is in the pH 5-6 range (Santucci *et al.*, 2009).

Thus, it is clear that the fibril, once formed, has two fates: a soluble fibril (detected by Congo red) or an amorphous aggregate (detected by turbidity) (Fig. 4.17). During this process three different kinetic phases are evident: lag, elongation (or growth), and monomer-fibril equilibrium phase. The lag phase refers to the period of time where no aggregation is observed. Elongation or growth phase refers to the addition of monomers on pre-existing fibrils (Caflisch and Pellarin, 2006). The monomer-fibril equilibrium refers to the reversibility of monomers associating into fibrillar aggregates and fibrillar aggregates dissociating into monomers. Moreover, the formation of a protofilament (Fig 4.17) is an intermediate step from a monomer to fibril (Fülöp *et al.*, 2006). It must be noted, however, that not all amyloid peptides are converted into aggregates via the protofilament step.

### 4.6.3 Thioflavin-T (ThT) assay

When each of the amyloid peptides [$A\beta_{1-40}$, $A\beta_{22-35}$, $A\beta_{17-28}$, $A\beta_{32-35}$ and $A\beta_{25-35}$] at increasing concentrations was incubated with nNOS in the presence of thioflavin-T there was a gradual increase in fluorescence up to a maximum at saturation (Fig. 4.18). This change in fluorescence initially appeared to be linear (Fig. 4.19), not only reflecting that nNOS was indeed catalytic towards fibril formation, but indicated a direct estimation of both the concentration and rate of formation of fibrils. This was consistent with the possibility that amyloid peptides were converted into a form that could no longer bind to the enzyme. nNOS induced $A\beta_{17-28}$ to produce fibrils both four-fold faster and more concentrated than those from $A\beta_{32-35}$ and the change in fluorescence reflected that fibril production from $A\beta_{17-28}$ was 10-fold greater than $A\beta_{32-35}$ (Fig. 4.19). The other peptides [$A\beta_{1-40}$, $A\beta_{22-35}$, and $A\beta_{25-35}$] afforded rates of formation and concentrations only two to three-fold more (Fig. 4.18). Also, change in fluorescence for these peptides [$A\beta_{1-40}$, $A\beta_{22-35}$ and $A\beta_{25-35}$] reflected that fibril production was also two - three-fold less than $A\beta_{17-28}$.

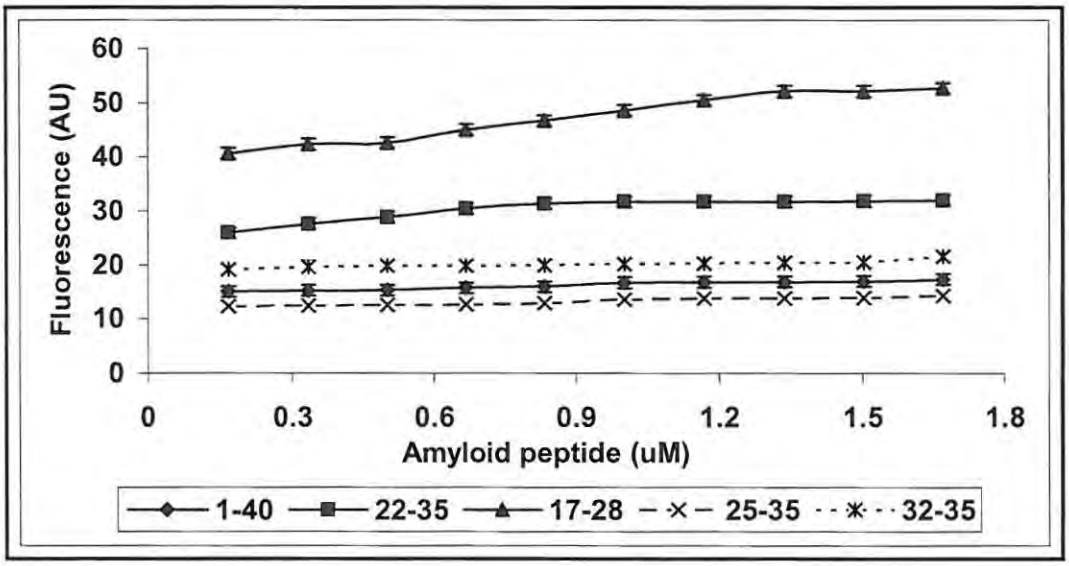


**Figure 4.18 nNOS catalyzed fibrillogenesis of amyloid peptide fragments [$A\beta_{1-40}$, $A\beta_{22-35}$, $A\beta_{17-28}$, $A\beta_{32-35}$ and $A\beta_{25-35}$] quantified by thioflavin-T fluorescence, values represent the mean (± S.E.M) of three trials.**

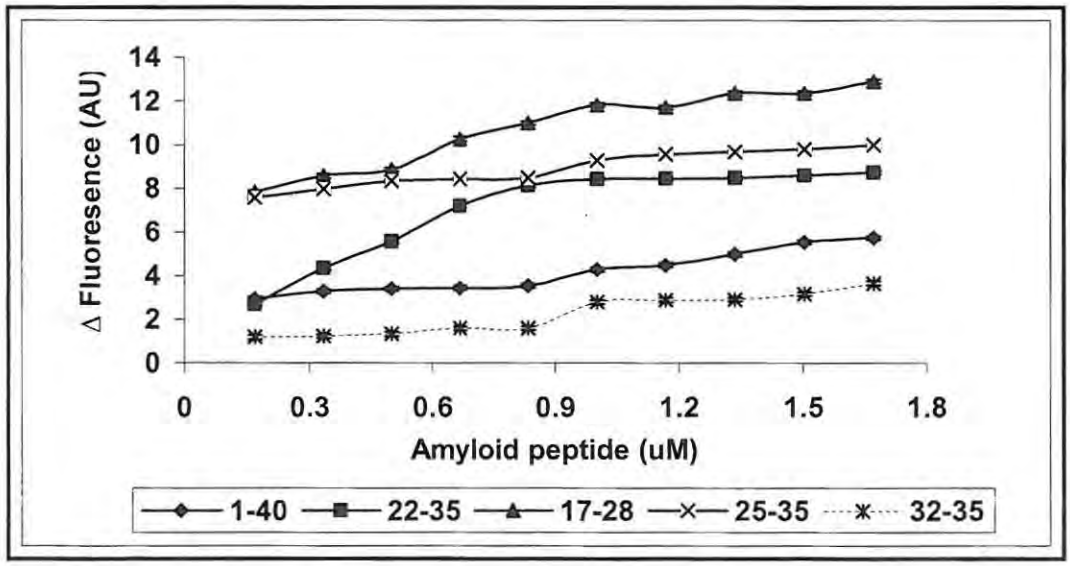


**Figure 4.19 Change in fluorescence plot of nNOS catalyzed fibrillogenesis of amyloid peptide fragments [$A\beta_{1-40}$, $A\beta_{22-35}$, $A\beta_{17-28}$, $A\beta_{32-35}$ and $A\beta_{25-35}$] quantified by thioflavin-T, values represent the mean (± S.E.M) of three trials.**

The incubation of nNOS with amyloid peptides and thioflavin-T (Fig. 4.18 and Fig. 4.19) was performed for 30 min and substantiated the results obtained for Congo red and turbidity (4.6.1 and 4.6.2). This was the case as fibrils began to rapidly form within a similar time frame of 0.5 h, irrespective of whether the fibril was soluble or insoluble for the thioflavin-T assay. The possible explanation of rapid fibril formation as detected by thioflavin-T could be similarly explained via the nucleation effect which was accelerated by seeding. An ordered nucleus was formed only after a lag phase and in a 'supersaturated' solution of fibrils formed from 'seeds' (initially present) which eventually exceeded the critical concentration (c*) of amyloid peptide and any fibrils already present in solution (Lansbury and Rochet, 2000). This effect was enhanced by micelle formation which provided nuclei for new fibrils, thus allowing for spontaneous formation of fibrils with time just as was the case in the Congo red assay. In addition, the presence of pre-fibril species called protofibrils may have also undergone lateral or 'end-to-end' fusion to form short thick fibrils that were detected by thioflavin-T, as documented in literature (Lansbury and Rochet, 2000).

### 4.6.4 Transmission electron microscopy (TEM)

The structure of the insoluble amyloid fibrils generated from the proteolytic action of nNOS with $A\beta_{17-28}$ was examined under TEM to investigate aggregate morphology. Within the first 30 min, fibrils appeared mainly as short, rod-like structures (Fig 4.20, C) and after 24 h, fibrillization of amyloid peptides appeared to have progressed from short discrete fibrils to a mass of much longer fibrils in a branched network (Fig 4.20, D). This supported the morphology pattern of fibrils as illustrated from literature (McLaurin *et al.*,1998; Fülop *et al.*, 2006; Chakrabartty *et al.*, 2000). These observations also substantiate Congo red, turbidity and thioflavin-T results which showed that fibrils were produced rapidly within 0.5 h and steadily increased in quantity after 24 h. This was especially true for turbidity results (4.6.2) which pointed to a steady increase in insoluble fibrils being formed between 24-120 h. This indicated that the fibrils that initially formed within 30 min remained soluble and then after 24 h aggregated to form a mass of slender, long fibrils in a typical branched network (Fig 4.20, D).

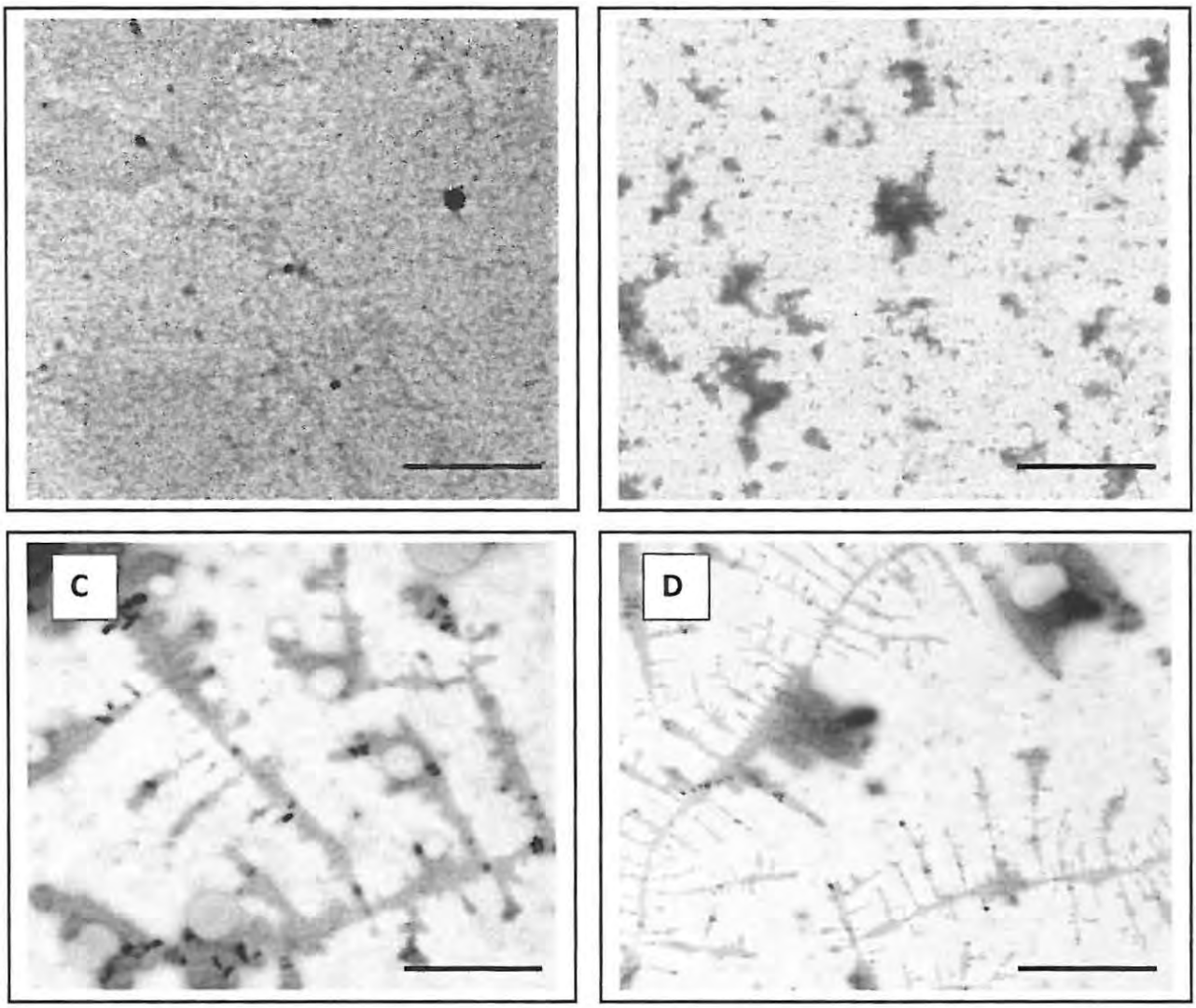


**Figure 4.20 Transmission electron microscopy views of: (A.) nNOS alone (B.) Peptide $A\beta_{17-28}$ alone (C.) short rod-like structures of $A\beta_{17-28}$ (D.) branched network of fibrils from $A\beta_{17-28}$ (scale bar = 100 nm).**

The observed structures above (Fig 4.20, C and D) could be confidently classified as fibrils of a length of between 100-200 nm because according to the schematic diagram (Fig. 4.21), fibrils have a maximum size range of 200 nm. Any monomers, small oligomers, and peptide aggregates in the protofibril (also called protofilament) size-range (< 200 nm) (Fig. 4.18) were, however, not visualized by TEM presumably because the lag time was too long and surpassed protofibril formation or the protofibrils rapidly dissolved into monomers in solution as suggested in literature (Lansbury and Rochet, 2000).

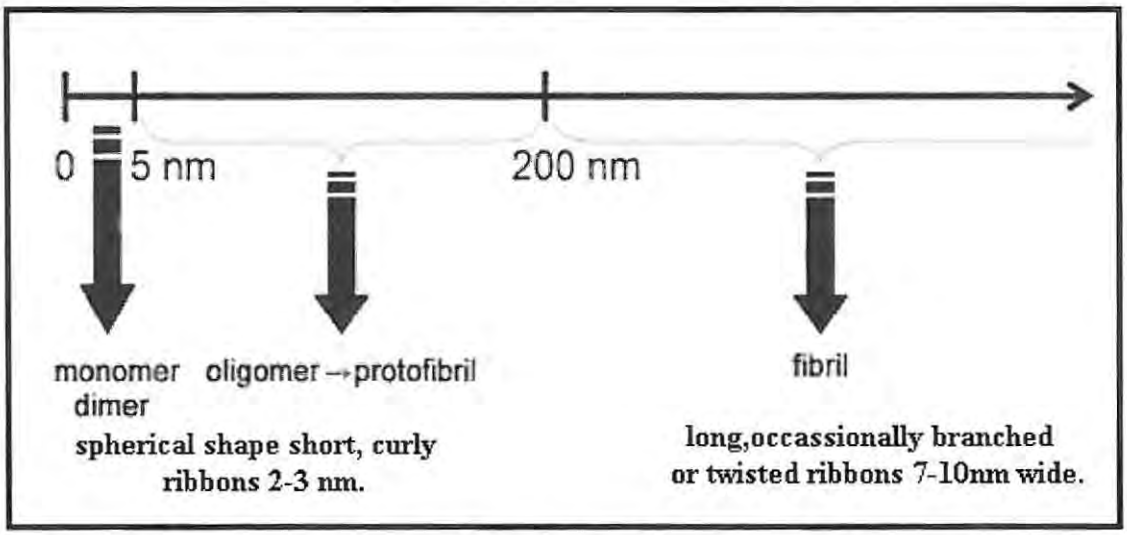


**Figure 4.21 Schematic diagram of fibril assembly processes (Fülop *et al.*, 2006)**

Moreover, $A\beta_{17-28}$ revealed extensive formation of fibrils (Fig. 4.20, C and D) compared to both of the controls (Fig. 4.20, A and B). This may indicate firstly that during conversion into fibrils, the native fold of $A\beta_{17-28}$ was destabilized through rapid unfolding and/or slower refolding of its amino acids and thus was associated with enhanced fibril formation. Such reasoning supports the principle that fibrillogenesis requires the partial unfolding of globular proteins or the partial folding of disordered proteins (Lansbury and Rochet, 2000). Moreover, secondly according to literature some amyloidogenic proteins (referred to as 'fragments') are released from precursors by proteolysis. Mutations that enhance the proteolytic sensitivity of the precursor promote fibril formation by causing an increase in the steady-state level of the fibrillogenic fragment (Lansbury and Rochet, 2000). In the current study of fibrillogenesis, the enzyme nNOS was the precursor and when $A\beta_{17-28}$ dissociated from the enzyme, a mutation in the native fold of the peptide promoted fibril formation. Thirdly, the greater mass of fibrils from $A\beta_{17-28}$ may be attributed to the secondary nucleation effect which involves the addition of monomers to existing fibrils as supported by literature. Recent literature (Rischel *et al.*, 2009) highlighted the positive feedback from secondary nucleation associated with exponential growth kinetics observed for many proteins including amyloid peptides.

It must be noted however, that the morphology of fibrils was different depending on the degree of aggregation. It was significant, therefore to carefully select the type of solvent in which to dissolve the peptide, because the different solvents applied for solubility promote different aggregation profiles, conformations, and consequently, different size distributions of the amyloid aggregates (Fülop *et al.*, 2006). In the current experiment, $A\beta_{1-40}$, $A\beta_{22-35}$, $A\beta_{17-28}$, $A\beta_{32-35}$ and $A\beta_{25-35}$ were dissolved in DMSO (dimethyl sulfoxide), an organic solvent which induced solubility of the peptide. Other organic solvents could have also been used such as TFE (trifluoroethanol); TFA (trifluoroacetic acid); HFIP (hexafluoroisopropanol) or concentrated base such as NaOH. Moreover, fibril formation was shown to be modulated by several factors, including pH. In the current chapter, amyloid fibrils were observed thin and branched at a pH 7. This was consistent with literature where fibril morphology alternated between short, thick fibrils and long, slender fibrils at the same pH (Chakrabartty *et al.*, 2000).

In addition, adsorption phenomena can also have a large influence on the accuracy of filament length measurements of fibrils. In fact, the lack of any protein adsorption to the grid is typically a good indication that there is little to no protein aggregation, amyloid or otherwise which was not the case in the present TEM results. The resultant filaments which were detected by TEM occurred only after adsorption of reaction products onto the hydrophobic surface of carbon nickel grids. Previous literature (Kuret and Necula, 2004) has shown that adsorption depends upon temperature, pH, ionic strength, and protein concentration. In addition, adsorption from protein mixtures can be a competitive and dynamic process, where initially adsorbed proteins can undergo conformational changes and displace other proteins in a time- and concentration-dependent manner. Thus, the branched network of fibrils observed by TEM could have likewise been influenced by the process of adsorption, thus affecting the formation of fibrils.

## 4.7 Conclusion

The Congo red assay (Klunk *et al.*, 1989) proved to be successful in the quantification of soluble fibrils. However, literature has shown that the dye can bind to both insoluble and soluble aggregates (Howlett *et al.*, 1995). Hence, Congo red was not able to clearly

distinguish between soluble and insoluble aggregates, both of which were formed by beta-amyloid in solution and this may have afforded the rather unexpected results with both the inhibition of the enzyme by amyloid peptides (chapter 3) and the binding of the Aß to the enzyme leading to fibrillogenesis. In addition, the assay was specific but not sensitive. This was because some amyloid deposits which formed fibrils upon staining with the dye generally had other characteristics of amyloid deposits. In addition, the amyloid deposits may, in turn, have had characteristics of other protein deposits which were not positive for Congo red staining. Additionally, the molecular packing of fibrils could have obscured Congo red binding. Thus, for these reasons, the use of Congo red as a rigid criterion for the identification of amyloid fibrils *in vitro* was critically considered. Nevertheless, the Congo red assay proved to be an objective assay as it was less prone to misinterpretation and was easily combined with microscopic analysis.

In addition, the turbidity assay (Evans *et al.*, 1995), proved to be a simple and reliable method in identifying the process of aggregation that was driven by the formation of insoluble fibrils. It was clear that the various Aß showed a quick tendency to self-assemble and form insoluble aggregates. Moreover, it is very likely that these amyloid fragments also tend to aggregate rapidly in the brain, thus contributing to the powerful toxic effects on neuronal activity which is influential in the onset of AD. Most importantly, results obtained thus far have shown that when Aß binds to nNOS, the enzyme is inhibited (chapter 3). Then, after several minutes, the peptide dissociates and is converted into a soluble fibril. There was a restoration of enzyme activity and a build up of soluble fibrils which remained attached to the enzyme but did not inhibit activity. Moreover, when a soluble fibril associated with nNOS, an enzyme-fibril complex in solution [nNOS + $(Fib)_{sol}$] was formed via the aggregation of more fibrils binding with time. Eventually the [nNOS + $(Fib)_{sol}$] complex reached a saturation point in solution resulting in a rapid dissociation of fibrils which accounted for the surprising increase in soluble fibrils with time as revealed by Congo red. The decrease in soluble fibrils was a reflection of an increase in insoluble fibril formation which was detected by turbidity. The thioflavin-T assay showed that some amyloid peptides produce more fibrils than others and indicated that $Aß_{17-28}$ was the most prominent peptide for fibrillogenesis.

The technique of transmission electron microscopy (TEM) was successful in visualizing the long, slender and branched network of fibrils and confirmed that $A\beta_{17-28}$ produced the most amount of fibrils. Moreover, the addition of nNOS to the $A\beta_{17-28}$ solution facilitated the process of fibrillogenesis and once again confirmed that nNOS is an amyloidogenic catalyst in fibrillogenesis. It may also suggest that amyloid fibril formation requires proteolysis and that different amyloid peptides produce different quantities of fibrils over a given time due the process of misfolding in proteins. Nevertheless, the technique of TEM has potential problems when visualizing fibrils on the carbon/formvar grids. This could occur when the composition of the protein sample solution damages the TEM grids or when salt crystals form and obscure the identification of fibrils. In addition, many things on a TEM grid can be mistaken for protein aggregates. For example, blemishes on formvar or carbon grids may be caused by some solvents or by a poor grid coating resulting in interesting shaped protein aggregates. Moreover, a completely blank grid is observed if the formvar or carbon has been torn. This usually occurs when too high a protein concentration is used or when all the protein in solution does not settle on the grid (Nilsson, 2004). However, none of these factors played a major role in the resolution and clarity of TEM photos from the present work. TEM proved to be an effective tool for the investigation of fibrils from amyloid peptides and demonstrated that Aß peptides are made up of soluble oligomers which do form fibrils when incubated with nNOS for a time period.

# V

# Fibrillogenesis: Quenching, FRET and computational molecular modeling.

## 5.1 Introduction

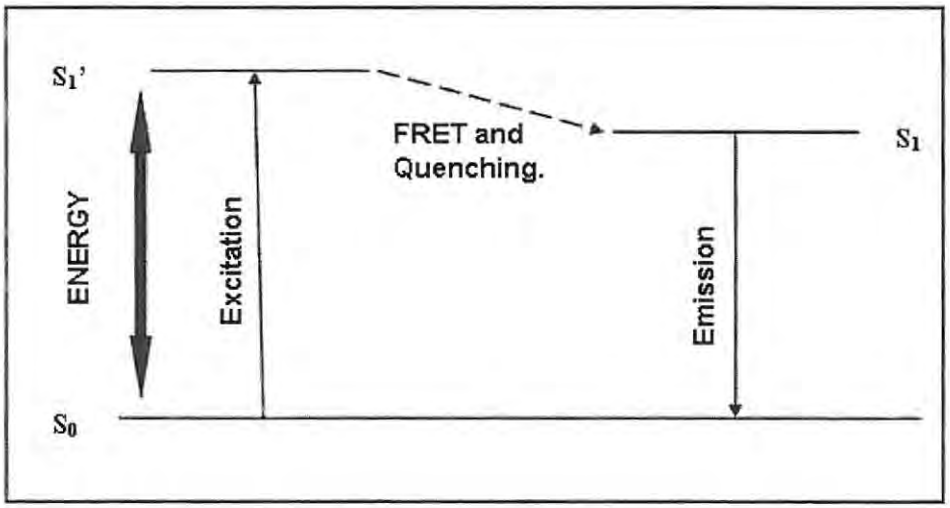


**Figure 5.1 Jablonski diagram illustrating the processes of absorption (excitation) and fluorescence (emission).**

Fluorescence spectroscopy involving FRET and quenching and computational molecular modeling are used as additional tools to examine protein/enzyme structure and dynamics. They are also used to study conformational changes induced when the amyloid peptide is bound to nNOS relative to the fraction and distance of significant tryptophan amino acids on the surface and around the active site of nNOS. The Jablonski diagram describes the absorption and emission of fluorescence by a molecule (Fig. 5.1). A chromophore within a molecule absorbs light energy to undergo the first step of electron excitation from the

ground state ($S_0$) to a singlet excited state ($S_1$'). The second step in the process involves collision quenching, fluorescence resonance energy transfer (FRET) and intersystem crossing which also results in energy loss (Fig. 5.1). The third step in the process occurs when the excited molecule undergoes energy loss and returns to the ground state by the emission of light which is termed fluorescence (Freifelder, 1976). Moreover, the probability of fluorescence is described by the quantum yield (Q) which is the ratio of the number of emitted to absorbed photons (unit of light). A reduction in Q results in quenching (Freifelder, 1976).

The instrumentation used to measure fluorescence is called a spectrofluorometer (Fig. 5.2). A high intensity light beam passes through a monochromator for the selection of an excitation wavelength (i.e., a wavelength efficiently absorbed by the fluor). The exciting light beam then passes through a cell containing the sample. Fluorescence is emitted in all directions by the sample, but most systems look at only that emitted at 90° with respect to the exciting light. This differs from an absorption spectrophotometer where only transmitted light would be detected. The fluorescence then passes through a monochromator for wavelength analysis and finally falls on a photosensitive detector (usually a photomultiplier tube) (Fig. 5.2) (Freifelder, 1976).

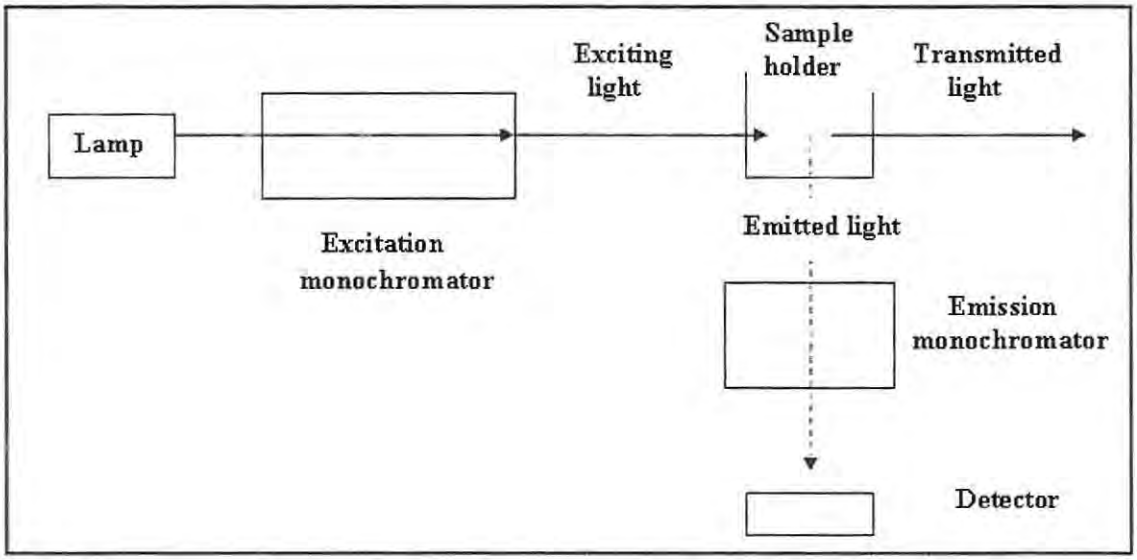


**Figure 5.2 Spectrofluorometer used in fluorescence analysis (Freifelder, 1976).**

In addition, the molecules involved in fluorescence are known as fluors. There are two types of fluors used in fluorescence analysis of proteins namely; intrinsic fluors (usually aromatic rings within the protein itself) and extrinsic fluors (added to the protein e.g., the quencher molecule fluorescein used in FRET). For proteins, there are only three intrinsic fluors, namely tryptophan, tyrosine and phenylalanine. However, phenylalanine has a very low quantum yield and tyrosine fluorescence is frequently very weak due to quenching (Freifelder, 1976). Thus, in this chapter tryptophan amino acids were involved in quenching and the subsequent estimation of the Stern-Volmer constant ($K_{SV}$). In addition, four empirical 'rules' obtained from studies of model compounds whose structure and conformation were well-known can be applied to fluorescence quenching (Freifelder, 1976).

1. The tryptophan must be internal and in a nonpolar environment when the maximum wavelength ($\lambda_{max}$) of fluorescence shifts to shorter wavelengths. On the other hand, the protein is in a nonpolar medium when tryptophan is either on the surface of the protein or the solvent induces conformational change to bring the amino acid to the surface.

2. If a substance is known to be a quencher, such as a fluorescent probe, and quenches the tryptophan fluorescence, the amino acids must be on the surface of the protein. If it fails to do so, the amino acid may be internal, in a crevice whose dimensions are too small for the quencher to enter or the amino acid may be in a highly charged region and the charge might repel the quencher.

3. If a substance affects the fluorescence of a protein, it must do so by producing a conformational change in the protein.

4. If a substance binds to a protein and tryptophan fluorescence is quenched, either there is a conformational change as a result of binding or a tryptophan is in or very near the binding site.

Moreover, computerized molecular modeling involves the use of graphical, mathematical or physical representations to help understand and predict the properties of 3-D protein molecules (Woodward and Li, 1999). This is significant as the design of novel

therapeutic agents in diagnostic disease research is based on the knowledge of the three-dimensional (3-D) structure of target proteins. Computerized molecular modeling helps determine four separate levels of protein structure: primary, secondary, tertiary and quaternary structures (Freifelder, 1976; Palmer, 1995).

1. *Primary structure*: refers to the sequence of amino acids making up the protein. A peptide bond connects the a-carboxyl group of each amino acid to the a–amino group of the next in the chain.

2. *Secondary structure*: refers to the regular, repeating patterns formed by the backbone of at least part of a polypeptide chain and stabilized by hydrogen bonding. It is associated with the orientation of each monomer within the protein.

3. *Tertiary structure*: refers to the 3-D structure associated with the relative orientation of the amino acid side chains which are in close proximity to each other and is stabilized by bonding between the chains.

4. *Quaternary structure*: refers to the interaction between several 3-D structures of proteins to form complex structures such as multi subunit proteins.

In case of AD, the beta-amyloid peptides form neurotoxic aggregates by a process called 'misfolding', which means that the peptides undergo a conformational change from the soluble a-helical/random coiled structure to a ß-hairpin with a high propensity towards aggregation (Fülop *et al.*, 2006). A number of models have been proposed for the actual peptide composition of fibrils, but it is generally accepted that the major ß-sheet regions of the peptide are formed by the hydrophobic internal residues $A\beta_{17-21}$ and C-terminal residues $A\beta_{29-42}$ (Lansbury and Rochet, 2000). Amyloid fibril formation is considered to be a consequence of the ability of the main chain of a protein to form hydrogen bonds. In addition, it is the competition between hydrophobic interactions (Fig. 5.3) and hydrogen bonding which is a major determinant of the aggregation process (Santucci *et al.*, 2009). Evidence for the importance of the competition between hydrogen bonding and hydrophobic interactions in the aggregation process was found in studies in which changes in solvent polarity resulted in a change in the hydrogen bonding interactions and subsequently in the formation of beta-amyloid aggregates (Calamai, 2005).

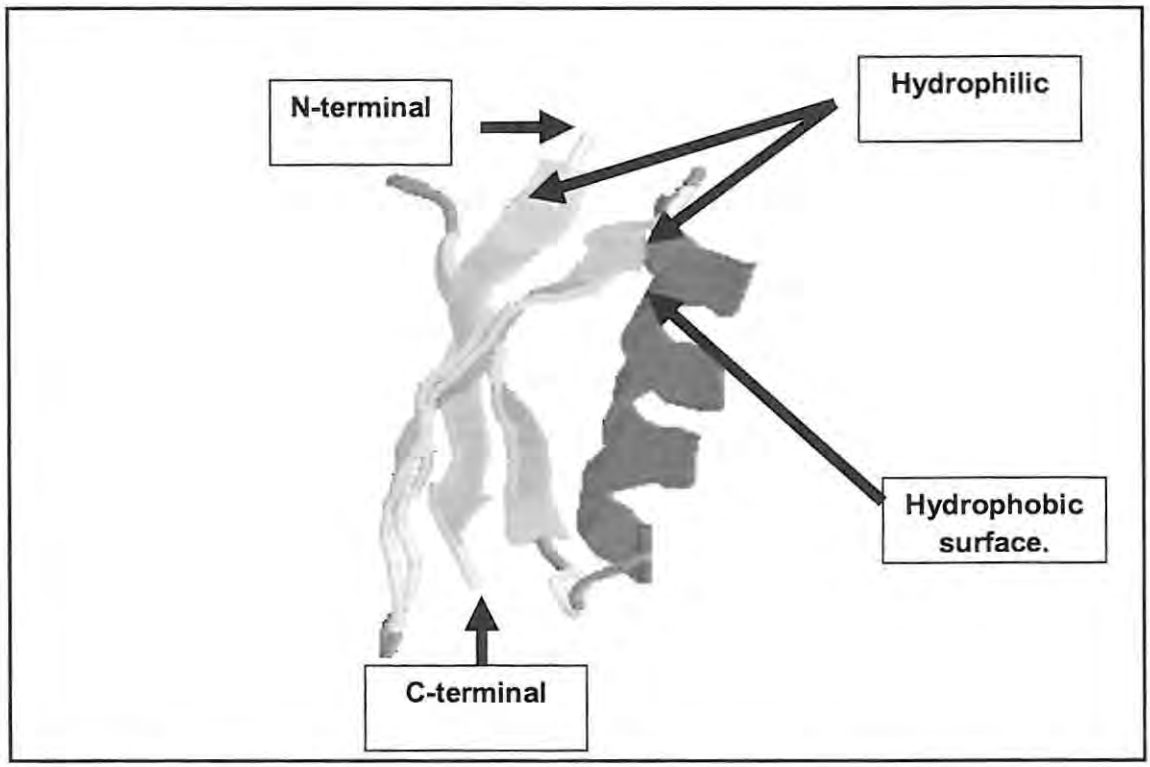


**Figure 5.3 Secondary structure of an arbitrary protein depicted in cartoon and coloured structure (Lesk, 2001).**

The alpha helix (magenta strand) and beta-pleated sheets (yellow strands) with the characteristic N and C-terminal is displayed (Fig. 5.3). The structure is depicting the hydrophobic effect which predicts the tendency of hydrophobic side chains to sequester themselves in the interior of a protein, away from contact with solvent, thus promoting aggregation affects significant to AD

# 5.2 Theory of techniques utilized

## 5.2.1 Quenching

Fluorescence quenching is an additional useful method to obtain information about the conformational and dynamic changes in proteins through the use of an intrinsic or extrinsic quencher. Fluor molecules within a protein such as tryptophans or other amino acids may behave as possible intrinsic quenchers thus decreasing the quantum yield of fluorescence (Q). Measuring the fluorophore accessibility to quenching using different quenchers allows estimation of the relative position of a fluorophore in the protein.

Moreover, such quenchers produce either static or dynamic quenching. Static quenching is between the quencher and a fluorophore, while dynamic quenching requires bimolecular collisions in which the quencher takes away the energy of the excitation previously absorbed, and leaves less energy for the process of fluorescence emission (Matyus *et al.*, 2006). In this chapter, quenching analysis was used to determine two parameters essential to studying conformational changes in nNOS. The first parameter was the Stern-Volmer constant ($K_{sv}$) which employed the dependence of the fluorescence intensity on the concentration of a quencher and reflected the degree of quenching.

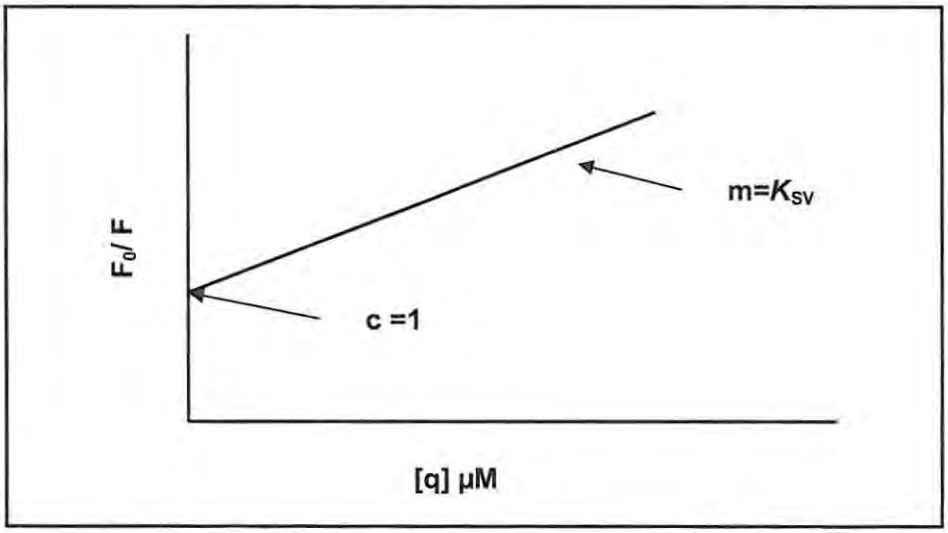


**Figure 5.4 Classical Stern-Volmer plot where $K_{SV}$ is equivalent to the gradient (m) and the intercept (c) must be equivalent to 1.**

$$\frac{F_0}{F} = 1 + Tk[q] \qquad \text{..... Eq (7).}$$

where $F_0$ = fluorescence in the absence of a quencher (q)

F = fluorescence in the presence of a quencher (q)

[q] = quencher

T = lifetime of excited fluor

k = rate constant

Tk = Stern-Volmer constant ($K_{sv}$).

The classical Stern-Volmer plot (Fig. 5.4) and its corresponding Stern-Volmer equation of the straight line (Equation 7) were used in the estimation of $K_{sv}$. In addition, the second parameter (Θ) was a reflection of the fraction of tryptophans near or on the surface of the enzyme. Θ may be determined from equation 8 which is also that of a straight line (Fig. 5.5).

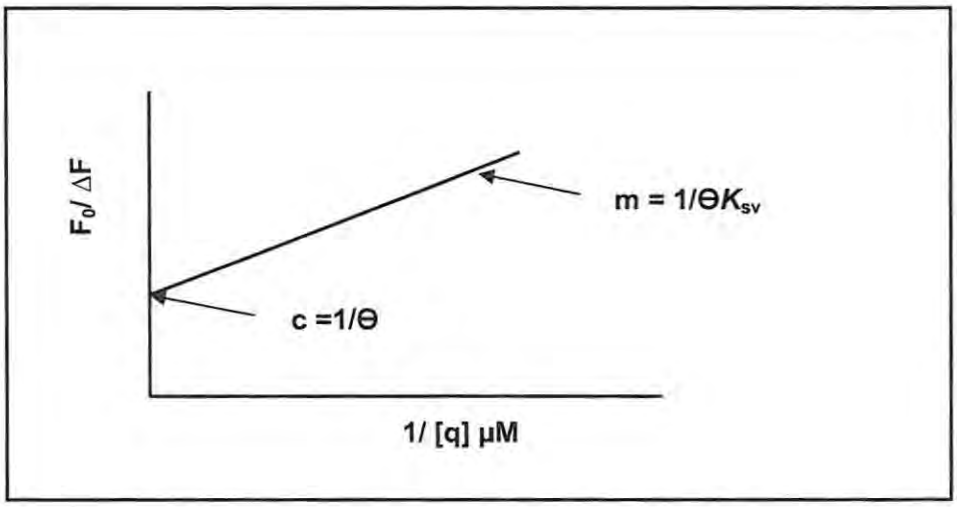


**Figure 5.5 Classical Θ spectrofluorimetric plot with Θ equivalent to the reciprocal of the intercept (c).**

$$\frac{F_0}{\Delta F} = \frac{1}{\Theta K_{SV}[q]} + \frac{1}{\Theta} \quad \text{..... Eq (8).}$$

where ΔF is change in fluorescence and [q] is concentration of the quencher.

### 5.2.2 Fluorescence resonance energy transfer (FRET)

The process called fluorescence resonance energy transfer (FRET) represents a special type of quenching and is used to measure intramolecular and intermolecular distances to provide valuable information regarding the dynamic properties of protein systems (Matyus *et al.*, 2006). An extrinsic type of quencher called fluorescein was used in FRET

studies. Fluorescein is covalently attached to the enzyme via a cysteine thiol group (Matyus *et al.*, 2006). The process of FRET is based on the dipolar coupling between the emission dipole of a donor and the absorption dipole of an acceptor (Fig. 5.6).

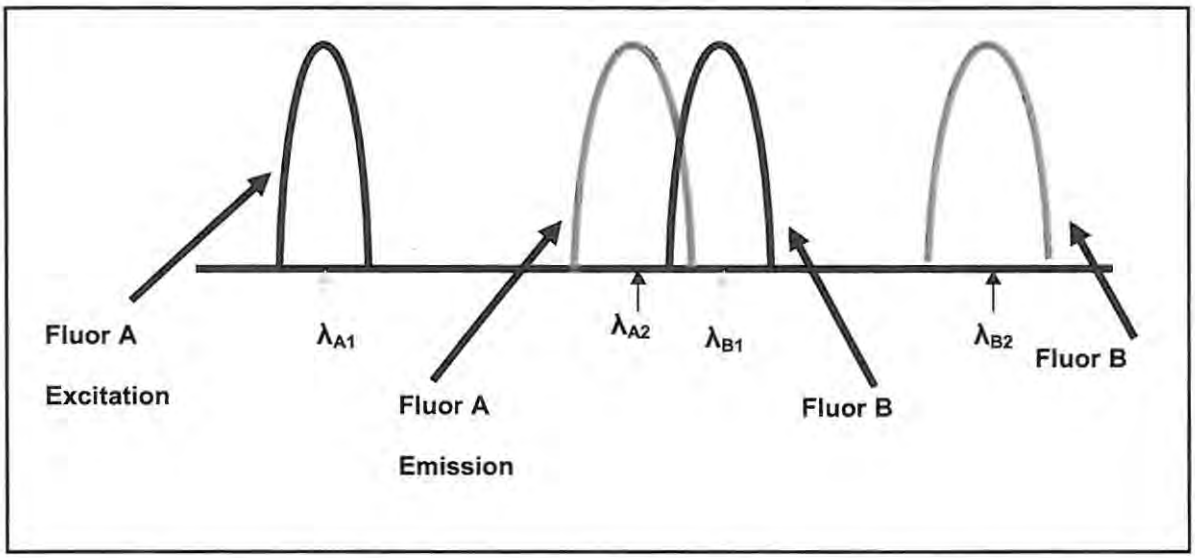


**Figure 5.6 Illustrative process of FRET involving the donor (fluor A) and the acceptor (fluor B).**

As illustrated (Fig. 5.6), the excitation energy of the donor molecule is transferred to an acceptor molecule without the emission of a photon. Absorption spectrum of the acceptor (fluor B) must overlap with the fluorescence emission spectrum of the donor (fluor A). This results in a decrease in donor emission intensity accompanied by an increase in acceptor emission intensity. If these fluors (fluor A and B) have unique locations in the protein, it will be possible to measure distances or changes in distances within proteins (Ishii *et al.*, 1999). In addition, the efficiency of energy transfer (E) is a quantitative measure of the number of quanta that are transferred from donor (D) to acceptor (A). In the most popular method of determining E, the steady-state donor fluorescence intensity is measured both from a sample containing only D (i.e., $F^D$) and from a corresponding sample containing acceptor (A) as well as donor (D) (i.e., $F^{D,A}$) . If the values of $F^D$ and $F^{D,A}$ are normalized to their respective concentrations of D, the efficiency for a single D-A pair can be calculated according to equation 9 (Clegg, 1995). Moreover, the use of FRET results from the strong dependence of the rate and efficiency of energy transfer on the sixth power of the distance R between D and A in equation 9. The strong dependence

of E on R has led to the often quoted reference to FRET as a 'spectroscopic ruler' (Clegg, 1995).

$$\text{Efficiency of Transfer} = 1 - \frac{F^{D,A}}{F^{D}} = \frac{1}{1+(R/R_0)^6} \qquad \text{..... Eq (9).}$$

where $F^{D,A}$ = fluorescence of donor (D) and acceptor (A)

$F^{D}$ = fluorescence of donor (D)

R = distance between donor and acceptor molecules

$R_0$ = Förster distance (52 Å).

The Förster distance ($R_0$) is derived from the Förster theory which was demonstrated using a series of polyproline oligomers having a naphthyl donor at one end and a dansyl acceptor at the other end. The theory established that $R_0$ values (in Å) represent the distance at which fluorescence resonance energy transfer from the donor to the acceptor molecule is 50 % efficient which allowed estimation of distances in the range from 10 to 100 Å (Ishii *et al.*, 1999). Moreover, the greater the $R_0$ value, the better the probability of FRET between fluorochromes. It should be noted that $R_0$ depends on the relative orientation of the donor and acceptor ($k^2$), the refractive index (n), the quantum yield of the donor ($Q_D$), and the overlap integral between the acceptor emission and donor excitation (J) as shown by the equation 10.

$$R_0 = 8.79 \times 10^{-5} (Q_D k^2 n^{-4} J) \qquad \text{..... Eq (10).}$$

Moreover, the following principles should be followed when conducting FRET experiments:

- The presence of a single donor and acceptor.

- $R_0$ (Förster distance) must be known depending on the nature of the donor-acceptor pair. Also, the donor and acceptor must be within 0.5x $R_0$ – 1.5x $R_0$ from each other. These measurements give the average distance between the two fluorphores.
- Relative orientation of donor and acceptor should be known.
- Addition of fluors should not alter the macromolecule being studied.

In this chapter, FRET was used to estimate the relative distances and the primary position of the tryptophan residues relative to the active site of nNOS in the presence of both inhibitor and substrate.

### 5.2.3 Computerized molecular modeling

There are essentially three structure-based design approaches that can be used to modify a 3-D protein structure (Chasman, 2003):

1. *Geometric searching:* an approach which enables finding molecules that match a set of distance and angular relationships between specific molecular features.
2. *De novo design*: an approach which constructs molecules directly within the receptor site, either by combining and linking separately docked fragments or by 'growing' molecules from a docked anchor fragment.
3. *Docking*: a method which fits a small molecule (ligand) into the binding site of a receptor (protein) by optimization of steric, hydrophobic, and electrostatic interactions. The first step in molecular docking is to identify those regions on the protein structure that, upon binding to a ligand, would interfere with normal function. These include the enzyme active site or the binding site of a receptor.

The aim of this chapter was to use a simple molecular modeling programme called RasMol (Raswin Molecular graphics) to analyze the active site of nNOS and the conformational changes induced when Aß peptide binds to the active site of the enzyme. Such analyses allowed the investigation and studying of the mechanisms of beta-amyloid and nNOS interaction. In addition, molecular docking was attempted in order to visualize

a suggested orientation of the Aß peptide within the receptor site of the enzyme. RasMol is a molecular graphics program intended for the visualization of proteins and reads in molecular co-ordinate files in a number of formats. This enables the molecule to be displayed on the screen in a variety of colour schemes and representations. The loaded molecule may be shown as wire frame, stick bonds, alpha-carbon trace, space filling (CPK) spheres, macromolecular ribbons (either smooth shaded solid ribbons or parallel strands), hydrogen bonding and dot surface. RasMol can further report information about atoms, including the atom's name, and the residue and macromolecular chain in which it resides; also bond distances and angles. However, RasMol cannot move two molecules, or two parts of a molecular complex, relative to each other.

## 5.3 Aims

To utilize the following techniques to study amyloid fibril formation:

- Technique of fluorescence quenching to calculate $K_{sv}$ (Stern-Volmer constant) and Θ (fraction of tryptophan residues near or on the surface of the enzyme) in order to measure the degree of quenching from amyloid peptides and the ease of accessibility of the various Aß to fluor molecules.

- Technique of fluorescence resonance energy transfer (FRET), using the quencher fluorescein to evaluate the distance of intrinsic fluors (tryptophan residues) from the active site of nNOS and to predict the conformational change of the enzyme via the shifting of these residues around the active site of nNOS.

- The use of RasMol (Raswin Molecular graphics) as a computerized modeling technique to understand the suggested orientation and nature of Aß binding to the nNOS active site.

## 5.4 Reagents and materials

### 5.4.1 Reagents

Amyloid peptides $A\beta_{1-40}$, $A\beta_{22-35}$, $A\beta_{17-28}$, $A\beta_{32-35}$ and $A\beta_{25-35}$; $N^a$-benzoyl-L-arginine ethyl ester hydrochloride (BAEE) and fluorescent buffer were obtained from Sigma-Aldrich (South Africa). Commercial neuronal nitric oxide synthase obtained from rat brain; thioflavin-T (ThT); Tris (hydroxymethyl) aminomethane; fluorescein and NaOH were obtained from Merck Chemicals (South Africa).

### 5.4.2 Materials

A fluorescence spectrophotometer (model F-2500, 230 V, 1.8 A, 50/60 Hz), obtained from Hitachi® was used to conduct fluorescence spectroscopy. A pH meter (Ionolab) was purchased from Sigma Aldrich (South Africa). Computerized molecular modeling was performed using Rasmol (Raswin Molecular graphics) (Sayle and Bernstein) [1998-2001] [V.2.7.2.1].

## 5.5 Methods

### 5.5.1 Estimation of $K_{sv}$ and Θ parameters in fluorescence quenching

Fluorescence quenching was performed using the graphical method of the Stern-Volmer and Θ plot sketching as previously described by (Lakos *et al.*, 1995; Matyus *et al.*, 2006). The thioflavin-T assay was the fluorescence quenching assay method performed as previously outlined in section 4.5.3 and $K_{SV}$ and Θ was obtained from the respective plots of equation 7 and 8.

### 5.5.2 Fluorescence energy transfer (FRET)

The FRET assay procedure was based on a method previously described but with slight modifications (Prostak *et al.*, 2005). The amyloid peptide, $A\beta_{17-28}$, was of particular interest in the quenching experiments due to it inhibiting nNOS more compared to the other peptides. Two separate reactions were performed: Reaction 1 was between the acceptor chromophore (BAEE) and fluorescein (donor chromophore). The reaction included fluorescein (200 µl); nNOS (50 µl), BAEE (200 µl) and fluorescent buffer (50 µl). Reaction 2 was between the acceptor chromophore ($A\beta_{17-28}$) and fluorescein (donor chromophore). The reaction included fluorescein (200 µl); nNOS (100 µl); $A\beta_{17-28}$ (100

µl) and fluorescent buffer (100 µl). Reaction controls were prepared in a similar way as mentioned above with the omission of BAEE and $A\beta_{17-28}$ in both reaction mixtures. An average Förster distance ($R_0$) of 52 Å was used in efficiency of energy transfer [E] calculations. After [E] was measured using equation 7, the distance between donor and acceptor molecules (R) was evaluated. Fluorescence was read at an excitation wavelength of 488 nm and an emission wavelength of 518 nm (fluorescein dependent excitation and emission).

### 5.5.3 Computerized molecular modeling

Graphic visualizations and attempted molecular docking was performed on a web programme called Rasmol (Raswin Molecular graphics) [V.2.7.2.1].

## 5.6 Results and discussion

### 5.6.1 Estimation of $K_{sv}$ and Θ parameters in fluorescence quenching

The fluorescence parameters of $K_{sv}$ and Θ were determined graphically for $A\beta_{17-28}$, $A\beta_{32-35}$ and $A\beta_{25-35}$ (Fig. 5.7 –Fig. 5.12).

#### *5.6.1.1 Stern Volmer and Θ plots for $A\beta_{17-28}$ to determine $K_{sv}$ and Θ.*

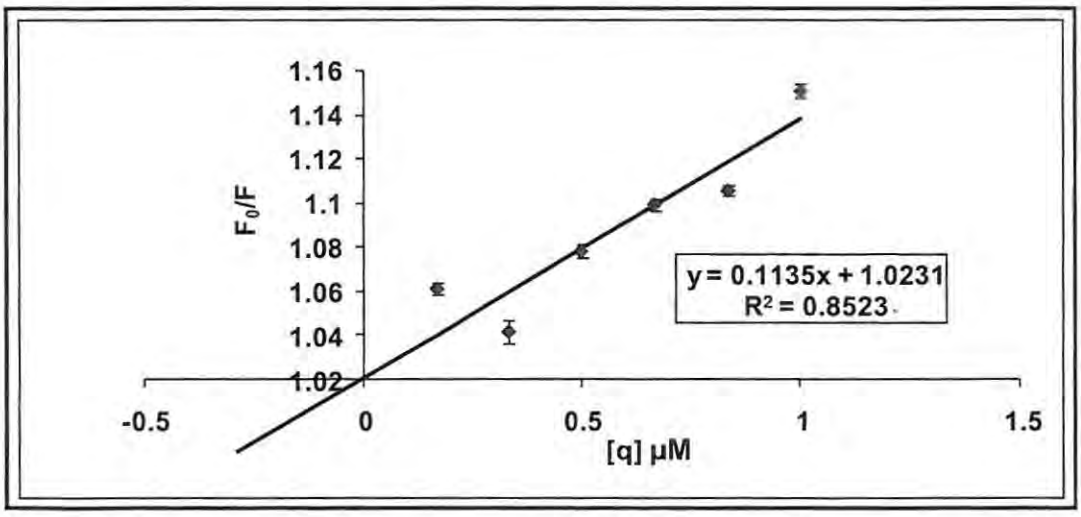


**Figure 5.7 Stern-Volmer plot of $A\beta_{17-28}$; values represent the mean (± S.E.M) of three trials.**

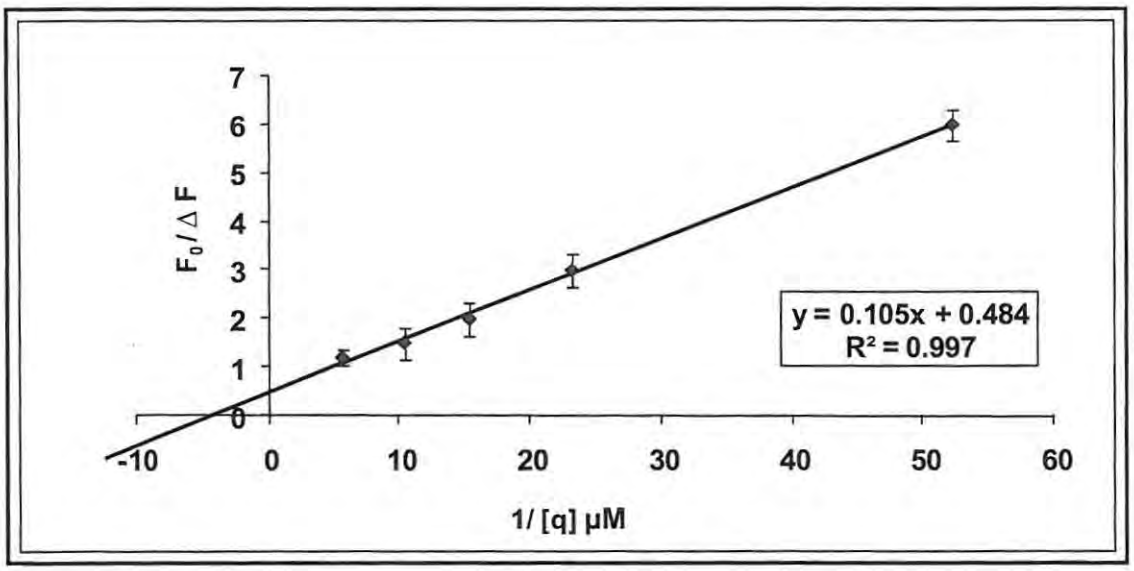


**Figure 5.8 Spectrofluorimetric plot to determine Θ for $A\beta_{17-28}$; values represent the mean (± S.E.M) of three trials.**

*5.6.1.2 Stern Volmer and Θ plots for $A\beta_{25-35}$ to determine $K_{sv}$ and Θ.*

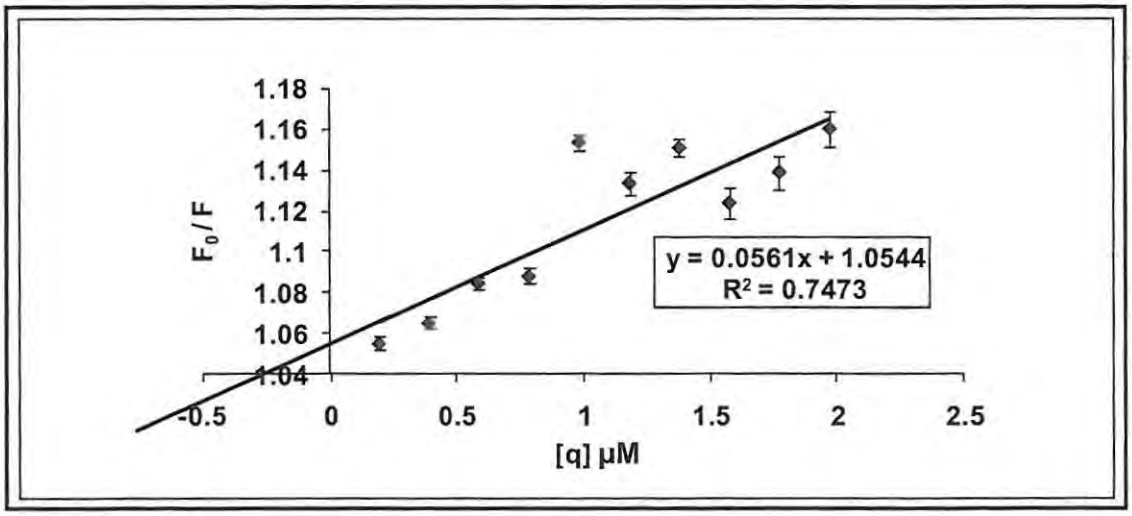


**Figure 5.9 Stern-Volmer plot for$A\beta_{25-35}$; values represent the mean (± S.E.M) of three trials.**

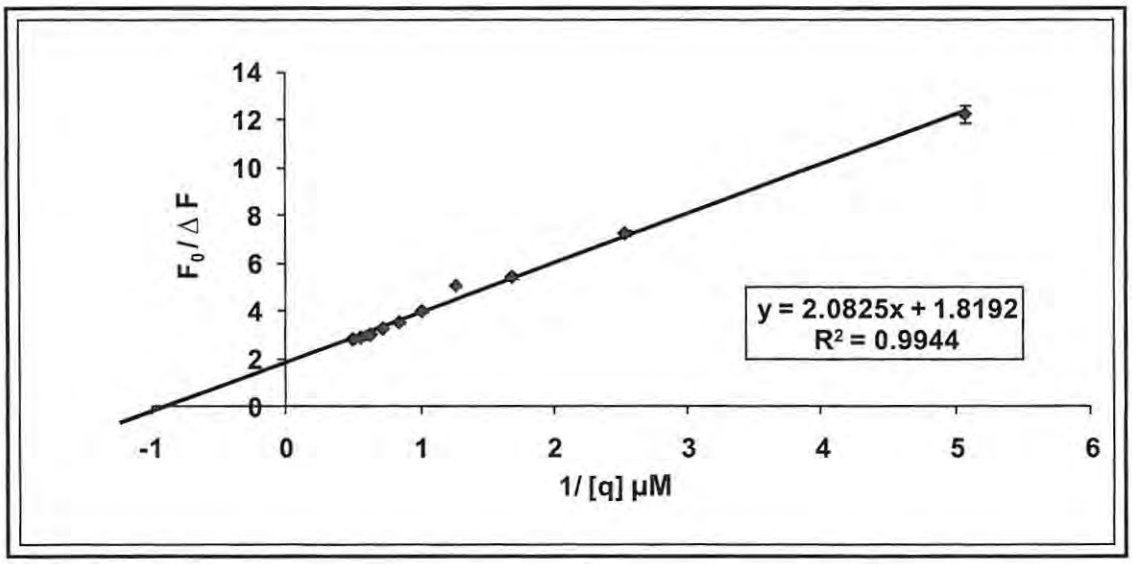


**Figure 5.10 Spectrofluorimetric plot to determine Θ for $A\beta_{25-35}$ ; values represent the mean (± S.E.M) of three trials.**

*5.6.1.3 Stern Volmer and Θ plots for $A\beta_{32-35}$ to determine $K_{sv}$ and Θ.*

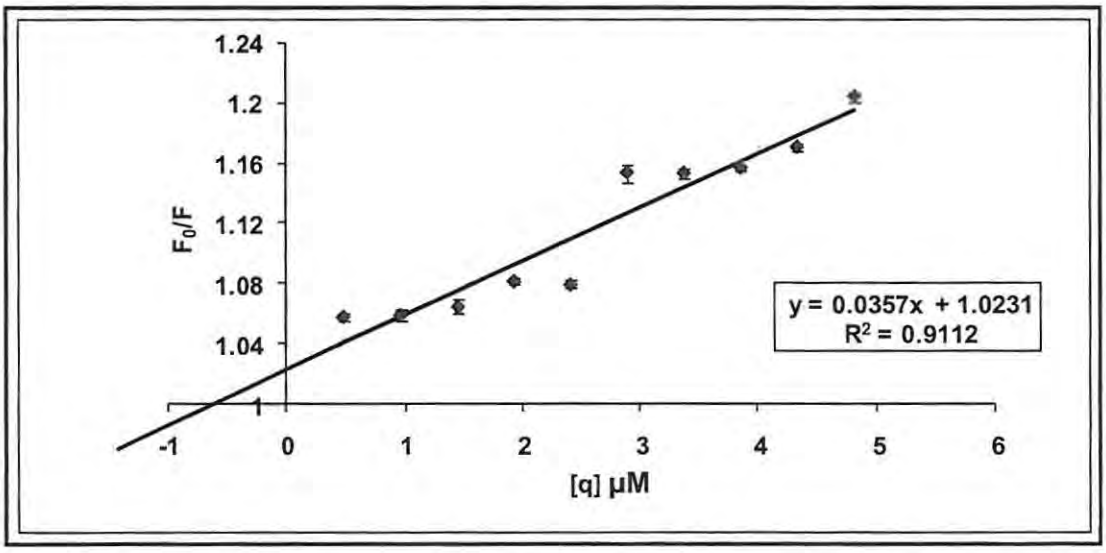


**Figure 5.11 Stern-Volmer plot for $A\beta_{32-35}$; values represent the mean (± S.E.M) of three trials.**

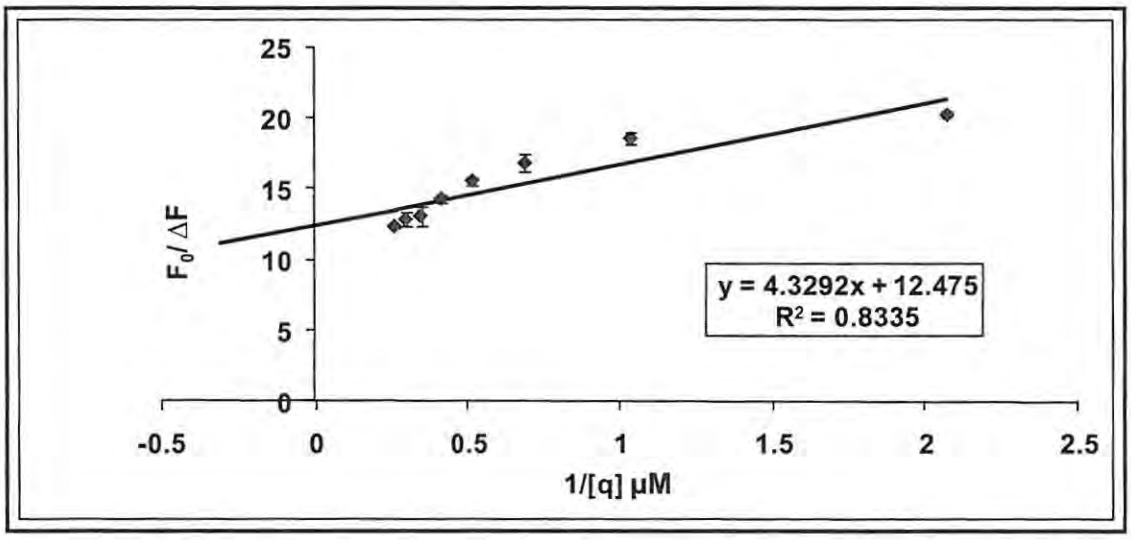


**Figure 5.12 Spectrofluorimetric plot to determine Θ for Aß$_{32-35}$; values represent the mean (± S.E.M) of three trials.**

**Table 5.1 Table of $K_{sv}$ and Θ values for Aß$_{17-28}$, Aß$_{32-35}$ and Aß$_{25-35}$.**

| Aß | $K_{SV}$ ($\mu M^{-1}$) | Θ |
|---|---|---|
| Aß$_{17-28}$ | 0.1135 | 2 |
| Aß$_{25-35}$ | 0.0561 | ~ 1 |
| Aß$_{32-35}$ | 0.0357 | ~ 0 |

The parameter $K_{SV}$ was equivalent to the gradient of the Stern-Volmer plots (Fig. 5.7; 5.9; 5.11). Generally, a greater $K_{SV}$ means the greater quenching and ease of accessibility to fluor molecules. It was observed that the $K_{SV}$ of Aß$_{17-28}$ was higher (0.1135 $\mu M^{-1}$) compared to the $K_{SV}$ of Aß$_{25-35}$ (0.0561 $\mu M^{-1}$) and $K_{SV}$ of Aß$_{32-35}$ (0.0357 $\mu M^{-1}$) (Table 5.1). Thus, the highest $K_{SV}$ value of 0.1135 $\mu M^{-1}$ which was estimated for Aß$_{17-28}$ indicated that this peptide had the greatest quenching ability and was easily accessible to flour molecules. In addition, the rule of fluorescence quenching states that if there is no internal quenching [IQ] and no external quenching [EQ], the overall fluorescence (F) must be equivalent to 1 (Freifelder, 1976). In the Stern-Volmer plots (Fig. 5.7; 5.9; 5.11),

the y intercept was equivalent to 1, thereby indicating that fluorescence was only due to internal quenching by amino acids within the amyloid peptide and not the interplay of other fluors in solution which may result in external quenching. Nevertheless, $A\beta_{1-40}$ and $A\beta_{22-35}$ showed an increase in overall fluorescence possibly due the simultaneous external and internal quenching of $A\beta_{1-40}$ and $A\beta_{22-35}$ such that F>>1. This meant that the rule of fluorescence quenching, generally applied to Stern-Volmer graphs was not allowed for $A\beta_{1-40}$ and $A\beta_{22-35}$. Hence Stern-Volmer graphs and calculations of $\Theta$ were limited to $A\beta_{17-28}$, $A\beta_{32-35}$ and $A\beta_{25-35}$ as shown in the results (Fig.5.7 –Fig. 5.12).

In addition, the fraction of tryptophans (TRP) near the enzyme surface ($\Theta$) was determined as the reciprocal of the y-intercept (Fig 5.8; 5.10; 5.12). The parameter $\Theta$ is generally dependent on the polarity of the solvent. Thus, the hydrophobic nature of the $A\beta_{17-28}$ sequence induced conformational change in nNOS, bringing two TRP residues to the surface of the enzyme ( $\Theta = 2$) for $A\beta_{17-28}$ (Table 5.1) as opposed to the binding of $A\beta_{25-35}$ to the enzyme where approximately one tryptophan residue was exposed on the enzyme surface ($\Theta \approx 1$). However, no tryptophan residue was exposed on the enzyme surface ($\Theta \tilde{} 0$) during the binding of $A\beta_{32-35}$. Moreover, the low $K_{SV}$ values for $A\beta_{32-35}$ and $A\beta_{25-35}$ (0.0357 $\mu M^{-1}$ and 0.0561 $\mu M^{-1}$) (Table 5.1) respectively, confirmed that the quencher accessibility by TRP residues was difficult. In consequence, lowering the ability of quenching and thus substantiating the $\Theta$ results obtained for $A\beta_{32-35}$ and $A\beta_{25-35}$.

### 5.6.2 FRET used to determine distance between TRP residues and nNOS active site as an indication of the binding mechanism between amyloid peptide and enzyme.

The distances of 28 Å between substrate (BAEE) and fluorescein and the distance of 14 Å between inhibitor ($A\beta_{17-28}$) and fluorescein (quencher) as calculated according to equation 9; pg 94, were proposed to be the distance that the tryptophan residue shifted once either the enzyme substrate binds or inhibitor binds to nNOS (Table 5.2). Moreover, the fluorescence intensity between BAEE and fluorescein was 129.6; relatively low fluorescence intensity compared to the higher fluorescence intensity of 270.3 between $A\beta_{17-28}$ and fluorescein.

**Table 5.2 Table of FRET results demonstrating effiency of energy transfer (E) and distance (R [Å]) between donor (D) and acceptor (A) molecules based on their combined (fluorescence of donor and acceptor) and individual fluorescence intensities (fluorescence of donor) ($F^{D,A}$ and $F^{D}$ ).**

| Acceptors | $F^{D,A}$ | $F^{D}$ | E (Joules) | $R^0$ (Forster distance) | R (Å) |
|---|---|---|---|---|---|
| **Substrate (BAEE)** | 129.6 | 46.42 | 1.792 | 52 | 28 |
| **Inhibitor ($A\beta_{17-28}$)** | 270.3 | 49.83 | 4.424 | 52 | 14 |

In addition, two possible mechanisms can explain FRET efficiency between fluorescein and substrate (BAEE) or inhibitor ($A\beta_{17-28}$), namely:

### *5.6.2.1. Conformational change*

The low fluorescent intensity was reflective of a low FRET efficiency when the substrate bound while the high fluorescent intensity was reflective of a high FRET efficiency when inhibitor bound to nNOS. These results were due to the orientation relationships associated with the binding of both BAEE and $A\beta_{17-28}$ which induced different conformational changes in nNOS. Since both acceptors had different binding natures, the position of the tryptophan residues around the enzyme active site became positioned differently; this factor took into account the quenching ability of the donor molecules as well.

### *5.6.2.2. Energy transfer mechanism*

For the inhibitor-acceptor ($A\beta_{17-28}$), the only intrinsic fluorophores present in the sequence were two phenyl rings ($Phe_{19}$ and $Phe_{20}$) which had low quantum yield and this was inadequate for sensitive determinations. Hence, the possibility of any internal quenching by aromatic amino acids when $A\beta_{17-28}$ was bound to nNOS was ruled out. In the absence of resonance energy transfer when nNOS (1.) (Fig. 5.13) and acceptor which

was either BAEE or Aß$_{17-28}$ (2.) remained unbound, the donor signal of fluorescein (F) was high and the emission of fluorescein acceptor (A) was low. However, when the enzyme-acceptor–donor (E-A-D) complex formed (3.), fluorescein (D) which was attached to the acceptor terminus (2.) behaved as a 'fluorescence resonance gate' for transferring excited energy to the acceptor. Both BAEE and Aß$_{17-28}$ thus experienced an increase in excitation energy after the emission by fluorescein. At the point of enzyme-inhibitor and enzyme-substrate complex, the donor signal was low (increased emission) and the acceptor signal was high (increased excitation) resulting in resonance energy transfer between donor and acceptor (Fig. 5.13).

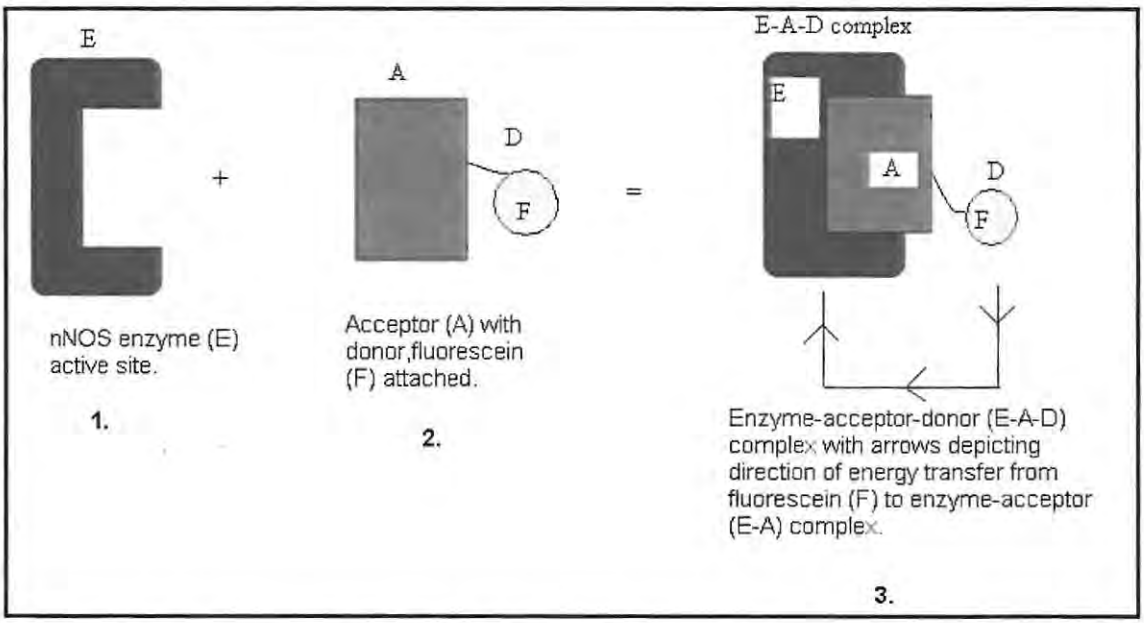


**Figure 5.13 Mechanism of FRET in binding studies of BAEE, Aß$_{17-28}$ (acceptor) and fluorescein (donor).**

## 5.6.3 Computerized molecular modeling

### *5.6.3.1 Secondary structure and 3-D models of rat nNOS active site*

It was necessary to model the interaction between enzyme (nNOS) and amyloid peptides (Aß) by studying the active site of nNOS and the possible conformational changes induced by beta-amyloid binding. This was significant as determination of the structure

of a protein with bound substrate/inhibitor/cofactor is often necessary to elucidate the mechanism of action. The secondary structure of nNOS constituted roughly equal parts of alpha-helical and beta-strand structures i.e., a total of 19 helices and 16 strands (Fig. 5.14). The oxygenase domain was found at the N-terminal of nNOS while the reductase domain having CaM-flavin and NADPH–binding sites were found within the C-terminal (carboxyl region) domain. The C-terminal part was inserted into the membrane and was predicted as a amphipathic helix and thus possessed both hydrophobic and hydrophilic characteristics. The oxygenase domain was the site of catalytic activity where the substrate arginine became bound and probably induced a conformational change in nNOS to reveal an inhibitor binding site to which Aß was bound.

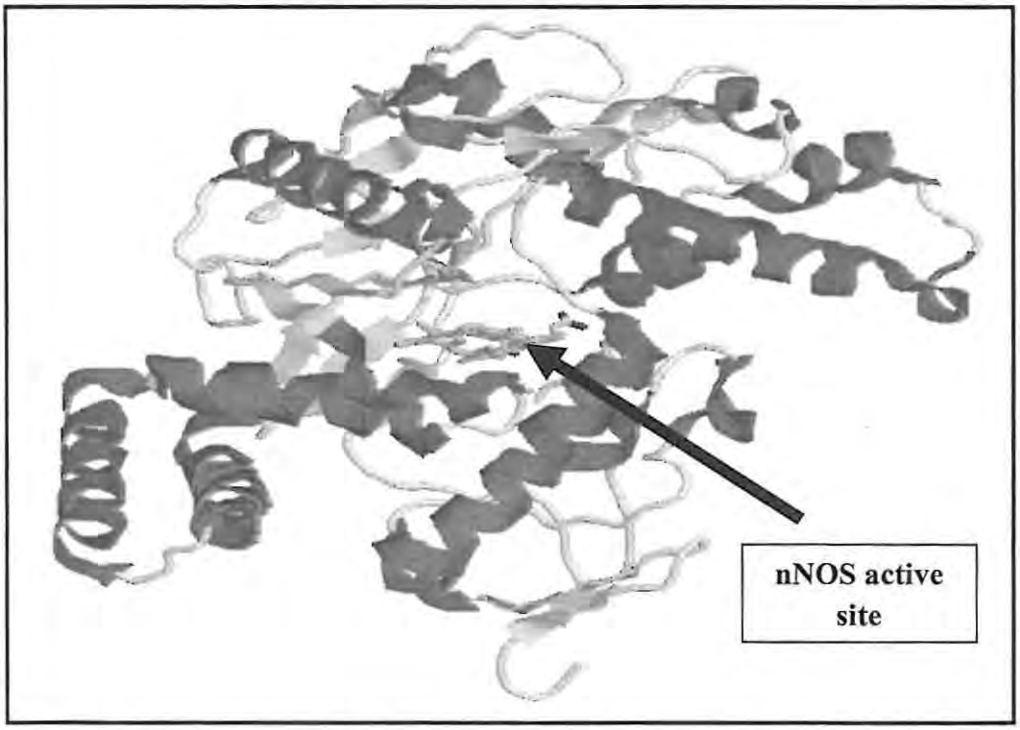


**Figure 5.14 Structure of at rat neuronal nitric oxide synthase showing active site (PDB1zvi) [cf Fig. 1.6; pg 12]**

***5.6.3.2 Secondary structure of rat neuronal nitric oxide synthase showing the relative distance of $TRP_{625}$ and $TRP_{716}$ from the arginine bound active site (purple).***

It is clear that fluorescence and internal quenching of tryptophan residues at or near the active site of nNOS can be used as to indicate the association between enzyme and substrate. The active site of the enzyme (coloured purple) in Figure 5.15 and 5.16 is a

reflection of arginine binding at this region since the active site contains an arginine binding site in the oxygenase domain of the enzyme (Stuehr, 1997). Moreover, from studies involving FRET (5.6.2) the distance at which tryptophan residues shifted when arginine was bound to the enzyme was approximately 28 Å and this correlated with computer modeling results which revealed that $TRP_{625}$ was 27.96 Å and $TRP_{716}$ was 29.32 Å away from the arginine bound active site (Fig. 5.15 and 5.16)

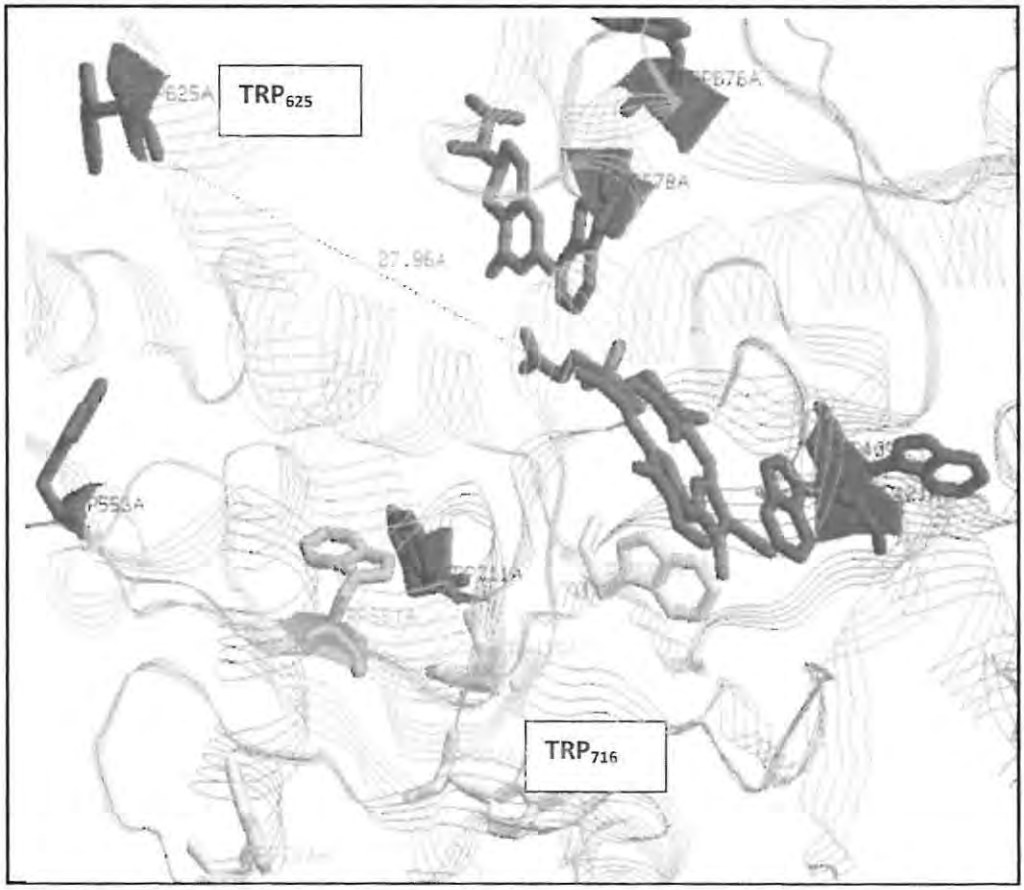


**Figure 5.15 Rat neuronal nitric oxide synthase showing active site and the relative distance of 27.96 Å of $TRP_{625}$ from the arginine bound active site (PDB: 1zvi)**

The results obtained from FRET and computerized modeling suggest that in the natural state of the enzyme with arginine bound to the active site, two TRP residues ($TRP_{625}$ and $TRP_{716}$) were positioned at the surface of the enzyme approximately 28.6 Å distance away. Nevertheless, when $A\beta_{17-28}$ was bound to the active site of nNOS, these same two

tryptophan residues ($TRP_{625}$ and $TRP_{716}$) moved 14 Å closer to the active site as substantiated by prior FRET results (5.6.2).

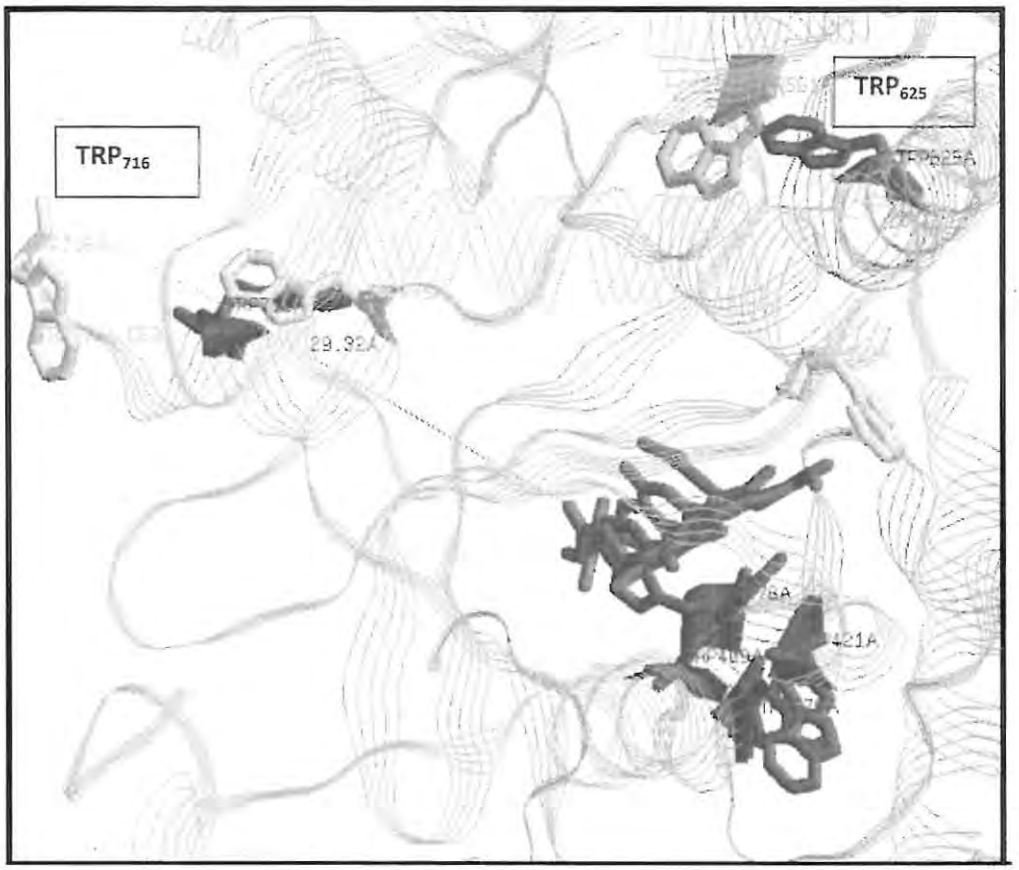


**Figure 5.16 Rat neuronal nitric oxide synthase showing active site and the relative distance of 29.32 Å of $TRP_{716}$ from the arginine bound active site (PDB: 1zvi)**

The relative distance of 11 tryptophan residues from the active site are shown in Table 5.3 since the distances of these TRPs were not shown on Figure 5.15 and 5.16.

**Table 5.3 Distance of tryptophan residues from the active site not shown on Figure 5.15 and 5.16.**

| TRP | $W_{625}$ | $W_{561}$ | $W_{421}$ | $W_{409}$ | $W_{587}$ | $W_{676}$ | $W_{678}$ | $W_{510}$ | $W_{306}$ | $W_{711}$ | $W_{716}$ |
|---|---|---|---|---|---|---|---|---|---|---|---|
| Å | 27.96* | 8.96 | 15.01 | 10.20 | 6.14 | 19.43 | 7.36 | 23.14 | 18.93 | 10.61 | 29.32 |

*5.6.3.3 Secondary structure and suggested 3-D models of $A\beta_{17-21}$ binding to nNOS.*

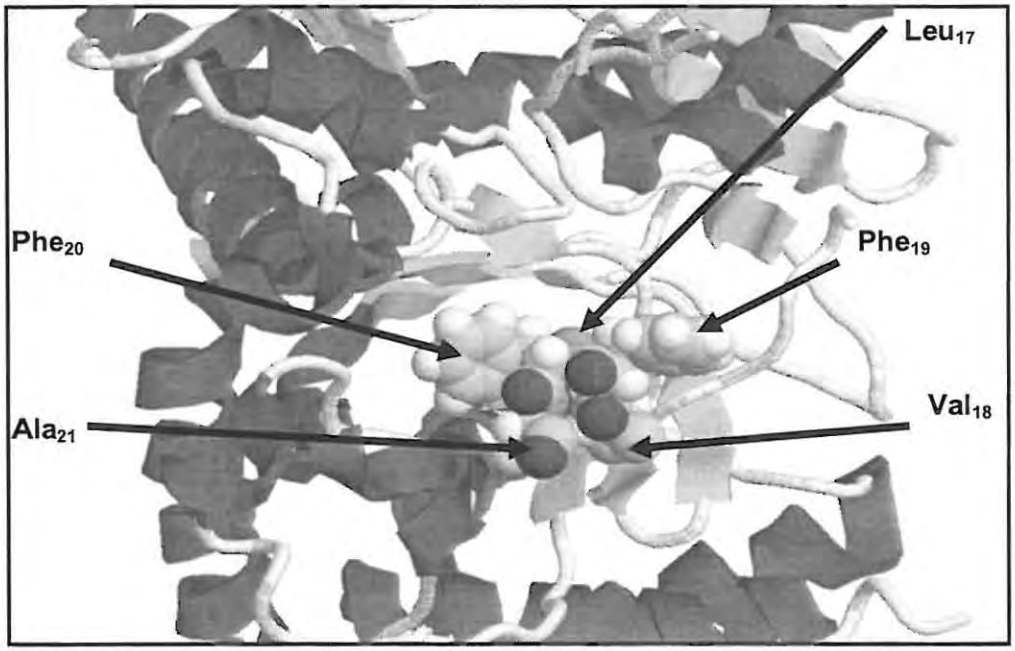


**Figure 5.17 Suggested binding of $A\beta_{17-21}$ to nNOS showing critical amino acid residues important in aggregation and inhibition (PDB: 1zvi).**

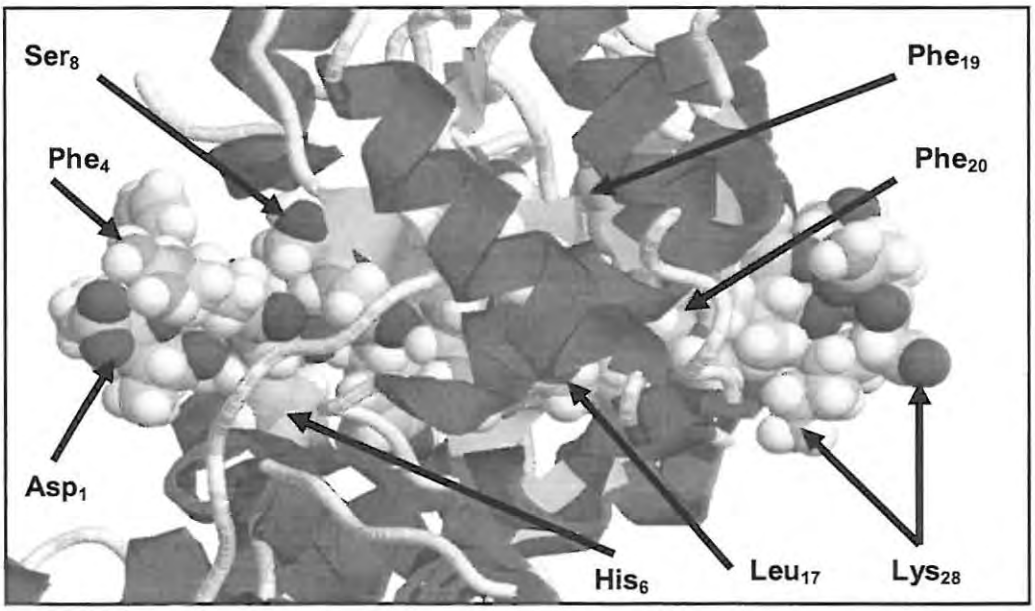


**Figure 5.18 Suggested binding of $A\beta_{1-28}$ to nNOS illustrating the 'barrel position' of some amino acid residues that may influence aggregation and inhibition effects (PDB: 1zvi).**

The suggested models predicted the possible binding of the $A\beta_{17-21}$ fragment and the $A\beta_{1-28}$ segment to the nNOS binding site (Fig. 5.17 and Fig. 5.18). The binding of $A\beta_{1-28}$ (Fig. 5.18) suggested that the peptide could bind to the active site of the enzyme in a 'barrel shaped position'. The middle of the 'barrel' was made up of residues $A\beta_{17-21}$ which were more in contact with the enzyme (Fig. 5.17) while $A\beta_{1-16}$ and $A\beta_{22-28}$ peptide segments seemed to 'stick out' on either side of the enzyme with little or no contact and was likened to the edges of a 'barrel' (Fig. 5.18). These findings suggested that the pentapeptide, $A\beta_{17-21}$, may be crucial in binding of Aß and inhibition of nNOS. Literature (Soto *et al.*, 2007) has shown that $A\beta_{17-21}$ possesses a series of promising properties: it has been shown to cross the blood brain barrier, to inhibit (and disassemble) the formation of amyloid fibrils *in vitro* and *in vivo*, to prevent Aß neurotoxicity in cell culture, to arrest amyloid deposition and to induce dissolution of preformed plaques in rat brain model of the amyloidogenic pathway. Thus, the use of $A\beta_{17-21}$ as a possible pseudoligand to block the process of fibrillogenesis shows promising future potential in treatment of AD.

Moreover, based on general molecular models, (Wouters, 1998) which described the interactions of a monoamine oxidase inhibitor with the active site of an enzyme, it was assumed that the peptide inhibitors in the current study were engaged in a molecular association with nNOS through a double attachment at a primary and secondary binding site. It was reasonable to suggest this as the molecular models of the active site of nNOS showed binding sites for flavins, haem and pterin cofactors. Thus, it was possible that when the peptide inhibitor was bound to either a primary or secondary cofactor site on the enzyme, there was a charge transfer interaction with the ring moiety of the flavin cofactor in the reductase domain. In consequence, efficient electron transfer to flavin may have increased due to an increase in oxidation of NADPH. This resulted in a stronger interaction of the peptide inhibitor (Aß) with nNOS.

## 5.7 Conclusion

Fluorescence quenching indicated that $A\beta_{17-28}$ caused the greatest quenching and the lowest quantum yield (Q) and was easily accessible to fluor molecules due to its highest $K_{SV}$ value of 0.1135 $\mu M^{-1}$ compared to $A\beta_{25-35}$ and $A\beta_{32-35}$. It was also revealed that two tryptophan residues ($TRP_{625}$ and $TRP_{716}$) were exposed on the surface of the enzyme during the binding of either arginine or $A\beta_{17-28}$ to the nNOS active site. In addition, the technique of FRET correlated with computerized molecular modeling in indicating that $TRP_{625}$ and $TRP_{716}$ were an average distance of 28.6 Å away from the active site when the enzyme existed in its native conformation. However when $A\beta_{17-28}$ was bound to the active site of the enzyme, these same tryptophan residues shifted 14 Å closer to the active site. Thus, the distance values were reflective of important structural modifications within nNOS active site when either inhibitor or substrate was bound.

# VI

# Final conclusions and future perspectives

## 6.1 General discussion

### 6.1.1 Isolation, purification and characterization of nNOS

Given its important catalytic function in the metabolism of arginine and, hence, its application in Alzheimer's disease, the use of nNOS as a biomarker in the disease is indispensable. In this project, the neuronal isoform of nitric oxide synthase (NOS) was purified and biochemically characterized. Bovine brain was an excellent and convenient source for the enzyme as the neuronal isoform of the enzyme is widely distributed in general tissue cells but high concentrations and corresponding high activity is normally found in the cerebella regions of bovine brain. However, nNOS has also been characterized in 28 regions of human, bovine and rat brain according to previous literature (Blum-Degan *et al.*, 1999). These regions included the cortical and subcortical areas, basal ganglia, the limbic system, thalamus and brainstem. In this project, it was difficult to estimate the exact region of localization of nNOS within the brain as the entire brain was homogenized. Nevertheless, based on enzyme activity calculations during purification it could be deduced that the cerebrum was the most likely region of the brain in which nNOS was located.

For the characterization and application of the enzyme, the purification was unsuccessful using two methods of precipitation: poly (ethylene glycol) 20 000 (PEG) and ammonium sulphate [$(NH_4)_2SO_4$] as no fold increase in purity was produced. Thus, a single main

purification step was performed; namely, anion exchange chromatography on DEAE-Sepharose. However, it was only after dialysis of the pooled 8 x 5 ml fractions that a 38 % yield and three-fold purification was produced with the highest specific activity of 2.27 U/mg. The purified nNOS was shown to be a heterodimeric protein ($M_r$ ± 225 kDa) consisting of two different subunits (95 and 130 kDa, respectively). The optimum pH and temperature of nNOS from bovine brain were determined to be 6.5 and 40 °C and it had a half-life of 3 h under these conditions. The turn-over number ($k_{cat}$) for nNOS was calculated to be 50.95 $min^{-1}$ and its catalytic effiency ($k_{cat}/K_M$) was determined to be 0.73 $min^{-1}.\mu M^{-1}$. Compared to other literature values (Riveros-Moreno *et al.*, 1995; Snyder and Bredt, 1990; Zweier and Giraldez, 1998; Hiki *et al.*, 1992), the partially purified enzyme affinity for the substrate arginine was lower ($K_M$ = 70 µM) and its $V_{max}$ (0.332 $\mu mol.min^{-1}$) were both lower than reported values.

### 6.1.2 Inhibition studies of ß-amyloid peptides with nNOS

Accumulation of ß-amyloid peptides in the form of senile plaques is central to the pathogenesis of Alzheimer's disease. The extracellularly located plaques subsequently cause formation of intracellularly located neurofibrillary tangles, another essential feature of the Alzheimer's brain and neuronal death. Due to the fact that nNOS and its metabolic substrate arginine along with the accumulation of amyloid peptides are all located in the astrocytes of an Alzheimer's patients brain, it was significant that $A\beta_{1-40}$, $A\beta_{22-35}$, $A\beta_{32-35}$ and $A\beta_{25-35}$ bound to nNOS and inhibited the enzyme to varying degrees with respective $K_i$ values of 14.4 µM; 7.4 µM; 8.8 µM and 10 µM. The $K_i$ value for $A\beta_{17-28}$ was the lowest; namely, 1.92 µM, indicating that this fragment inhibited the activity of nNOS the most. Moreover, the interaction of the various amyloid peptide fragments with nNOS further showed an association–dissociation suggesting that that enzyme behaved as an amyloidogenic catalyst and converted the peptide into a form which could no longer bind, later deduced as a fibril. To our knowledge, there are no studies in literature showing that nNOS catalyses the formation of fibrils.

### 6.1.3 Techniques to study amyloid fibril formation *in vitro*

The discovery of amyloid fibrils as a major constituent of protein deposition in neurons and their correlation with Alzheimer's disease has led to intense study of the formation and structure of such fibrils. Amyloid fibrils are ordered aggregates of a normally soluble peptide or protein. Four techniques were used to characterize and detect the presence of amyloid fibrils; namely, Congo red, turbidity, spectrofluorimetry using thioflavin-T (ThT) and transmission electron microscopy. Thioflavin-T staining fluorescence, Congo red and turbidity assays at 400 nm indicated that $A\beta_{17-28}$ was the most prominent peptide fragment for fibrillogenesis. Also, by correlating the time dependent inhibition data, the thioflavin-T fluorescence data and the Congo red assay and turbidity assays data for the affinity of several amyloid peptides with nNOS, there was evidence to support a two-stage transition. Although, there was no definite proof whether the original peptide fragments were random coils or a-helices, there was evidence of a rapid conversion (within 30 min) of the peptide, initiated by the enzyme, into a soluble ß-conformation rendering it no longer able to bind to the enzyme. Then, after approximately 24 h, there was a further change, also initiated by nNOS and the formation of insoluble fibrils as detected by turbidity. These aggregates were the final step in the process of fibril formation as they remained insoluble over some time and did not redissolve into soluble fibrils. The technique of transmission electron microscopy (TEM) successfully described the morphology of fibrils to be a branched network with $A\beta_{17-28}$ producing the most amount of fibrils. Thus, TEM pointed to the fact that different amyloid peptides produce different quantities of fibrils over a given time due the process of partial folding in proteins and proteolysis.

Fluorescence quenching showed that $A\beta_{17-28}$ exhibited the greatest degree of quenching and was easily accessible to fluor molecules as it had the highest $K_{SV}$ value of 0.11 $\mu M^{-1}$ compared to $A\beta_{25-35}$ and $A\beta_{32-35}$ which had $K_{SV}$ values of 0.0561 $\mu M^{-1}$ and 0.0357 $\mu M^{-1}$, respectively. The technique of FRET was useful in analyzing the conformational changes of $A\beta_{17-28}$ during binding to nNOS. Two surface tryptophans ($TRP_{625}$ and $TRP_{716}$) were an average distance of 28.6 Å away from the active site when arginine was bound to the

enzyme in its native conformation. The same two tryptophan residues moved 14 Å closer to the active site when the inhibitor ($A\beta_{17-28}$) was bound to the enzyme. Conformational change was induced due to the mechanism of energy transfer between fluorescein (donor) to arginine and $A\beta_{17-28}$ (acceptor). Attempted computerized modeling suggested that a pentapeptide; namely, $A\beta_{17-21}$ [$Leu_{17}$ – $Val_{18}$ – $Phe_{19}$ – $Phe_{20}$ – $Ala_{21}$] may be crucial in binding and inhibition of nNOS.

## 6.2 Future perspectives

To date there is no early diagnosis for Alzheimer's disease other than neuroimaging profiles of a deceased patient. In fact, the current treatment of Alzheimer's is largely symptomatic with different pharmacological drugs designed to temporarily suppress these debilitating symptoms. Hence, it is vital to identify suitable enzyme biomarkers like nNOS as the concentration level of the enzyme relative to its substrate concentration level may allow for a less invasive and more accurate diagnosis as well as serve as a predictor of future Alzheimer disease progression and treatment response.

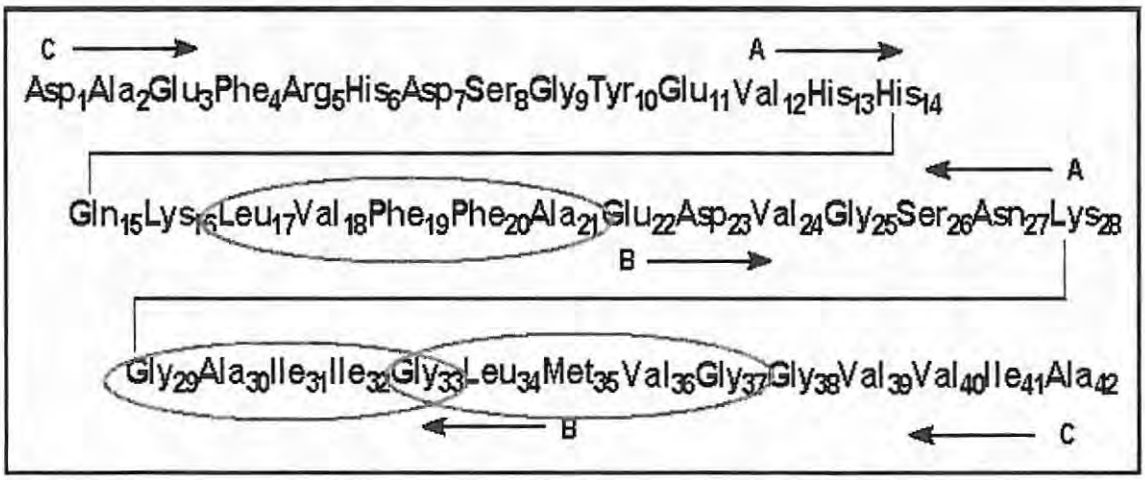


**Figure 6.1 The crucial pentapeptide motif ($A\beta_{17-21}$) and glycine zipper motifs ($A\beta_{29-33}$ and $A\beta_{33-37}$) as possible anti-aggregating agents within the 42 amino acid sequence.**

More specifically, future work should elucidate biochemical strategies targeted at selectively inhibiting the aggregation of fibrils or blocking the amyloid precursor protein (ß-secretase) pathway responsible for generating amyloid peptides in the first instance.

One approach is to use a small molecule called curcumin in turmeric spice as a prevention strategy as curcumin has been shown to inhibit the formation of fibrils.

Another approach is to use fragments of Aß such as $Aß_{17-21}$ and the hydrophobic pentapeptide $Gly_{29}$ –$Ala_{30}$ - $Ile_{31}$ – $Ile_{32}$ - $Gly_{33}$ - $Leu_{34}$ -$Met_{35}$-$Val_{36}$-$Gly_{37}$ which contains two G-X-X-X-G motifs called glycine zippers to selectively inhibit the formation of fibrils and the proteolytic amyloidogenic pathway responsible in generating amyloid peptides (Fig 6.1). In addition, mitochondrial NOS (mtNOS) is a new isoform of NOS which is found in brain mitochondria. This enzyme has the same cofactor and substrate requirements as neuronal nitric-oxide synthase and could be easily confused with neuronal nitric-oxide synthase itself. Future research could investigate the binding of mtNOS and Aß in mitochondria. This is significant as fibril formation could lead to mitochondrial dynamic imbalance. Hence, the binding of curcumin or $Aß_{17-21}$ pentapeptide stretch to mtNOS could restore mitochondrial stability.

The assumed inhibition and binding by these proposed anti-aggregating agents could be studied using molecular modelling programmes such as nanoscale molecular dynamics (NAMD), quartz crystal microbalance with dissipation monitoring (QCMD) and the incorporation of fluorescence recovery after photobleaching (FRAP) and fluorescence resonance energy transfer (FRET) to confirm results. Atomic force microscopy (AFM) is a novel technique that could also be employed to study Aß binding.

## 6.3 Conclusions

In the present study, a procedure was developed for the successful isolation and partial purification of neuronal nitric oxide synthase (nNOS) present in crude bovine brain extract. Three assays were compared with the citrulline assay and found to be faster and more economical and reliable. It was shown that nNOS was capable of metabolizing the substrate arginine. However further studies into regulation of nNOS based on arginine and citrulline levels in the brain need to be performed. This is significant as high levels of arginine and low levels of citrulline are found in the cerebrospinal fluid of Alzheimer's patients and warrant further research. The work also confirmed $Aß_{17-28}$ as a specialized peptide sequence and hinted at its possible anti-aggregating potential. $Aß_{17-28}$ peptide

inhibited the activity of nNOS extensively because it bound tightly to the inhibitor site on the enzyme and it was more in contact with fluorophores (two tryptophans) on the enzyme which were involved in energy transfer and conformational change. In addition, Congo red, turbidity and thioflavin-T (ThT) assays successfully detected the presence of fibrils and proved that as an amyloidogenic catalyst, nNOS converts the amyloid peptide into a soluble fibril rapidly and then with time precipitates the fibril out of solution to form an aggregate without hindering the activity of the enzyme. Nevertheless, fibril deposits have recently been found to deviate from the criteria for standard amyloid fibrils. This highlights the need to re-evaluate the techniques of Congo red, turbidity and ThT binding, since many other properties have been identified to be associated with amyloid fibrils such that a new *in vitro* classification system for amyloid fibrils may be warranted. Thus, in the future, it is expected that a broader classification of amyloid fibrils will emerge and traditional techniques will give way to novel techniques and new discoveries in the field of fibrillogenesis.

# References


Amersham Biosciences (2007). Produced by Wikstroms, Uppsala, Sweden (wwww.amershambiosciences.com), accessed 11/07/08

Archibald R.M. (1944). Determination of citrulline and allantoin and demonstration of citrulline in blood plasma. *Journal of Biological Chemistry.*, **156**: 121-142.

Blum-Degan D., Heinemann T., Lan J., Pedersen V., Leblhuber W.P., Riederer P. and Gerlach M. (1999). Characterization and regional distribution of nitric oxide synthase in the human brain during normal ageing. *Brain Research.*, **834**: 128-135.

Bonnerjera J., Oh S., Hoare M. and Dunhill P. (1986). The right step at the right time. *Biotechnology.*, **4**: 954-958.

Boyde T.R.C. and Rahmatullah M. (1980). Optimization of conditions for the colorimetric determination of citrulline using diacetyl monoxime. *Analytical Biochemistry.*, **107**: 424-431.

Bradford M.M. (1976). A rapid and sensitive method for quantitation of microgram quantities of protein utilizing the principle of protein-dye-binding. *Analytical Biochemistry.*, **72**: 248-254.

Bruckdorfer R. (2005). The basics about nitric oxide. *Molecular Aspects of Medicine.*, **26**: 3-31.

Caflisch A. and Pellarin R. (2006). Interpreting the aggregation kinetics of amyloid peptides. *Journal of Molecular Biology.*, **360**: 882-892

Calamai M., Chiti F. and Dobson C.M. (2005). Amyloid fibril formation can proceed from different conformations of a partially unfolded protein. *Biophysical Journal.*, **89**: 4201-4210.

Campos K.L., Giovanelli J., Kaufman S. (1995). Characteristics of the nitric oxide synthase-catalyzed conversion of arginine to *N*-hydroxyarginine, the first oxygenation step in the enzymatic synthesis of nitric oxide. *Journal of Biological Chemistry.*, **270**: 1721-1728.

Cantoni O., Palomba L., Musci G., Ascenzi P., Fioravanti E., Persichini T., Colasanti M. and Venturini G. (2002). ß–amyloid inhibits NOS activity by subtracting NADPH availability. *FASEB Journal.*, **10**: 1096.

Carrillo M.C., Blackwell A., Hampel H., Lindborg J., Sperling R., Schenk D., Sevigny J.J., Ferris S., Bennett D.A., Craft S., Hsu T. and Klunk W. (2009). Early risk assessment for Alzheimer's disease. *Alzheimers & Dementia.*, **5:** 182-196.

Castellani R.J., Shah R.S., Lee H.G., Xiongwei Z., Perry G., Smith M.A. (2008). Current approaches in the treatment of Alzheimer's disease. *Biomedicine and Pharmacotherapy.*, **62**: 199-207.

Citron M. (2002). Alzheimers disease: treatments in discovery and development. *Nature neuroscience supplement.*, **5**: 1055-1057.

Chabrier P., Auguet M., Spinnewyn B., Auvin S., Cornet S., Demerle-Pallardy C., Guilmard-Favre C., Marin J., Pignol B., Gillard-Roubert V., Roussillot-Charnet C., Schulz J., Viossat I., Bigg D. and Moncada S. (1999). BN 80933, a dual inhibitor of neuronal nitric oxide synthase and lipid peroxidation: A promising neuroprotective strategy. *Proceedings of the National Academy of Sciences.*, **96**: 10824-10829.

Chakrabartty A., Fraser P.E., Yip C.M., Go S., Plaskos N.P., Yang D. and Huang T.H.J. (2000). Structural studies of soluble oligomers of the Alzheimer ß-amyloid peptide. *Journal of Molecular Biology.*, **297**: 73-87.

Chasman D.I. (2003). Protein structure: determination, analysis and applications for drug discovery. Variagenics Inc. Cambridge, Massachusetts. U.S.A.

Choo-Smith L.P., Garzon-Rodriguez W., Glabe C.G., Surewicz W.K. (1997). Acceleration of amyloid fibril formation by specific binding of $A\beta_{1-40}$ peptide to ganglioside-containing membrane vesicles. *Journal of Biological Chemistry.*, **272**: 22987-22990.

Clegg R.M. (1995). Fluorescence resonance energy transfer. *Current opinion in Biotechnology.*, **6**:103-110.

Cooper J.H. (1974). Selective amyloid staining as a function of amyloid composition and structure. *Laboratory Investigation.*, **31**: 232.

Cosslett V.E. (1985). The early years of electron microscopy in biology. *Trends in Biochemical Sciences.*, **10**: 361-363.

Craig-Schapiro R., Fagan A.M., Holtzman D.M. (2009). Biomarkers of Alzheimers disease. *Neurobiology of Disease.*, **35**: 128-140.

Cromwell M.E.M., Hilario E. and Jacobson F. (2006). Protein aggregation and bioprocessing. *The AAPS Journal.*, **8**: 3-8.

Cummings J.L. (2003). The neuropsychiatry of Alzheimer's disease and related dementias. Taylor and Francis. London and New York.

De Felice F.G. and Ferreira S.T. (2002). ß-amyloid production, aggregation, and clearance as targets in Alzheimers disease. *Cellular and Molecular Neurobiology.*, **22**: 125-130.

De Lellis R.A., Glenner G.G. and Ram J.S. (1968). Histochemical observations on amyloid with reference to polarization microscopy. *Journal of Histochemistry and Cytochemistry.*, **16**: 663.

De Meyer G.R.Y., Martinet W., Van De Parre T.J.L., Herman A.G., Bult H., Kockx M.M. and Jans D.M. (2006). Processing of amyloid precursor protein as a biochemical link between Atherosclerosis and Alzheimer disease. *Cardiovascular & Haematological Disorders-Drug Targets.*, **6**: 21-34.

Deutscher M.P. (1990). Methods in Enzymology-Guide to Protein Purification. Academic Press Inc. San Diego, California. **182**: 38-49.

Dirsch V.M., Vollmar A.M., Leikert J.F. and Rathel T.R. (2003). Application of 4,5-diaminofluorescein to reliably measure nitric oxide released from endothelial cells *in vitro*. *Biological Proceedings.*, **5**:136-142.

Drake A.F., Arvinte T., Bui T.T.T., Dahab A.A., Demeule B., Elhag D. and King P. (2004). The multi-mode polarization modulation spectrometer- Part 1: simultaneous detection of absorption, turbidity, and optical activity. *Analytical Biochemistry.*, **332**: 46-57.

Espinosa A., Vivo A., Gallo M.A., Tapias V., Acuna-Castroviejo D., Escames G., Leon J., Velasco G., Lopez –Cara L.C., Carrion M.D., Camacho M.E. and Entrena A. (2005). Kynurenamines as neural nitric oxide synthase inhibitors. *Journal of Medicinal Chemistry.*, **48**: 8174-8181

Evans K.C., Berger E.P., Cho C., Weisgraber K.H. and Lansbury P.T. Jnr. (1995) Apolipoprotein E is a kinetic but not thermodynamic inhibitor of amyloid formation : Implications for the pathogenesis and treatment of Alzheimers disease,. *Proceedings of the National Academy of Sciences,* **92**: 763-767.

Feelisch M., Wink D., Dahmann R. and Kelm M. (1997). The Nitric oxide/Superoxide Assay: Insights into the biological chemistry of the NO/Superoxide interaction. *Journal of Biological Chemistry.*, **272**: 9922-9932.

Fink A.L. and Munishkina L.A. (2007). Fluorescence as a method to reveal structures and membrane-interactions of amyloidogenic proteins. *Biochimica et Biophysica Acta.*, **1768**: 1862-1885.

Fraser P.E., Levesque L. and Mclachlan D.R. (1993). Biochemistry of Alzheimers disease plaques. *Clinical Biochemistry.*, **26**: 339-349.

Freifelder D. (1976). Physical Biochemistry: applications to Biochemistry and Molecular biology. W.H. Freeman and Company, United States of America.

Fülop L., Zarándi M., Soos K. and Penke B. (2006). Self-assembly of Alzheimer's disease-related amyloid peptides into highly ordered nanostructures. *Nanopages 1.*, **1**: 69-83.

Glabe C.G. (2006). Review: common mechanisms of amyloid oligomer pathogenesis in degenerative disease. *Neurobiology of Aging.*, **27**: 570-575.

Giacomo C.D., Sorrenti V., Salerno L., Cardile V., Guerrera F., Siracusa M.A., Avitabile M. and Vanella A. (2003). Novel inhibitors of neuronal nitric oxide synthase. *Experimental Biology and Medicine.*, **228**: 486-490.

Grisham M.B. and Bryan N.S. (2007). Methods to detect nitric oxide and its metabolites in biological samples. *Free Radical Biology & Medicine*.,**43**: 645-657.

Grisham C.M. and Garrett R H. (2006). Biochemistry.Brooks/Cole Publishing Company. United States of America.

Guex N., Peitsch M., Schwede T. and Diemand A. (1995-2001) Deepview/Swiss –Pdb viewer [V.3.7], GlaxoSmithKline (http://www.expasy.org.spdv).

Hafiz A. (2005). Principles and reactions of protein extraction, purification and characterization. CRC Press, Florida.

Harris E.L.V. and S Angal. (1994). Protein purification and methods: A practical approach. Oxford University Press Inc, New York.

Hiki K., Hattori R., Kawai C. and Yui Y. (1992). Purification of insoluble nitric oxide synthase from rat cerebellum. *Journal of Biochemistry*., **111**, 556-558.

Howlett D.R., Jennings K.H., Lee D.C., Clark M.S.G., Brown F., Wetzel R., Wood S.J., Camilleri P and Roberts G.W. (1995). Aggregation state and neurotoxic properties of Alzheimer beta-amyloid peptide. *Neurodegeneration*., **4**: 23-32.

http://www.ahaf.org/alzdis/about/AmyloidPlaques.htm. (Accessed 24/10/09).

http://www.unl.edu/CMRAcfem/em.htm. (Accessed 17/01/10).

http://www.waters.com/waters/nav.htm. (Accessed 24/10/09).

http:// www.britannica.com. (Accessed 10/10/09).

Ishii Y., Yoshida T., Funatsu T., Wazawa T. and Yanagida T. (1999). Fluorescence resonance energy transfer between single fluorophores attached to a coiled-coil protein in aqueous solution. *Chemical Physics*., **247**: 163-173.

Kajava A., Squire J.M. and Parry D.A.D. (2006). Fibrous proteins: amyloids, prions and beta proteins. *Advances in Protein Chemistry*., **73**: 1-320.

Kelly J.W., Balch W.E., Marks M.S., Alory-Jost C., Koulov A.V., Fowler D.M. (2005). Functional amyloid formation within mammalian tissue. *PLoS Biology*., **4**: 0001-0008.

Klunk W.E., Pettegrew J.W. and Abraham D.J. (1989). Quantitative evaluation of Congo red binding to amyloid –like proteins with beta-pleated sheet conformation. *Journal of Histochemistry and Cytochemistry*., **37**:1 273-1281.

Knowles R.G., Alderton W.K. and Cooper C.E. (2001). Nitric oxide synthases: structure, function and inhibition. *Journal of Biochemistry*., **357**: 593-615.

Kontush A. (2001). Alzheimers amyloid-ß as a preventive antioxidant for brain lipoproteins. *Cellular and Molecular Neurobiology*., **21**: 299-315.

Krebs M.R.H., Bromley E.H.C. and Donald A.M. (2005). The binding of thioflavin-T to amyloid fibrils: localization and implications. *Journal of Structural Biology.*, **149**: 30-37.

Kuret J. and Necula M. (2004). Electron microscopy as a quantitative method for investigating tau fibrillization. *Analytical Biochemistry.*, **329**: 238-246.

Laemmli U.K. (1970). Cleavage of structural proteins during the assembly of the head of bacteriophage T4. *Nature.*, **227**: 680-685.

Lakos Z., Szarka A., Koszorfis L and Somogyi B.(1995) Quenching-resolved emission anisotropy: a steady state fluorescence method to study protein dynamics. *Journal of Photochemistry and Photobiology.*, **27**:55-60.

Lansbury P. Jnr and Rochet J. (2000). Amyloid fibrillogenesis: themes and variations. *Current Opinion in Structural Biology.*, **10**: 60-68.

Lesk A. (2001). Introduction to Protein Architecture. University of Cambridge, Oxford university press, New York.

LeVine H. (1993). Thioflavine T interaction with synthetic Alzheimer disease ß-amyloid peptides: detection of amyloid aggregation in solution. *Protein Science.*, **2**: 404-410

Lomakin A., Teplow D.B., Kirschner D.A. and Benedek G.B. (1997). Kinetic theory of fibrillogenesis of amyloid ß–protein (Alzheimer disease/light scattering). *Proceedings of the National Academy of Sciences.*, **94**: 7942-7947.

Marletta M.A., Hurshmen A.R. and Kristin M.R. (1998). Catalysis by Nitric oxide synthase. *Current opinion in Chemical Biology.*, **2**: 656-663.

Mathis C.A., Lopresti B.J., Klunk W.E. (2007). Impact of amyloid imaging on drug development in Alzheimers disease. *Nuclear Medicine and Biology.*, **34**: 809-822.

Matyus L., Szo J. and Jenei A. (2006). Steady-state fluorescence quenching applications for studying protein structure and dynamics. *Journal of Photochemistry and Photobiology B: Biology.*, **83**: 223-236

McLaurin J.A., Franklin T., Fraser P.E., Chakrabartty A. (1998) Structural transitions associated with the interaction of Alzheimer ß-amyloid peptides with gangliosides. *Journal of Biological Chemistry.*, **273**: 4506-4515.

McLaurin J., Yang D.S., Yip C.M. and Fraser P.E. (2000). Modulating factors in amyloid-ß fibril formation. *Journal of Structural Biology.*, **130**: 259-270.

Mebane-Sims I. (2009). 2009 Alzheimer's disease facts and figures. *Alzheimers & Dementia.*, **5**: 234-270.

Munter L.M., Voigt P., Harmeier A., Kaden D.,Gottschalk K.E., Weise C., Pipkorn R., Schaefer M., Langosch D and Multhaup G .(2007). GxxxG motifs within the amyloid precursor protein transmembrane sequence are critical for the etiology of $A\beta_{1-42}$. *EMBO Journal.*, **26**:1702-1712.

National Institute of aging. (1998). Progress report on Alzheimers disease. National Institute on Aging, Bethesda, U.S.A.

Nilsson M.R. (2004). Techniques to study amyloid fibril formation *in vitro*. *Methods.*, **34**: 151-160.

Nunomura A., Perry G., Zhang J., Montine T., Takeda A., Chiba S. and Smith M.A. (1999). RNA oxidation in Alzheimer and Parkinsons diseases. *Journal of Anti-Aging Medicine.*, **2**: 227-230.

Nunomura A., Perry G., Pappolla M.A., Friedland R.P., Hirai K., Chiba S. and Smith M.A. (2000). Neuronal oxidative stress precedes amyloid-beta deposition in Down Syndrome. *Journal of Neuropathology and Experimental Neurology.*, **59**: 1011-1017.

Packer L. (1994). Methods in Enzymology- oxygen radicals in biological systems: Part C. Academic Press Inc, USA. 233.

Palmer T. (1995). Understanding enzymes, 4th Edition. Ellis Horwood, Great Britain.

Parihar M.S. and Hemnani T. (2004). Alzheimers disease pathogenesis and therapeutic interventions. *Journal of Clinical Neuroscience.*, **11**: 456-467.

Perry G., Moreira P.I., Oliveira C.R., Santos M.S., Nunomura A., Honda K., Zhu X. and Smith M.A. (2005). A second look in to the oxidant mechanisms in Alzheimers disease. *Current Neurovascular research.*, **2**:179-184.

Plourde G., Lavoie J.P., Rousseau-Migneron S. and Nadeau A. (1991). Validation of the polyethylene glycol precipitation techniques for the characterization of rat ventricular beta-adrenoceptors. *Analytica .Biochemistry.*, **192**: 426-428.

Poulos T.L., Li H., Shimizu H., Flinspach M., Jamal J., Yang W., Xian M., Cai T., Zhong W.E., Jia Q., Wang P.G. (2002). The novel binding mode of *N*-Alkyl-*N'*-hydroxyguanidine to neuronal nitric oxide synthase provides mechanistic insights into NO biosynthesis. *Biochemistry.*, **41**:13868-13875.

Prostak L., Barnea E., Yaish P. and Zharhary D. (2005). The Sigma-Aldrich BACE1 activity assay kit- a FRET based assay designed for BACE1 inhibitor screening. Sigma-Aldrich Inc .St.Louis, MO, USA.

Reymond J.L. and Sicard R. (2006). Enzyme assays: High–throughput screening, genetic selection and fingerprinting. Wiley-VCH Verlag GmbH & Co. KGaA, Weinheim.

Rischel C., Goto Y., Otzen D.E., Christiansen G., Ban T., Martorana V., Manno M., Yagi H., Anderson C.B. (2009). Branching in amyloid fibril growth. *Biophysical Journal.*, **96**: 1529-1536.

Riveros-Moreno V., Heffernan B., Torres B., Chubb A., Charles I. and Moncada S. (1995). Purification to homogeneity and characterization of rat brain recombinant nitric oxide synthase. *European Journal of Biochemistry.*, **230**: 52-57.

Rodgers A.B. (2003). Alzheimers disease: unravelling the mystery. National Institute on Aging, National Institute of Health, U.S.Department of Health and Human Services

Rosazza J. P. N. and Chen C. (1996) Purified nitric oxide synthase from rat brain. University of Iowa Research Foundation, **675**: 821.

Ruben G.C., Iqbal K.,Wisniewski H.M., Johnson J.E Jr. and Grundke-Iqbal I.(1992). Alzheimer neurofibrillary tangles contain 2.1 nm filaments structurally identical to the microtubule-associated protein tau: a high resolution transmission electron microscope study of tangles and senile plaque core amyloid., *Brain Research*, **590**: 164-179.

Santucci, A., Terstappen G., Franceschini D., Raggiaschi R. and Millucci L. (2009). Rapid aggregation and assembly in aqueous solution of Aß (25-35) peptide. *Journal of Bioscience.*, **34**: 293-303.

Sayle R. and Bernstein H. (1998-2001). Rasmol (Raswin molecular graphics) [V.2.7.2.1]. University of Edinburgh's Biocomputing research unit and the Biomolecular structure Department at Glaxo research and development, Greenford, UK.

Sigel A., Sigel H., Sigel K.O. (2006). Neurodegenerative diseases and metal ions-Volume 1. John Wiley & Sons Ltd, England.

Sakakibara Y. and Yanagisawa H. (2003). Agmatine deiminase from cucumber seedlings is a mono-specific enzyme: purification and characteristics. *Protein Expression and Purification.*, **30**: 88-93

Smith M.A. and Perry G. (1998). What are the facts and artifacts of the pathogenesis and etiology of Alzheimers disease? *Journal of Neuroanalytical Chemistry.*, **16**: 35-41.

Snyder S.H. and Bredt D.S. (1990). Isolation of nitric oxide synthetase, a calmodulin-requiring enzyme. *Proceedings of the National Academy of Sciences.*, **87**: 682-685.

Soto P., Griffin M.A. and Shea J. (2007). New insights into the mechanism of Alzheimer amyloid-ß fibrillogenesis inhibition by *N*-methylated peptides. *Biophysical Journal.*, **93**: 3015-3025.

Stuehr D.J. (1997), Structure-function aspects in the nitric oxide synthases. *Annual Review of Pharmacology and Toxicology.*, **37**: 339-59.

Thrash S.L., Otto J.C. Jnr. and Deits T.L. (1991). Effect of divalent ions on protein precipitation and polyethylene glycol: mechanism of action and applications. *Protein Expression and Purification.*, **2**: 83-89.

Vadimsky R.G. (1980). Electron microscopy. *Methods in Experimental Physics.*, **16**: 185-235.

Virchow R.Z. (1854). Weitere Mittheilungen uber das Vorkommen der pflanzlichen Cellulose beim Menschen. *Virchows Arch.*, **6**: 268-71.

Wang S.S.S., Chen Y., Chen P. and Liu K. (2006). A kinetic study on the aggregation behavior of amyloid peptides in different initial solvent environments. *Biochemical Engineering Journal.*, **29**: 129-138.

Wiesinger H. (2001). Arginine metabolism and the synthesis of nitric oxide in the nervous system. *Progress in Neurobiology.*, **64**: 365-391.

Wilson K and Walker J. (2000). Practical Biochemistry-Principles and Techniques, 5th Edition. Cambridge University Press, London.

Woodward C. and Li R.H. (1999). The hydrogen exchange core and protein folding. *Protein Science.*, **8**: 1571-1590.

Wouters J. (1998). Structural aspects of monoamine oxidase and its reversible inhibition. *Current Medicinal Chemistry.*, **5**: 137-162.

Zhang J., Snyder S.H. (1995). Nitric oxide in the nervous system. *Annuual Reveiw of Pharmacology and Toxicology* ., **35**: 213-233.

Zweier J.L.and Giraldez R.R. (1998). An improved assay for the measurement of nitric oxide synthase activity in biological tissues. *Analytical Biochemistry.*, **261**: 29-35.